
# Las Vegas Valley Visibility and $PM_{2.5}$ Study

Final Report

PREPARED BY:

Mark C. Green
Judith C. Chow
Arsineh Hecobian
Vicken Etyemezian
Hampden Kuhns
John G. Watson

DESERT RESEARCH INSTITUTE
755 East Flamingo Road
Las Vegas, NV 89119

PREPARED FOR:

Clark County Department of Air Quality Management
500 South Grand Central Parkway
P.O. Box 551741
Las Vegas, NV 89155

May 6, 2002

# Las Vegas Valley Visibility and $PM_{2.5}$ Study

Final Report


PREPARED BY:

Mark C. Green
Judith C. Chow
Arsineh Hecobian
Vicken Etyemezian
Hampden Kuhns
John G. Watson

DESERT RESEARCH INSTITUTE
755 East Flamingo Road
Las Vegas, NV 89119


PREPARED FOR:

Clark County Department of Air Quality Management
500 South Grand Central Parkway
P.O. Box 551741
Las Vegas, NV 89155

May 6, 2002

TABLE OF CONTENTS

Page

TABLE OF CONTENTS (continued)

LIST OF FIGURES

LIST OF FIGURES (continued)

LIST OF FIGURES (continued)

LIST OF FIGURES (continued)

Page

LIST OF FIGURES (continued)

Page

LIST OF TABLES

# EXECUTIVE SUMMARY

The Desert Research Institute conducted a year-long study of haze and fine particulate matter ($PM_{2.5}$) chemical composition at three sites in southern Nevada from July 2000 to July 2001. The results of the study are presented in this report. The study was funded by the Nevada Department of Motor Vehicles and administered by the Clark County Department of Air Quality Management (CCDAQM). Major objectives of the study were to:

- Characterize the chemical composition of $PM_{2.5}$ at urban, suburban, and background locations. What can be said about source contributions to $PM_{2.5}$?
- Determine the fraction of dust (crustal material) in $PM_{2.5}$ and coarse ($PM_{10}$ minus $PM_{2.5}$) size ranges. Do dust sources contribute significantly to $PM_{2.5}$?
- Determine the background levels of $PM_{2.5}$ that are transported into the Las Vegas Valley from outside sources.
- Estimate the chemical component contributions to haze (i.e., crustal, organic carbon, elemental carbon, sulfates, nitrates). What can be said about source contributions to haze?
- How much haze is locally generated and how much is transported into the Las Vegas Valley from outside sources?
- Characterize diurnal and seasonal patterns in haze and seasonal patterns in $PM_{2.5}$.

Measurements were made at three monitoring sites intended to represent urban, suburban, and background areas in and around Las Vegas. The sites were East Charleston east of Fremont Street, Palo Verde High School in Summerlin, and just west of Jean, Nevada. Instruments were deployed at these sites to measure light scattering and absorption, which are the major components of haze, as well as particulate matter less than 2.5 microns in diameter ($PM_{2.5}$). At the East Charleston site, $PM_{10}$ was also sampled. Suspended particulate matter is the main cause of haze. The USEPA has established National Ambient Air Quality Standards for $PM_{2.5}$ to protect public health. Detailed chemical analysis was done on about half of the $PM_{2.5}$ and $PM_{10}$ samples, which were collected every third day during the one-year field study. The chemical analysis of these samples allows us to help understand the sources that contribute to $PM_{2.5}$ and haze in the Las Vegas Valley. The measurements at Jean provide an estimate of the levels of haze and $PM_{2.5}$ that are transported into our area from outside (e.g., southern California). The difference between levels at the Jean background site and our suburban and urban sites can be attributed to sources within the Las Vegas urban area.

The results showed that haze and $PM_{2.5}$ levels at the urban site were much higher than the suburban and background sites. The suburban site was influenced by local sources, but was closer to the background site than the urban site in the levels of haze and $PM_{2.5}$. At the urban site, haze and $PM_{2.5}$ were highest in winter; at the backgound site, winter tended to be

the cleanest. At the urban site, haze levels decreased substantially during afternoon hours. The worst levels were during early morning hours.

Background sources outside the valley were estimated to contribute about two-thirds of the $PM_{2.5}$ and a little over half of the haze at the suburban Palo Verde site, on average. At the urban East Charleston site, over three-quarters of the $PM_{2.5}$ and haze were caused by local (Las Vegas urban area) sources. The local and background contributions to haze at the east Charleston and Palo Verde sites are shown for each chemical component in the figures below. The major components are organic compounds (OMC), elemental carbon or soot (EC), sulfates ($SO_4$), nitrate ($NO_3$), fine soil and coarse mass (mainly crustal or dust). The fine soil and coarse mass components are mainly due to disturbed land, construction activity, and road dust.

Local and background average non-Rayleigh light extinction at East Charleston by component

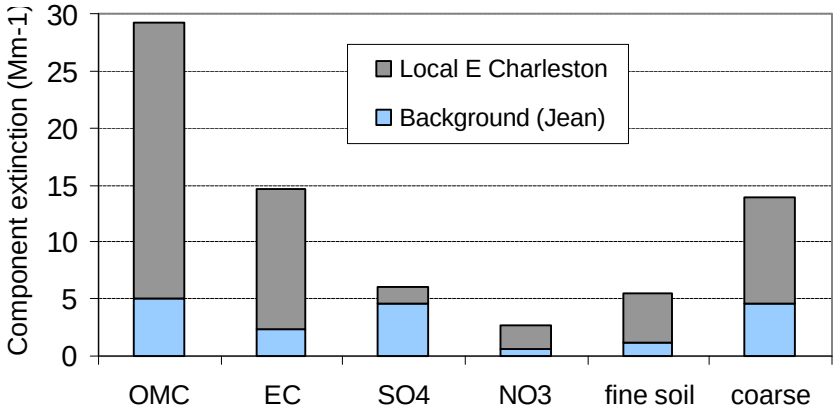


Local and background average non-Rayleigh light extinction at Palo Verde by component

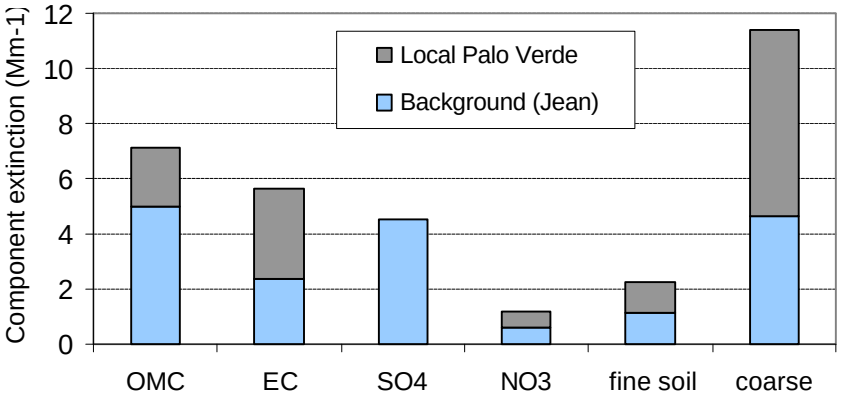


Most of the increase in $PM_{2.5}$ and haze over the background level is due to particles containing organic carbon, elemental carbon, and soil or crustal material. At the East Charleston site, organic and elemental carbon compounds account for over half of the $PM_{2.5}$

mass and about 60% of the haze at East Charleston. At Palo Verde, 42% of $PM_{2.5}$ mass and 40% of haze is caused by carbonaceous compounds. Crustal components were estimated to contribute 25% of $PM_{2.5}$ and 27% of haze at East Charleston, and about 26% of $PM_{2.5}$ and 42% of haze at Palo Verde. At both sites, the amount of crustal material in the $PM_{2.5}$ size range may be overestimated by the measurement techniques used; this will not substantially affect the estimated contribution of crustal material to haze.

The sources of the increased crustal concentrations in the Las Vegas Valley are well known and are dominated by disturbed vacant land, construction activity, and road dust. There is some uncertainty over the relative importance of the major source categories, however. The sources of organic and elemental carbon are also well identified, but there is large uncertainty over the relative contribution from each of the major source types. Sources of concern include gasoline and diesel on-road and off-road vehicles, construction equipment, aircraft, burning, meat cooking, dry cleaning, and lawn and gardening equipment. It is expected that on-road vehicles are dominant sources, with a significant contribution from construction equipment as well. Study data shows that the Palo Verde site was significantly impacted during mornings for a portion of the study period from construction equipment working on the I-215 beltway west of the high school.

Nitrate levels were usually low and contributed significantly to $PM_{2.5}$ and haze only on a few days in winter. Nitrates are formed from reactions of nitrogen oxides (released from combustion processes such as in vehicles) with ammonia gas. Sulfate concentrations in the valley were near background levels, indicated little contribution from local sources.

Recommendations in Section 8 focus on improving knowledge of the contributions from each source type to organic and elemental carbon compounds. Additional chemical analysis and emission inventory work is recommended to help define the source contributions. It is also recommended that additional work be done to better define emissions of crustal material. Sources of elemental carbon are of particular concern because diesel emissions (high in elemental carbon) have been linked to adverse health effects, in particular respiratory distress and lung cancer (Lloyd and Cackette, 2001).

To improve visibility and reduce $PM_{2.5}$ levels in the Las Vegas Valley, reductions in organic and elemental carbon and crustal material emissions are required. Levels of $PM_{2.5}$ and $PM_{10}$ meeting National Ambient Air Quality Standards are not sufficient to prevent significant visibility effects. It is also likely that emissions of visibility-reducing pollutants will need to be reduced in order to comply with the Clean Air Act's regional haze requirements. These regulations require states to make continued progress toward no manmade visibility impairment at mandatory Class I areas in their state and in states where they are contributing to haze. Areas that could be affected by Las Vegas include national parks in southern Utah, such as Zion and Bryce Canyon, and the Grand Canyon in northern Arizona. The Jarbidge Wilderness area in far northern Nevada is the only Class I area in the state.

# 1. INTRODUCTION

The U.S. Environmental Protection Agency has established health-based National Ambient Air Quality Standards (NAAQS) for fine particulate matter less than 2.5 microns in diameter ($PM_{2.5}$) and less than 10 microns in diameter ($PM_{10}$). The Las Vegas urban area is in non-attainment of the $PM_{10}$ NAAQS, due mainly to crustal elements from sources such as construction activities, disturbed vacant land, and road dust. Clark County has only recently begun to measure $PM_{2.5}$ concentrations with USEPA-designated Federal Reference Method (FRM) monitors. The data from these monitors will be used to determine $PM_{2.5}$ compliance status for the area.

While it is well established that crustal compounds dominate $PM_{10}$ mass, the composition of $PM_{2.5}$ had not been established prior to this study. Review of chemically speciated $PM_{10}$ data from a 1996 study of $PM_{10}$ in Las Vegas (Chow and Watson, 1997) suggested that a significant portion of the fine ($PM_{2.5}$) mass at the urban site of East Charleston was organic and elemental carbon, with minor contributions from crustal, sulfate, and nitrate (Green and Chow, 1997). However, because the analysis was for $PM_{10}$ rather than $PM_{2.5}$, this relied particularly upon some assumptions regarding the relative amounts of crustal and organic carbon material in the coarse ($PM_{10}$ minus $PM_{2.5}$) and fine fractions of the $PM_{10}$. In addition, the 1996 study's chemical analyses focused on worst-case episodes for $PM_{10}$ (typically windy days) and one long winter stagnation period. This subset of days selected for chemical analysis was not expected to be representative of annual average conditions, especially when extrapolated to $PM_{2.5}$. Subsequent to the 1996 $PM_{10}$ study, DRI prepared a program plan for $PM_{2.5}$ and haze in the Las Vegas Valley (Green and Chow, 1997).

Visibility impairment (haze) is of concern for multiple reasons. Unlike many pollutants (such as CO and ozone) which are invisible, haze is obvious to the general public and is widely used as an indicator of air quality. The Clean Air Act requires visibility protection for mandatory Class I areas, several of which could be impacted by pollution from the Las Vegas urban area. In the Project MOHAVE final report (Pitchford et al., 1999), there was some discussion about the impact of Las Vegas pollution on visibility at Grand Canyon National Park, but no conclusions were reached. The State of Nevada will be required to prepare a State Implementation Plan (SIP) in accordance with EPA's regional haze regulations. The SIP must provide a plan for the gradual elimination of all manmade visibility impairment at Class I areas within the state (Jarbidge Wilderness area), as well eliminating Nevada's contributions to haze in downwind Class I areas (Zion National Park, for example). Just as the Las Vegas area will transport haze downwind, it will receive haze from upwind areas such as southern California. The amount of haze that is transported into Las Vegas versus locally generated haze is of interest.

As a large fraction of haze is typically caused by fine particles, it is natural to combine a $PM_{2.5}$ study with a visibility study (some basics of visibility science are presented in Section 6). The current study was funded by the State of Nevada Department of Motor Vehicles and administered by the Clark County Department of Air Quality Management (CCDAQM). The field study was conducted from July 2000 to July 2001 and included

measurements at three sites: a background/transport site (Jean), a suburban site (Palo Verde High School), and an urban site (East Charleston east of Fremont Street). The measurement program is fully described in Section 2 and included one-in-three-day filter sampling for $PM_{2.5}$ at the three sites, $PM_{10}$ filter sampling at East Charleston, and light scattering and light absorption (haze components) measurements at the three sites. Full chemical analysis was conducted on about half of the particulate samples. Data collected by the CCDAQM was also used. Digital photographs were taken of the Las Vegas Valley from the roofs of Palo Verde High School and the Humanities Building at UNLV.

Technical objectives of the study included:

- Characterize the chemical composition of $PM_{2.5}$ at urban, suburban, and background locations. What can be said about source contributions to $PM_{2.5}$?

- Determine the fraction of dust (crustal material) in the $PM_{2.5}$ and coarse mass ($PM_{10}$ minus $PM_{2.5}$) size range. Do dust sources contribute significantly to $PM_{2.5}$?

- Determine the background levels of $PM_{2.5}$ that are transported into the Las Vegas Valley from outside sources

- Estimate the chemical component contributions to haze (i.e., crustal, organic carbon, elemental carbon, sulfates, nitrates). What can be said about source contributions to haze?

- How much haze is locally generated and how much is transported into the Las Vegas Valley from outside sources?

- Characterize diurnal and seasonal patterns in haze and seasonal patterns in $PM_{2.5}$.

Public outreach objectives include presenting the results of the study in an easy-to-understand format on DRI's website and making public presentations regarding the study results.

The measurement network and instrumentation used are described in Section 2. In Section 3, database structure, data validation, and data comparability measures are presented. Particulate measurements, including chemical speciation, and temporal and spatial patterns are shown in Section 4. Spatial, seasonal, and diurnal patterns in visibility measurements are discussed in Section 5. Section 6 presents the analysis of the chemical composition of haze. In Section 7, source type contributions to haze are discussed. Recommendations for additional work are made in Section 8. References cited appear in Section 9.

# 2. AMBIENT MEASUREMENTS

## 2.1 Network Description

The ambient monitoring network shown in Figure 2-1 was designed to represent boundary/ background, source, and receptor areas that characterize $PM_{2.5}$ and visibility in the Las Vegas Valley. The network consisted of one urban commercial/ residential site on East Charleston Blvd., one suburban residential site at Palo Verde High School, and one background/transport site at Jean. These sites are adjacent to or part of sites in the current Clark County Department of Air Quality Monitoring (CCDAQM) monitoring network. Concurrent gas and meteorological measurements have been acquired as part of the long-term network, shown in Figure 2-2. Table 2-1 summarizes site surroundings along with site locations, UTM coordinates, and site elevations. Collocated or nearby measurements from this study and from CCDAQM are listed in Table 2-2.

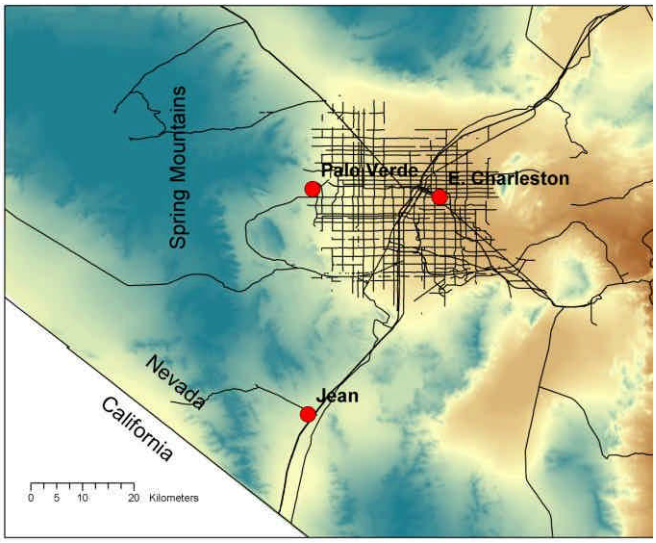


**Figure 2-1.** Topographic map of the study area.

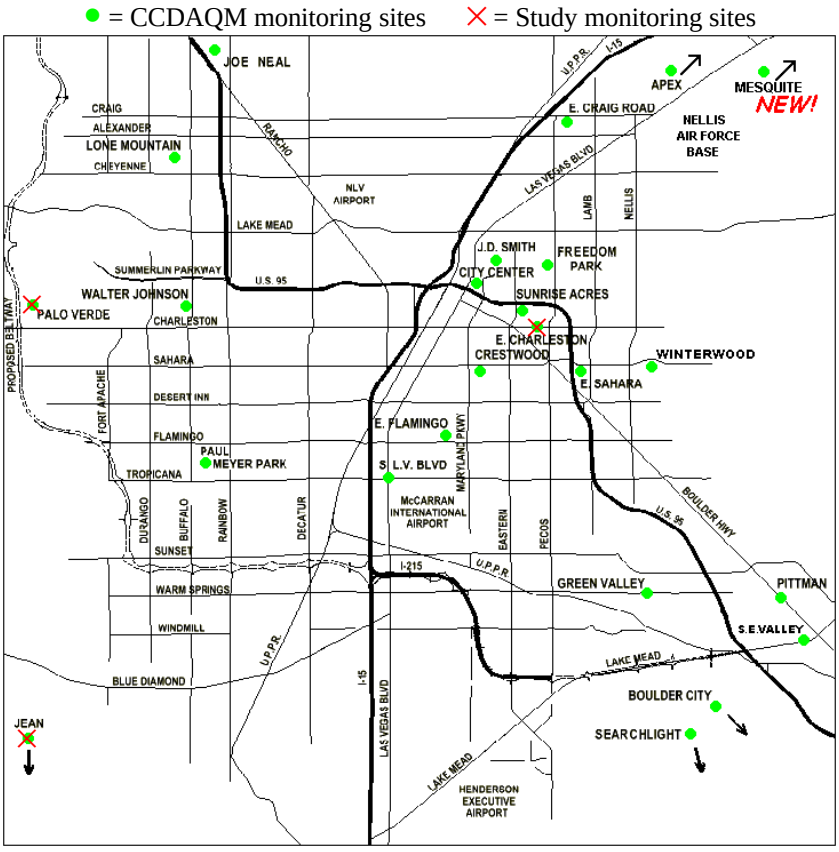


**Figure 2-2.** Ambient monitoring network.

**Table 2-1.** Description of the monitoring sites.

| *Site Name and Location* | *UTM Coordinates* | *Elevation above Mean Sea Level (MSL)* | *Site Description* |
|---|---|---|---|
| **East Charleston**<br><br>2801 E. Charleston Blvd., Las Vegas | 36.159 N, 115.110 W | 567 m | An urban/commercial/residential site in eastern Las Vegas. The site is approximate 40 meters north of East Charleston St., a moderately to heavily traveled thoroughfare, and adjacent to a Mexican fast-food restaurant to the east. The site is in an area that is designated as being in non-attainment for CO, although exceedences have not been recently recorded; the SIP has been submitted to the USEPA and is pending final approval. It is expected to have among the highest $PM_{2.5}$ levels in the Las Vegas Valley. About 15 meters to the north of the SNAQS site is a Clark County Department of Air Quality Monitoring (CCDAQM) site. |
| **Palo Verde**<br><br>Palo Verde High School, 333 Pavillion Center Dr. Las Vegas | 36.173 N, 115.332 W | 909 m | A suburban residential site located a short distance east of the Spring Mountains at the far western edge of the Las Vegas urbanized area and at an elevation 342 m higher than the East Charleston site. This is the existing CCDAQM site next to Pavillion Center Dr. at an entrance/exit of a high school parking lot. Immediately west of the high school, construction began on a segment of the I-215 beltway during the beginning of the field study. The site recorded among the highest ozone ($O_3$) within the Las Vegas area. |
| **Jean**<br><br>T25S R59E S10 | 35.78 N, 115.34 W | 979 m | A background/transport site in relatively undisturbed desert environs about 30 km southwest of the Las Vegas urban area on an east-facing slope about 115 m above Jean, between the Ivanpah Valley and the southern end of the Spring Mountains. This site is next to a CCDAQM site. The site is off a dirt path about 2 km west of Jean and I-15 and about 800 m south of Nevada State Highway 53. On occasion, emissions from vehicular traffic on I-15 may affect the site, although typical wind patterns would not cause direct impacts from the highway. Also, the dirt road to the site may cause elevated concentrations of crustal material. |

**Table 2-2.** Air quality measurements acquired.

| | East Charleston (urban commercial/ residential site) | Palo Verde (suburban residential site) | Jean (background/transport site) |
|---|---|---|---|
| Ammonia, $PM_{2.5}$ mass, chemistry [a] | DRI | DRI | DRI |
| $PM_{10}$ mass and chemistry | DRI | n/a | n/a |
| Particle size distribution [b] | DRI | n/a | n/a |
| Light scattering by particles ($b_{scat}$) [c]<br>– $PM_{2.5}$ $b_{scat}$ (dry)<br>– Total $b_{scat}$ (dry)<br>– Total $b_{scat}$ (ambient) | <br>DRI<br>DRI<br>DRI | <br>n/a<br>n/a<br>DRI | <br>n/a<br>n/a<br>DRI |
| Light absorption by particles ($b_{abs}$) [d] | DRI | DRI | DRI |
| $PM_{2.5}$ by Federal Reference Method | CCDAQM | n/a | CCDAQM |
| $PM_{10}$ by Beta Attenuation Monitor | CCDAQM | CCDAQM | CCDAQM |
| Ozone ($O_3$) | n/a | CCDAQM | CCDAQM |
| Carbon monoxide (CO) | CCDAQM (nearby at Sunrise Acres) | n/a | n/a |
| Wind speed | CCDAQM | CCDAQM | CCDAQM |
| Wind direction | CCDAQM | CCDAQM | CCDAQM |
| Temperature | CCDAQM | CCDAQM | CCDAQM |

[a] 24-hour-average (midnight to midnight) $PM_{2.5}$ and ammonia measurements were acquired on an every-third-day basis by DRI medium-volume sequential gas samplers (SGS) between 07/20/00 and 07/21/01 for mass, elements, ions, and carbon measurements at the three sites, with additional $PM_{10}$ mass and chemical measurements at the East Charleston site.

[b] Particle size distribution measurements were acquired at East Charleston with Climet Model CI-500 optical particle counter to acquire size distributions from 0.3 to 10 µm in 16 bins.

[c] 2-minute-average total particle light scattering ($b_{scat}$) measurements at ambient temperature were acquired at three sites using Optec NGN-2 nephelometers (Air Resource Specialists, Fort Collins, CO). In addition, 5-minute-average dry particle scattering by $PM_{2.5}$ and total particles were acquired with a Radiance M903 nephelometer with smart heater (only heats sample stream when relative humidity exceeds 60%) at the East Charleston site.

[d] 5-minute-average particle light absorption ($b_{abs}$) measurements were acquired with an Andersen AE30S seven-color aethalometer (Andersen Instruments, Smyrna, GA) at the East Charleston site.

## 2.2 $PM_{2.5}$, $PM_{10}$, and Ammonia Measurements

Desert Research Institute (DRI) sequential gas sampling systems (SGS), shown schematically in Figure 2-3, were used at the three study sites. The SGS was equipped with either a Sensidyne/Bendix 240 cyclone or an Andersen SA-254 size-selective inlet to sample $PM_{2.5}$ or $PM_{10}$, respectively, at a flow rate of 113 L/min. The SGS was configured to take two simultaneous samples (i.e., Teflon-membrane/citric-acid-impregnated cellulose-fiber and quartz-fiber/sodium-chloride-impregnated cellulose-fiber filter packs) at 20 L/min through each sampling port. An anodized aluminum denuder was located between the plenum base

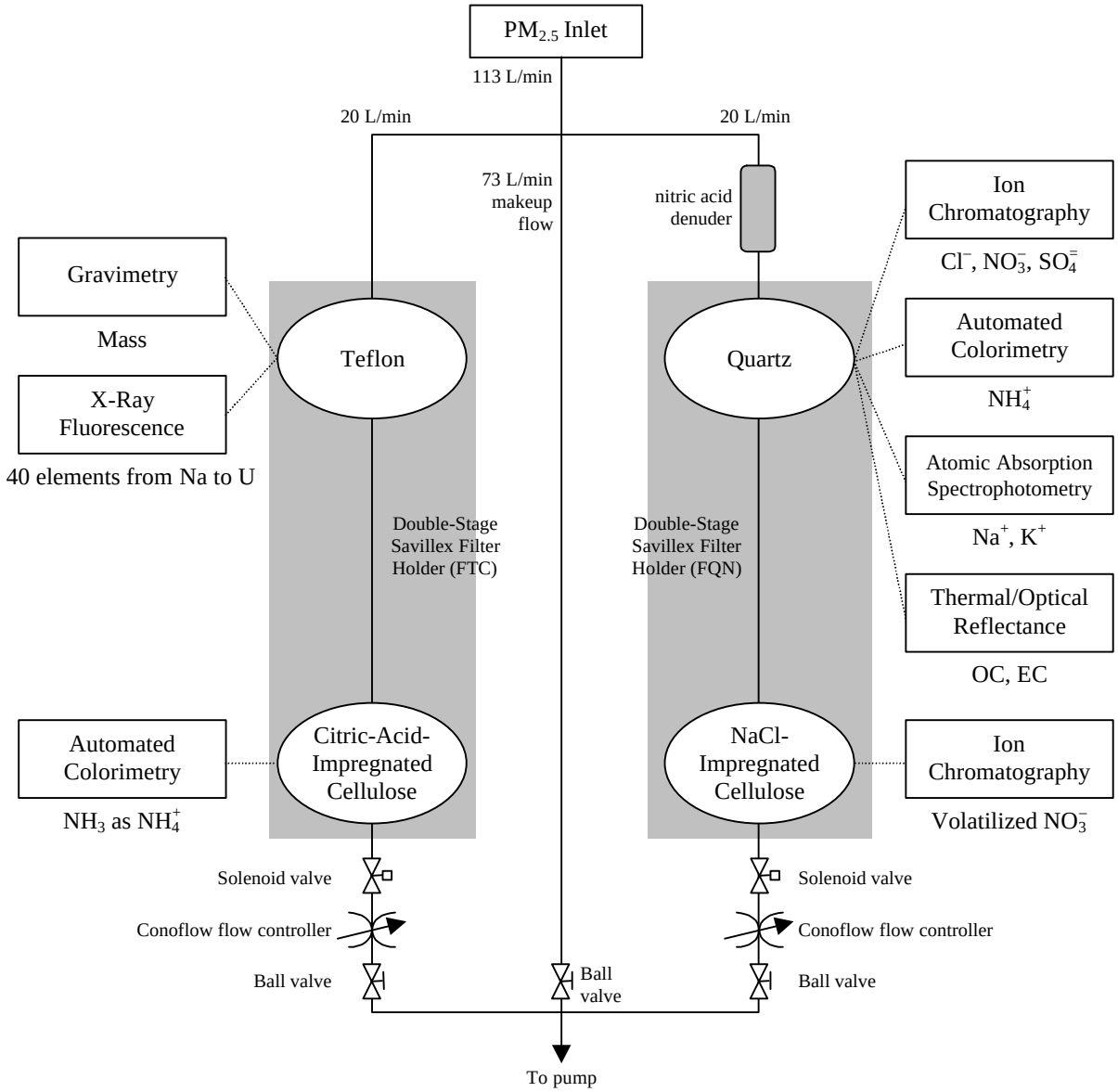


**Figure 2-3.** $PM_{2.5}$ sequential gas sampler (SGS) configuration for the study.

and the filter pack in the SGS to remove gaseous nitric acid. The remaining 73 L/min required for the 113 L/min total inlet flow was drawn through a makeup air sampling port inside the plenum. A vacuum pump drew air through the paired filter packs when the valves were open. The flow rate was controlled by maintaining a constant pressure across a valve with a differential pressure regulator.

Twenty-four-hour (midnight to midnight) filter pack samples were acquired over a yearlong period between 07/20/00 and 07/21/01 on an every-third-day schedule by SGS for $NH_3$ (a precursor gas), $PM_{2.5}$ mass, and chemistry at all three sites. In addition, $PM_{10}$ mass and chemistry were acquired concurrently at the East Charleston site.

The filters were loaded into perfluoralkoxy (PFA) Teflon filter holders at DRI's Environmental Analysis Facility laboratory in Reno, NV. Each filter holder has a tapered extender section (called a receptacle) that mates to the sampler plenum by means of an O-ring and a retainer ring. As shown in Figure 2-3, the Teflon-membrane filter collected particles for mass analysis by gravimetry and elemental analysis (40 elements including Na, Mg, Al, Si, P, S, Cl, K, Ca, Ti, V, Cr, Mn, Fe, Co, Ni, Cu, Zn, Ga, As, Se, Br, Rb, Sr, Y, Zr, Mo, Pd, Ag, Cd, In, Sn, Sb, Ba, La, Au, Hg, Tl, Pb, and U) by x-ray fluorescence (Watson et al., 1999). The citric-acid-impregnated backup filter on a separate stage behind the Teflon-membrane filter was used to acquire gaseous ammonia ($NH_3$) for determination by automated colorimetry. The parallel filter pack contained a 47-mm diameter quartz-fiber front filter with a sodium-chloride-impregnated cellulose-fiber backup filter on a separate stage. The deposit on the quartz-fiber filter was analyzed for chloride ($Cl^-$), nitrate ($NO_3^-$), and sulfate ($SO_4^=$) by ion chromatography, for ammonium ($NH_4^+$) by automated colorimetry, for water-soluble sodium ($Na^+$) and potassium ($K^+$) by atomic absorption spectrophotometry, and for organic and elemental carbon by thermal/optical reflectance (Chow et al., 1993b, 2001). The sodium-chloride-impregnated cellulose-fiber backup filter was analyzed for nitrate to estimate losses due to volatilization of ammonium nitrate from the front filter during sampling.

## 2.3 Nephelometer

The Optec NGN-2 nephelometer uses an open-air design that allows accurate measurement of the scattering extinction coefficient of ambient air. Because of the open-air design, relative humidity and temperature of the air sample are essentially unchanged, thus the aerosol is negligibly modified when brought into the optical measuring chamber. The nephelometer consists of a large inlet with motorized door, measuring chamber, clean air pump for calibration, blower, solenoid activated inlet for span gas, temperature sensor, and real time clock. Clean-air calibrations can be done by the nephelometer, using a clean air filter; but the operator should perform the span gas calibrations manually. Clean (Rayleigh-quality) air is obtained by recirculating the measuring chamber air through a 0.3-µm glass microfiber filter with the inlet door closed. This filter retains 99.97% of all particles larger than 0.3 µm (Optec, 1999). Clean air values were collected by the nephelometer every 6 hours at each site. This was done using a clean air filter installed at the clean air inlet of the nephelometer. For quality control purposes, span gas calibration (using SUVA 134a) was done every 15 days, or more often if required. The lamp brightness levels were set to 1,000

for the nephelometers. Old lamps with low brightness levels were replaced with new ones about every month. The primary format of the nephelometer data is as follows:

000523 1041
RUN Mode 1
SN 11
Intervals 72
Auto span 1=on
baud rate 9600
Auto test 1=on
total run time 4613 hours
low lamp limit 1600
Fog limit 1500
Analog -1 multiplier = 1

| | | | | | | | |
|---|---|---|---|---|---|---|---|
| 1 | 117 | 3326 | 70 | 1 | 37.24 | 0523 | 1042 |
| 2 | 81 | 3416 | 47 | 10 | 37.88 | 0523 | 1049 |
| 3 | 185 | 3383 | 109 | 10 | 38.53 | 0523 | 1109 |

Figure 2-4 illustrates the procedures that have been followed to collect data from three monitoring sites. The data were collected on the site computers. Each host PC captured data to files via communications ports (RS-232 or USB) connected to instruments. An application called HyperACCESS controlled the capture of data to files and ran a script upon connection which enables the capture-text-to-file feature 0 to 59 minutes before the current hour and disables text capture exactly on the hour. There was a default capture file located in the directory where data was being captured to file; it was located in this directory as a requirement by a rename-by-date capability within HyperACCESS. Each host PC had PCAnywhere installed on it and launched a PCAnywhere host to await a call from the remote PC. The remote PC called the host PCs in sequence at 10 minutes after every hour using the Windows 98 Task Scheduler that called a script from PCAnywhere. During the connection, the previous hour's data was transferred from the host PC to the remote PC. The data was imported as text files to a Microsoft ACCESS database

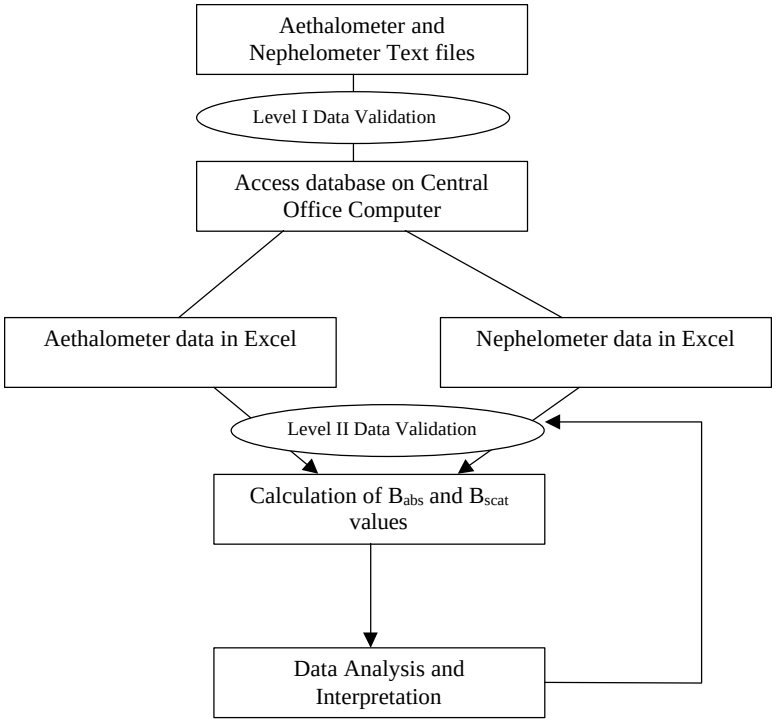


**Figure 2-4.** Flow diagram of nephelometer and aethalometer data collection processes.

using the Data Junction software application, which is a database utility. This database was queried and sorted for light scattering computations and the results were placed into Excel for further analysis and control. Data from the nephelometer was calculated to show the light scattering coefficient for every two minutes of data collection.

## 2.4 Aethalometer

Magee Scientific seven-wavelength (350, 450, 571, 590, 660, 880, and 950 nm) aethalometers were used to measure light absorption. The aethalometer measures changes in transmission of light through a paper tape onto which air is sampled. The calculated light absorption is then converted to a "black carbon" concentration by using a wavelength-dependent absorption efficient (10 $m^2/g$ at 550 nm). The aerosol is collected on an area of a fibrous filter at a moderate face velocity (Hansen, 1999). The aethalometers collected 5-minute continuous data. Each aethalometer was connected to an external pump. The flow rates of the aethalometers were set to 2.5 L/min at the East Charleston site and to 5.0 L/min at the Palo Verde and Jean sites. Each aethalometer stored measurement data on floppy disks and used the aethalometer's internal computer as a backup system for data collection. Aethalometer data was remotely retrieved in the manner described above for the nephelometers. The resulting database was queried and sorted for light absorption computations and the results were placed into Excel for further analysis and control.

## 2.5 Optical Particle Counter

An optical particle counter was used at the East Charleston site. The instrument used was a Climet Spectro .3 Laser Particle Spectrometer, a laser-diode-based aerosol particle counter. The instrument samples air at about one liter per minute and counts and sorts by size individual particles by the amount of light scattered by each particle. The instrument is able to detect optically important particles greater than 0.3 µm in diameter that may significantly affect visibility. The instrument gives a number count of particles per minute in the following size (diameter) bins in µm: 0.3-0.4, 0.4-0.5, 0.5-0.63, 0.63-0.8, 0.8-1.0, 1.0-1.3, 1.3-1.6, 1.6-2, 2-2.5, 2.5-3.2, 3.2-4, 4.0-5.0, 5-6.3, 6.3-8, 8.0-10.0, and >10.

The total counts per minute in each of the bins are written to a file along with the relative humidity, temperature, and flow rate in liters per minute. By dividing the number count by the flow rate, a particle count per liter is obtained for each size range. By multiplying particle count by the cross-sectional area of the particles, an area distribution of particles can be estimated. By multiplying by volume and making assumptions about particle density, a mass distribution can be estimated as well.

# 3. DATABASE AND DATA VALIDATION

This section evaluates the precision, accuracy, and validity of SNAQS aerosol measurements. Numerous air quality studies have been conducted over the past decade, but the data obtained are often not available or applicable for data analysis and modeling because the databases lack documentation with regard to sampling and analysis methods, quality control/quality assurance procedures, accuracy specifications, precision calculations, and data validity. Lioy et al. (1980), Chow and Watson (1989), Watson and Chow (1992), and Chow and Watson (1994) summarize the requirements, limitations, and current availability of ambient and source databases in the United States. The SNAQS data sets intend to meet these requirements. The data files for these studies have the following attributes:

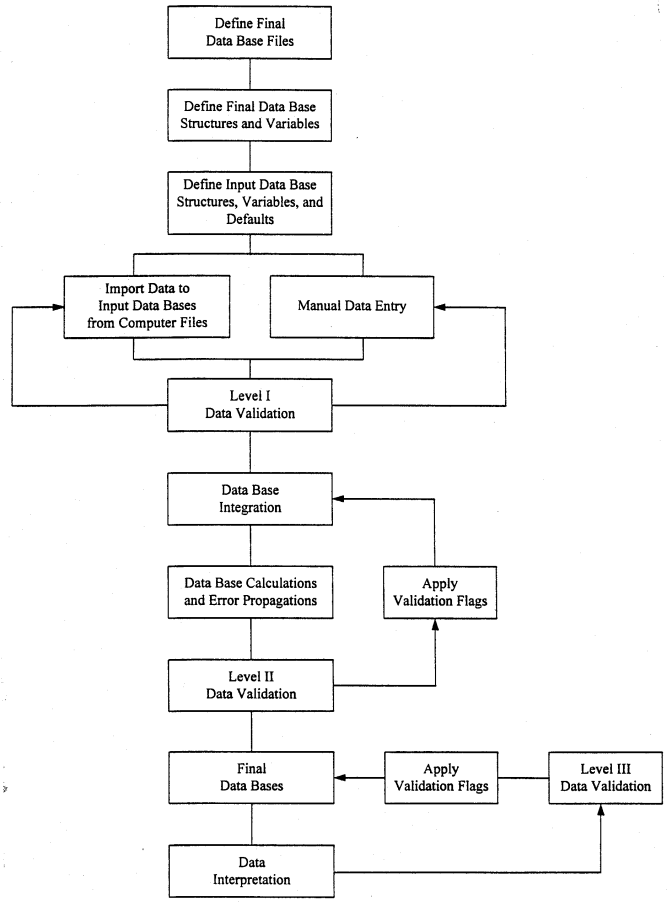


**Figure 3-1.** Flow diagram of the database management system.

- They contain the ambient observables needed to assess source/receptor relationships.
- They are available in a well-documented, computerized form accessible by personal computers and over the Internet.
- Measurement methods, locations, and schedules are documented.
- Precision and accuracy estimates are reported.
- Validation flags are assigned.

This section introduces the features, data structures, and contents of the SNAQS data archive. The approach that was followed to obtain the final data files is illustrated in Figure 3-1. Detailed data processing and data validation procedures are documented in Section 3.2. These data are available on floppy diskettes in Microsoft Excel (.xls) format for convenient

distribution to data users. The file extension identifies the file type according to the following definitions:

- TXT = ASCII text file
- DOC = Microsoft Word document
- XLS = Microsoft Excel spreadsheet

The assembled aerosol database for filter pack measurements taken during SNAQS is fully described by the file "SNAQSFLDNAME.XLS" (see Table 3-1) which documents variable names, descriptions, and measurement units.

## 3.1 Database Structures and Features

The raw SNAQS data was processed with Microsoft FoxPro 2.6 for Windows (Micrsosoft Corp., 1994), a commercially available relational database management system. FoxPro can handle 256 fields of up to 4,000 characters per record and up to one billion records per file. This system can be implemented on most IBM PC-compatible desktop computers. The data base files (∗.DBF) can also be read directly into a variety of popular statistical, plotting, data base, and spreadsheet programs without having to use any specific conversion software. After processing, the final SNAQS data was converted from FoxPro to Microsoft Excel format for reporting purposes.

In FoxPro, one of five field types (character, date, numerical, logical, or memo) was assigned to each observable. Sampling sites and particle size fractions are defined as "Character" fields, sampling dates are defined as "Date" fields, and measured data are defined as "Numeric" fields. "Logical" fields are used to represent a "yes" or "no" value applied to a variable, and "Memo" fields accommodate large blocks of textual information and are used to document the data validation results.

Data contained in different XBase files can be linked by indexing on and relating to common attributes in each file. Sampling site, sampling hour, sampling period, particle size, and sampling substrate IDs are, typically, the common fields among various data files that can be used to relate data in one file to the corresponding data in another file.

To assemble the final data files, information was merged from many data files derived from field monitoring and laboratory analyses by relating information on the common fields cited above.

Four data files resulted from the SNAQS aerosol measurements:

- Filter-based 24-hour $PM_{10}$ aerosol mass data (every third day) from the entire sampling period (07/20/00 to 07/21/01).
- Filter-based 24-hour $PM_{2.5}$ aerosol mass data (every third day) from the entire sampling period (07/20/00 to 07/21/01).

**Table 3-1.** Variable names, descriptions, and measurement units in the assembled aerosol database for filter pack measurements taken during the study.

| Field Code | Description | Measurement Unit |
|---|---|---|
| SITE | Sampling site | |
| DATE | Sampling date | |
| SIZE | Sampler particle size cut | µm |
| STRTHHMM | Sample start time | |
| STOPHHMM | Sample end time | |
| TID | Teflon filter pack ID | |
| QID | Quartz filter pack ID | |
| TFFLG | Teflon filter pack field flag | |
| QFFLG | Quartz filter pack field flag | |
| MSGF | Gravimetry analysis flag | |
| NHCF | Ammonia analysis flag | |
| HNIF | Volatilized nitrate analysis flag | |
| ANIF | Anion analysis flag | |
| N4CF | Ammonium analysis flag | |
| KPAF | Soluble potassium analysis flag | |
| OETF | Carbon analysis flag | |
| ELXF | XRF analysis flag | |
| TVOC | Teflon filter volume | $m^3$ |
| TVOU | Teflon filter volume uncertainty | $m^3$ |
| QVOC | Quartz filter volume | $m^3$ |
| QVOU | Quartz filter volume uncertainty | $m^3$ |
| MSGC | Mass concentration | $\mu g/m^3$ |
| MSGU | Mass concentration uncertainty | $\mu g/m^3$ |
| NHCC | NH3 concentration | $\mu g/m^3$ |
| NHCU | NH3 concentration uncertainty | $\mu g/m^3$ |
| HNIC | Volatilized nitrate concentration | $\mu g/m^3$ |
| HNIU | Volatilized nitrate concentration uncertainty | $\mu g/m^3$ |
| CLIC | Chloride concentration | $\mu g/m^3$ |
| CLIU | Chloride concentration uncertainty | $\mu g/m^3$ |
| N3IC | Nitrate concentration | $\mu g/m^3$ |
| N3IU | Nitrate concentration uncertainty | $\mu g/m^3$ |
| S4IC | Sulfate concentration | $\mu g/m^3$ |
| S4IU | Sulfate concentration uncertainty | $\mu g/m^3$ |
| N4CC | Ammonium concentration | $\mu g/m^3$ |
| N4CU | Ammonium concentration uncertainty | $\mu g/m^3$ |
| KPAC | Soluble Potassium concentration | $\mu g/m^3$ |
| KPAU | Soluble Potassium concentration uncertainty | $\mu g/m^3$ |
| OCTC | Organic Carbon concentration | $\mu g/m^3$ |
| OCTU | Organic Carbon concentration uncertainty | $\mu g/m^3$ |
| ECTC | Elemental Carbon concentration | $\mu g/m^3$ |
| ECTU | Elemental Carbon concentration uncertainty | $\mu g/m^3$ |

**Table 3-1.** (continued)

| Field Code | Description | Measurement Unit |
|---|---|---|
| TCTC | Total Carbon concentration | $\mu g/m^3$ |
| TCTU | Total Carbon concentration uncertainty | $\mu g/m^3$ |
| NAXC | Sodium concentration | $\mu g/m^3$ |
| NAXU | Sodium concentration uncertainty | $\mu g/m^3$ |
| MGXC | Magnesium concentration | $\mu g/m^3$ |
| MGXU | Magnesium concentration uncertainty | $\mu g/m^3$ |
| ALXC | Aluminum concentration | $\mu g/m^3$ |
| ALXU | Aluminum concentration uncertainty | $\mu g/m^3$ |
| SIXC | Silicon concentration | $\mu g/m^3$ |
| SIXU | Silicon concentration uncertainty | $\mu g/m^3$ |
| PHXC | Phosphorous concentration | $\mu g/m^3$ |
| PHXU | Phosphorous concentration uncertainty | $\mu g/m^3$ |
| SUXC | Sulfur concentration | $\mu g/m^3$ |
| SUXU | Sulfur concentration uncertainty | $\mu g/m^3$ |
| CLXC | Chlorine concentration | $\mu g/m^3$ |
| CLXU | Chlorine concentration uncertainty | $\mu g/m^3$ |
| KPXC | Potassium concentration | $\mu g/m^3$ |
| KPXU | Potassium concentration uncertainty | $\mu g/m^3$ |
| CAXC | Calcium concentration | $\mu g/m^3$ |
| CAXU | Calcium concentration uncertainty | $\mu g/m^3$ |
| TIXC | Titanium concentration | $\mu g/m^3$ |
| TIXU | Titanium concentration uncertainty | $\mu g/m^3$ |
| VAXC | Vanadium concentration | $\mu g/m^3$ |
| VAXU | Vanadium concentration uncertainty | $\mu g/m^3$ |
| CRXC | Chromium concentration | $\mu g/m^3$ |
| CRXU | Chromium concentration uncertainty | $\mu g/m^3$ |
| MNXC | Manganese concentration | $\mu g/m^3$ |
| MNXU | Manganese concentration uncertainty | $\mu g/m^3$ |
| FEXC | Iron concentration | $\mu g/m^3$ |
| FEXU | Iron concentration uncertainty | $\mu g/m^3$ |
| COXC | Cobalt concentration | $\mu g/m^3$ |
| COXU | Cobalt concentration uncertainty | $\mu g/m^3$ |
| NIXC | Nickel concentration | $\mu g/m^3$ |
| NIXU | Nickel concentration uncertainty | $\mu g/m^3$ |
| CUXC | Copper concentration | $\mu g/m^3$ |
| CUXU | Copper concentration uncertainty | $\mu g/m^3$ |
| ZNXC | Zinc concentration | $\mu g/m^3$ |
| ZNXU | Zinc concentration uncertainty | $\mu g/m^3$ |
| GAXC | Gallium concentration | $\mu g/m^3$ |
| GAXU | Gallium concentration uncertainty | $\mu g/m^3$ |
| ASXC | Arsenic concentration | $\mu g/m^3$ |
| ASXU | Arsenic concentration uncertainty | $\mu g/m^3$ |

**Table 3-1.** (continued)

| Field Code | Description | Measurement Unit |
|---|---|---|
| SEXC | Selenium concentration | µg/m$^3$ |
| SEXU | Selenium concentration uncertainty | µg/m$^3$ |
| BRXC | Bromine concentration | µg/m$^3$ |
| BRXU | Bromine concentration uncertainty | µg/m$^3$ |
| RBXC | Rubidium concentration | µg/m$^3$ |
| RBXU | Rubidium concentration uncertainty | µg/m$^3$ |
| SRXC | Strontium concentration | µg/m$^3$ |
| SRXU | Strontium concentration uncertainty | µg/m$^3$ |
| YTXC | Yttrium concentration | µg/m$^3$ |
| YTXU | Yttrium concentration uncertainty | µg/m$^3$ |
| ZRXC | Zirconium concentration | µg/m$^3$ |
| ZRXU | Zirconium concentration uncertainty | µg/m$^3$ |
| MOXC | Molybdenum concentration | µg/m$^3$ |
| MOXU | Molybdenum concentration uncertainty | µg/m$^3$ |
| PDXC | Palladium concentration | µg/m$^3$ |
| PDXU | Palladium concentration uncertainty | µg/m$^3$ |
| AGXC | Silver concentration | µg/m$^3$ |
| AGXU | Silver concentration uncertainty | µg/m$^3$ |
| CDXC | Cadmium concentration | µg/m$^3$ |
| CDXU | Cadmium concentration uncertainty | µg/m$^3$ |
| INXC | Indium concentration | µg/m$^3$ |
| INXU | Indium concentration uncertainty | µg/m$^3$ |
| SNXC | Tin concentration | µg/m$^3$ |
| SNXU | Tin concentration uncertainty | µg/m$^3$ |
| SBXC | Antimony concentration | µg/m$^3$ |
| SBXU | Antimony concentration uncertainty | µg/m$^3$ |
| BAXC | Barium concentration | µg/m$^3$ |
| BAXU | Barium concentration uncertainty | µg/m$^3$ |
| LAXC | Lanthanum concentration | µg/m$^3$ |
| LAXU | Lanthanum concentration uncertainty | µg/m$^3$ |
| AUXC | Gold concentration | µg/m$^3$ |
| AUXU | Gold concentration uncertainty | µg/m$^3$ |
| HGXC | Mercury concentration | µg/m$^3$ |
| HGXU | Mercury concentration uncertainty | µg/m$^3$ |
| TLXC | Thallium concentration | µg/m$^3$ |
| TLXU | Thallium concentration uncertainty | µg/m$^3$ |
| PBXC | Lead concentration | µg/m$^3$ |
| PBXU | Lead concentration uncertainty | µg/m$^3$ |
| URXC | Uranium concentration | µg/m$^3$ |
| URXU | Uranium concentration uncertainty | µg/m$^3$ |
| COMMENT | Sampling and/or analysis comments | |

- Filter-based $PM_{10}$ chemical concentration data (episodic) from the entire sampling period (07/20/00 to 07/21/01).

- Filter-based $PM_{2.5}$ chemical concentration data (episodic) from the entire sampling period (07/20/00 to 07/21/01).

Table 3-2 lists the contents of each data file. Each observable is identified by a field name which follows a pattern for that type of observable. For example, in the filter-based aerosol concentration file, the first two characters represent the measured species (e.g., AL for aluminum, SI for silicon, CA for calcium), the third character designates the analysis method (i.e., "G" for gravimetric weighing, "D" for optical densitometry, "X" for x-ray fluorescence analysis, "I" for ion chromatography, "A" for atomic absorption spectrophotometry, "C" for automated colorimetry, "T" for thermal/optical carbon analysis), and the last character uses a "C" to identify a species concentration or a "U" to identify the uncertainty (i.e., precision) of the corresponding measurement. Each measurement method is associated with a separate validation field to document the sample validity for that method. Missing or invalidated measurements have been removed and replaced with –99. All times are in Pacific Standard Time (PST) and sample times show the start of an averaging period.

## 3.2 Measurement and Analytical Specifications

Every measurement consists of: 1) a value; 2) a precision; 3) an accuracy; and 4) a validity (Hidy, 1985; Watson et al., 1989, 1995). The measurement methods described in this volume are used to obtain the value. Performance testing via regular submission of standards, blank analysis, and replicate analysis are used to estimate precision. These precisions are reported in the data files described in Section 3.1 so that they can be propagated through air quality models and used to evaluate how well different values compare with one another. The submission and evaluation of independent standards through quality audits are used to estimate accuracy. Validity applies both to the measurement method and to each measurement taken with that method. The validity of each measurement is indicated by appropriate flagging within the data base, while the validity of the methods has been evaluated in this study by tests described in Section 3.4.

### 3.2.1 Definitions of Measurement Attributes

The precision, accuracy, and validity of the SNAQS aerosol measurements are defined as follows (Chow et al., 1993a):

- A **measurement** is an observation at a specific time and place which possesses: 1) value – the center of the measurement interval; 2) precision – the width of the measurement interval; 3) accuracy – the difference between measured and reference values; and 4) validity – the compliance with assumptions made in the measurement method.

- A **measurement method** is the combination of equipment, reagents, and procedures which provide the value of a measurement. The full description of the

**Table 3-2.** Summary of aerosol databases.

| Category | Database File | Database Description |
|---|---|---|
| I. DATABASE DOCUMENTATION | | |
| | README.DOC | Project and data description file. |
| | SNAQSFLDNAME.XLS | Defines the field names, measurement units, and formats used in the ambient database |
| II. MASS AND CHEMICAL DATA | | |
| $PM_{10}$ | VGSTTM.XLS | Contains 24-hour $PM_{10}$ mass data collected with a sequential filter sampler at the East Charleston site between 07/20/00 and 07/21/01 |
| $PM_{10}$ | VGSTTC.XLS | Contains 24-hour $PM_{10}$ mass and chemical data[a,b,c,d] collected with a sequential filter sampler at the East Charleston site on selected days between 07/20/00 and 07/21/01 |
| $PM_{2.5}$ | VGSFFM.XLS | Contains 24-hour $PM_{2.5}$ mass data collected at three sites with sequential filter samplers between 07/20/00 and 07/21/01 |
| $PM_{2.5}$ | VGSFFC.XLS | Contains 24-hour $PM_{2.5}$ mass and chemical data[a,b,c,d] collected with sequential filter samplers at three sites on selected days between 07/20/00 and 07/21/01 |
| III. NEPHELOMETER, AETHALOMETER, AND OPC DATA | | |
| $b_{scat}$ –hourly | BSCAT.XLS | Contains hourly average particle light scattering data collected with Optec NGN-2 nephelometers at three sites between June 2000 and July 2001 |
| $b_{scat}$- 2 minute | JN_BSCAT.XLS, PB_BSCAT.XLS, EC_BSCAT.XLS | Contain 2-minute-average particle light scattering data collected with Optec NGN-2 nephelometers at three sites between June 2000 and July 2001 |
| $b_{abs}$-hourly | BABS.XLS | Contains hourly average particle light absorption data collected with aethalometers at three sites between June 2000 and July 2001 |
| $b_{abs}$-5 minute | JN_BABS.XLS, PV_BABS.XLS, EC_BABS.XLS | Contains 5-minute-average particle light absorption data collected with aethalometers at three sites between June 2000 and July 2001 |
| Particle number | CLIMET.MDB | Contains particle size counts for 1-minute data from July 2000- July 2001 at East Charleston for 16 size ranges (0.3->10 μm) |
| IV. DATABASE VALIDATION | | |
| | FLDFLAGS.DOC | Contains the field sampling data validation flags |
| | CHEMFLAG.DOC | Contains the chemical analysis data validation flags |

[a] Includes 40 elements (sodium to uranium) by x-ray fluorescence.

[b] Includes chloride, nitrate, and sulfate by ion chromatography; ammonium by automated colorimetry; water-soluble sodium and potassium by atomic absorption spectrophotometry; and organic and elemental carbon by thermal/optical reflectance.

[c] Includes volatilized nitrate by ion chromatography.

[d] Includes ammonia by automated colorimetry.

measurement method requires substantial documentation. For example, two methods may use the same sampling systems and the same analysis systems. These are not identical methods, however, if one performs acceptance testing on filter media and the other does not. Seemingly minor differences between methods can result in major differences between measurement values.

- **Measurement method validity** is the identification of measurement method assumptions, the quantification of effects of deviations from those assumptions, the evaluation that deviations are within reasonable tolerances for the specific application, and the creation of procedures to quantify and minimize those deviations during a specific application. A substantial effort was expended during SNAQS to establish the validity of measurement methods, especially for the measurements of elemental carbon, light absorption, and particle nitrate.

- **Sample validation** is accomplished by procedures that identify deviations from measurement assumptions and the assignment of flags to individual measurements for potential deviations from assumptions.

- The **comparability and equivalence of sampling and analysis methods** are established by the comparison of values and precisions for the same measurement obtained by different measurement methods. Interlaboratory and intralaboratory comparisons are usually made to establish this comparability. Simultaneous measurements of the same observable are considered equivalent when more than 90% of the values differ by no more than the sum of two one-sigma precision intervals for each measurement.

- **Completeness** measures how many environmental measurements with specified values, precisions, accuracies, and validities were obtained out of the total number attainable. It measures the practicability of applying the selected measurement processes throughout the measurement period. Databases which have excellent precision, accuracy, and validity may be of little use if they contain so many missing values that data interpretation is impossible.

Over 11,000 filter-pack samples were acquired during SNAQS. Selected samples were submitted for comprehensive chemical analyses which resulted in 14,000 data points, as documented in Section 3.1.

A database with numerous data points, such as the one used in this study, requires detailed documentation of precision, accuracy, and validity of the measurements. This section addresses the procedures followed to define these quantities and presents the results of those procedures.

### 3.2.2 Definitions of Measurement Precision

Measurement precisions were propagated from precisions of the volumetric measurements, the chemical composition measurements, and the field blank variability using

the methods of Bevington (1969) and Watson et al. (1995). The following equations calculated the precision associated with filter-based measurements:

$$C_i = (M_i - B_i)/V \quad (3\text{-}1)$$

$$V = F \times t \quad (3\text{-}2)$$

$$B_i = \frac{1}{n}\sum_{j=1}^{n} B_{ij} \quad \text{for } B_i > \sigma_{Bi} \quad (3\text{-}3)$$

$$B_i = 0 \quad \text{for } B_i \le \sigma_{Bi} \quad (3\text{-}4)$$

$$\sigma_{Bi} = STD_{Bi} = [\frac{1}{n-1}\sum_{j=1}^{n}(B_{ij} - B_i)^2]^{1/2} \quad \text{for } STD_{Bi} > SIG_{Bi} \quad (3\text{-}5)$$

$$\sigma_{Bi} = SIG_{Bi} = [\frac{1}{n}\sum_{j=1}^{n}(s_{Bij})^2]^{1/2} \quad \text{for } STD_{Bi} \le SIG_{4Bi} \quad (3\text{-}6)$$

$$\sigma_{Ci} = [\frac{s_{Mi}^2 + s_{Bi}^2}{V^2} + \frac{s_V^2 (M_i - B_i)^2}{V^4}]^{1/2} \quad (3\text{-}7)$$

$$\sigma_{RMS_i} = (\frac{1}{n}\sum_{j=1}^{n} s_{Ci}^2)^{1/2} \quad (3\text{-}8)$$

$$\sigma_V/V = 0.05 \quad (3\text{-}9)$$

where:

$B_i$ = average amount of species i on field blanks

$B_{ij}$ = the amount of species i found on field blank j

$C_i$ = the ambient concentration of species i

F = flow rate throughout sampling period

$M_i$ = amount of species i on the substrate

$M_{ijf}$ = amount of species i on sample j from original analysis

$M_{ijr}$ = amount of species i on sample j from replicate analysis

n = total number of samples in the sum

$SIG_{Bi}$ = the root mean square error (RMSE), the square root of the averaged sum of the squared of $\sigma_{Bij}$.

$STD_{Bi}$ = standard deviation of the blank

$\sigma_{Bi}$ = blank precision for species i

$\sigma_{Bij}$ = precision of the species i found on field blank j

$\sigma_{Ci}$ = propagated precision for the concentration of species i

$\sigma_{Mi}$ = precision of amount of species i on the substrate

$\sigma_{RMS_i}$ = root mean square precision for species i

$\sigma_V$ = precision of sample volume

t = sample duration

V = volume of air sampled

Dynamic field blanks were periodically placed in each sampling system without air being drawn through them to estimate the magnitude of passive deposition for the period of time which filter packs remained in a sampler (typically 24 hours). No statistically significant inter-site differences in field blank concentrations were found for any species after removal of outliers (i.e., concentration exceeding three times the standard deviations of the field blanks). The average field blank concentrations (with outliers removed) were calculated for each species on each substrate (e.g., Teflon-membrane, quartz-fiber), irrespective of the sites.

### 3.2.3 Analytical Specifications

Blank precisions ($\sigma_{Bi}$) are defined as the higher value of the standard deviation of the blank measurements, $STD_{Bi}$, or the square root of the averaged squared uncertainties of the blank concentrations, $SIG_{Bi}$. If the average blank for a species was less than its precision, the blank was set to zero (as shown in Equation 3-4). Dynamic field blank concentrations in µg/filter are given in Table 3-3 for $PM_{2.5}$ and $PM_{10}$ samples collected with sequential gas samplers (SGS) during the study.

The precisions ($\sigma_{Mi}$) for x-ray fluorescence analysis were determined from counting statistics unique to each sample. Hence, the $\sigma_{Mi}$ is a function of the energy-specific peak area, the background, and the area under the baseline.

As shown in Table 3-3, the standard deviation of the field blank is more than twice its corresponding root mean square error (RMSE) for ammonia ($NH_3$), chloride ($Cl^-$), soluble sodium ($Na^+$), soluble potassium ($K^+$), organic carbon (OC), silicon (Si), calcium (Ca), and iron (Fe). Some of these field blanks may have been contaminated during the passive deposition period and during sample changing while the plenum was open. Examining the individual field blank values shows that these values are well within the range of the standard deviation of the average blank concentrations.

**Table 3-3.** $PM_{2.5}$ and $PM_{10}$ SGS dynamic field blank concentrations at the East Charleston, Palo Verde and Jean sites.

| | Concentrations in µg/47-mm filter | | | | | |
|---|---|---|---|---|---|---|
| Species | Blank Subtracted[a] ($B_j$) | Blank Subtracted Precision[b] ($s_{Bi}$) | Average Field Blank | Field Blank Std. Dev. ($STD_{Bi}$) | Root Mean Squared Blank Precision[c] ($s_{RMS}$) | Total No. of Blanks in Average |
| Mass | 0.0000 | 10.1176 | -13.5660 | 10.1176 | 5.7925 | 53 |
| Chloride ($Cl^-$) | 0.0000 | 2.2445 | 0.9508 | 2.2445 | 0.5038 | 26 |
| Nonvolatilized Nitrate ($NO_3^-$) | 0.0000 | 0.5000 | 0.0000 | 0.0000 | 0.5000 | 26 |
| Volatilized Nitrate ($NO_3^-$) | 0.0000 | 0.3333 | 0.0000 | 0.0000 | 0.3333 | 26 |
| Sulfate ($SO_4^=$) | 0.0000 | 0.5000 | 0.0335 | 0.1706 | 0.5000 | 26 |
| Ammonium ($NH4^+$) | 0.9061 | 0.5015 | 0.9061 | 0.3000 | 0.5015 | 26 |
| Soluble Sodium ($Na^+$) | 0.0000 | 0.2769 | 0.2395 | 0.2769 | 0.0306 | 26 |
| Soluble Potassium ($K^+$) | 0.1508 | 0.1300 | 0.1508 | 0.1300 | 0.0508 | 26 |
| Organic Carbon (OC) | 37.3269 | 15.5558 | 37.3269 | 15.5558 | 4.2198 | 26 |
| Elemental Carbon (EC) | 0.0000 | 0.9000 | 0.2769 | 0.5701 | 0.9000 | 26 |
| Sodium (Na) | 0.0000 | 2.9240 | 1.5619 | 2.9240 | 2.1027 | 26 |
| Magnesium (Mg) | 0.0000 | 0.4344 | 0.3491 | 0.4344 | 0.2254 | 26 |
| Aluminum (Al) | 0.0000 | 0.2249 | 0.1511 | 0.2025 | 0.2249 | 26 |
| Silicon (Si) | 0.0000 | 0.5380 | 0.3585 | 0.5380 | 0.1914 | 26 |
| Phosphorus (P) | 0.0000 | 0.0670 | 0.0633 | 0.0610 | 0.0670 | 26 |
| Sulfur (S) | 0.0000 | 0.0594 | 0.0423 | 0.0472 | 0.0594 | 26 |
| Chlorine (Cl) | 0.0000 | 0.1427 | 0.0772 | 0.1427 | 0.1223 | 26 |
| Potassium (K) | 0.0000 | 0.1197 | 0.0008 | 0.0567 | 0.1197 | 26 |
| Calcium (Ca) | 0.0000 | 0.2896 | 0.1973 | 0.2896 | 0.1147 | 26 |
| Titanium (Ti) | 0.0000 | 0.5227 | -0.1059 | 0.1778 | 0.5227 | 26 |
| Vanadium (V) | 0.0000 | 0.2393 | -0.0589 | 0.1077 | 0.2393 | 26 |
| Chromium (Cr) | 0.0000 | 0.0602 | -0.0255 | 0.0348 | 0.0602 | 26 |
| Manganese (Mn) | 0.0000 | 0.0339 | -0.0043 | 0.0129 | 0.0339 | 26 |
| Iron (Fe) | 0.0000 | 0.0974 | 0.0085 | 0.0974 | 0.0268 | 26 |
| Cobalt (Co) | 0.0000 | 0.0195 | -0.0044 | 0.0057 | 0.0195 | 26 |
| Nickel (Ni) | 0.0000 | 0.0188 | -0.0055 | 0.0066 | 0.0188 | 26 |
| Copper (Cu) | 0.0000 | 0.0218 | -0.0095 | 0.0111 | 0.0218 | 26 |
| Zinc (Zn) | 0.0000 | 0.0229 | -0.0083 | 0.0135 | 0.0229 | 26 |
| Gallium (Ga) | 0.0000 | 0.0358 | -0.0092 | 0.0173 | 0.0358 | 26 |
| Arsenic (As) | 0.0000 | 0.0400 | -0.0087 | 0.0115 | 0.0400 | 26 |
| Selenium (Se) | 0.0000 | 0.0216 | -0.0056 | 0.0080 | 0.0216 | 26 |
| Bromine (Br) | 0.0000 | 0.0200 | -0.0023 | 0.0059 | 0.0200 | 26 |
| Rubidium (Rb) | 0.0000 | 0.0186 | 0.0019 | 0.0064 | 0.0186 | 26 |
| Strontium (Sr) | 0.0000 | 0.0212 | -0.0029 | 0.0057 | 0.0212 | 26 |
| Yttrium (Y) | 0.0000 | 0.0262 | -0.0004 | 0.0081 | 0.0262 | 26 |
| Zirconium (Zr) | 0.0000 | 0.0308 | 0.0000 | 0.0097 | 0.0308 | 26 |

**Table 3-3.** (continued)

| Species | Concentrations in µg/47-mm filter: Blank Subtracted[a] ($B_j$) | Blank Subtracted Precision[b] ($s_{Bi}$) | Average Field Blank | Field Blank Std. Dev. ($STD_{Bi}$) | Root Mean Squared Blank Precision[c] ($s_{RMS}$) | Total No. of Blanks in Average |
|---|---|---|---|---|---|---|
| Molybdenum (Mo) | 0.0000 | 0.0555 | -0.0091 | 0.0178 | 0.0555 | 26 |
| Palladium (Pd) | 0.0000 | 0.1542 | -0.0139 | 0.0594 | 0.1542 | 26 |
| Silver (Ag) | 0.0000 | 0.1823 | 0.0260 | 0.0592 | 0.1823 | 26 |
| Cadmium (Cd) | 0.0000 | 0.1916 | -0.0049 | 0.0572 | 0.1916 | 26 |
| Indium (In) | 0.0000 | 0.2123 | 0.0552 | 0.0784 | 0.2123 | 26 |
| Tin (Sn) | 0.0000 | 0.2782 | 0.0244 | 0.0829 | 0.2782 | 26 |
| Antimony (Sb) | 0.0000 | 0.3274 | 0.0687 | 0.0952 | 0.3274 | 26 |
| Barium (Ba) | 0.0000 | 1.2490 | 0.1936 | 0.4325 | 1.2490 | 26 |
| Lanthanum (La) | 0.0000 | 1.7027 | 0.0163 | 0.7267 | 1.7027 | 26 |
| Gold (Au) | 0.0000 | 0.0568 | -0.0227 | 0.0273 | 0.0568 | 26 |
| Mercury (Hg) | 0.0000 | 0.0466 | -0.0059 | 0.0164 | 0.0466 | 26 |
| Thallium (Tl) | 0.0000 | 0.0452 | 0.0043 | 0.0144 | 0.0452 | 26 |
| Lead (Pb) | 0.0000 | 0.0628 | -0.0200 | 0.0259 | 0.0628 | 26 |
| Uranium (U) | 0.0000 | 0.0455 | 0.0057 | 0.0116 | 0.0455 | 26 |
| Ammonia ($NH_3$) | 3.2750 | 1.2272 | 3.2750 | 1.2272 | 0.3383 | 26 |

[a] Values used in data processing. Non-zero average blank concentrations are subtracted when the average blank exceeds its standard deviation.

[b] Larger of either the analytical precision or standard deviation from the field.

[c] RMS precision is the square root of the sum of the squared uncertainties of the observations divided by the number of observations.

$PM_{2.5}$ and $PM_{10}$ mass blank values averaged –13.6±10.1 µg/47-mm filter and were thus set to zero (Equation 3-4) for blank subtraction. The largest variation was found for organic carbon, with an average of 37.3±15.6 µg/47-mm filter. The large standard deviations in blank samples were mainly due to the adsorption of gaseous organic carbon which occurred during the passive sampling period when filters were left in the sampler prior to and after sampling. These values were comparable with those reported in other studies (e.g., Watson et al., 1988; Chow et al., 1997).

Table 3-4 summarizes the analytical specifications for the 24-hour $PM_{2.5}$ and $PM_{10}$ measurements obtained during the study. Minimum detectable limits (MDL), root mean squared (RMS) precisions, and lower quantifiable limits (LQL) are given. The MDL is defined as the concentration at which the instrument response equals three times the standard deviation of the response to a known concentration of zero. RMS precision is the square root

**Table 3-4.** Analytical specifications for 24-hour $PM_{2.5}$ and $PM_{10}$ measurements at the East Charleston, Palo Verde, and Jean sites.

| Species | Analysis Method[a] | MDL[b] (µg/m$^3$) | RMS[c] (µg/m$^3$) | LQL[d] (µg/m$^3$) | No. of Values[e] | No. > MDL | % > MDL | No. > LQL | % > LQL |
|---|---|---|---|---|---|---|---|---|---|
| Mass (all days) | Gravimetry | 0.2429 | 1.2291 | 0.7026 | 401 | 401 | 100% | 392 | 98% |
| Mass (chem analysis days) | Gravimetry | 0.2429 | 1.3639 | 0.7026 | 214 | 214 | 100% | 213 | 100% |
| Chloride ($Cl^-$) | IC | 0.0521 | 0.0322 | 0.1559 | 214 | 93 | 43% | 180 | 84% |
| Nonvolatilized Nitrate ($NO_3^-$) | IC | 0.0521 | 0.0606 | 0.0347 | 214 | 209 | 98% | 212 | 99% |
| Volatilized Nitrate ($NO_3^-$) | IC | 0.0521 | 0.0263 | 0.0231 | 214 | 159 | 74% | 182 | 85% |
| Sulfate ($SO_4^=$) | IC | 0.0521 | 0.0843 | 0.0347 | 214 | 214 | 100% | 214 | 100% |
| Ammonium ($NH4^+$) | AC | 0.0521 | 0.0369 | 0.0348 | 214 | 212 | 99% | 214 | 100% |
| Soluble Sodium ($Na^+$) | AAS | 0.0104 | 0.0146 | 0.0192 | 214 | 213 | 100% | 205 | 96% |
| Soluble Potassium ($K^+$) | AAS | 0.0104 | 0.0127 | 0.0090 | 214 | 201 | 94% | 207 | 97% |
| Organic Carbon (OC) | TOR | 0.0958 | 0.6188 | 1.0803 | 214 | 201 | 94% | 158 | 74% |
| Elemental Carbon (EC) | TOR | 0.0958 | 0.1766 | 0.0625 | 214 | 214 | 100% | 214 | 100% |
| Sodium (Na) | XRF | 0.0331 | 0.2618 | 0.2031 | 214 | 100 | 47% | 8 | 4% |
| Magnesium (Mg) | XRF | 0.012 | 0.0229 | 0.0302 | 214 | 185 | 86% | 148 | 69% |
| Aluminum (Al) | XRF | 0.0048 | 0.2235 | 0.0156 | 214 | 213 | 100% | 208 | 97% |
| Silicon (Si) | XRF | 0.003 | 0.8906 | 0.0374 | 214 | 214 | 100% | 211 | 99% |
| Phosphorus (P) | XRF | 0.0027 | 0.0113 | 0.0047 | 214 | 39 | 18% | 27 | 13% |
| Sulfur (S) | XRF | 0.0024 | 0.0269 | 0.0041 | 214 | 214 | 100% | 214 | 100% |
| Chlorine (Cl) | XRF | 0.0048 | 0.0424 | 0.0099 | 214 | 105 | 49% | 92 | 43% |
| Potassium (K) | XRF | 0.0029 | 0.0718 | 0.0083 | 214 | 214 | 100% | 212 | 99% |
| Calcium (Ca) | XRF | 0.0022 | 0.4619 | 0.0201 | 214 | 214 | 100% | 212 | 99% |
| Titanium (Ti) | XRF | 0.0014 | 0.0237 | 0.0363 | 214 | 171 | 80% | 43 | 20% |
| Vanadium (V) | XRF | 0.0012 | 0.0120 | 0.0166 | 214 | 59 | 28% | 0 | 0% |
| Chromium (Cr) | XRF | 0.0009 | 0.0028 | 0.0042 | 214 | 41 | 19% | 5 | 2% |
| Manganese (Mn) | XRF | 0.0008 | 0.0014 | 0.0024 | 214 | 188 | 88% | 136 | 64% |
| Iron (Fe) | XRF | 0.0007 | 0.0352 | 0.0068 | 214 | 214 | 100% | 214 | 100% |
| Cobalt (Co) | XRF | 0.0004 | 0.0106 | 0.0014 | 214 | 73 | 34% | 36 | 17% |
| Nickel (Ni) | XRF | 0.0004 | 0.0008 | 0.0013 | 214 | 67 | 31% | 11 | 5% |
| Copper (Cu) | XRF | 0.0005 | 0.0010 | 0.0015 | 214 | 180 | 84% | 139 | 65% |
| Zinc (Zn) | XRF | 0.0005 | 0.0015 | 0.0016 | 214 | 213 | 100% | 193 | 90% |
| Gallium (Ga) | XRF | 0.0009 | 0.0016 | 0.0025 | 214 | 0 | 0% | 0 | 0% |
| Arsenic (As) | XRF | 0.0008 | 0.0021 | 0.0028 | 214 | 43 | 20% | 5 | 2% |
| Selenium (Se) | XRF | 0.0006 | 0.0009 | 0.0015 | 214 | 5 | 2% | 0 | 0% |
| Bromine (Br) | XRF | 0.0005 | 0.0007 | 0.0014 | 214 | 209 | 98% | 176 | 82% |
| Rubidium (Rb) | XRF | 0.0005 | 0.0008 | 0.0013 | 214 | 95 | 44% | 37 | 17% |
| Strontium (Sr) | XRF | 0.0005 | 0.0011 | 0.0015 | 214 | 187 | 87% | 136 | 64% |
| Yttrium (Y) | XRF | 0.0006 | 0.0012 | 0.0018 | 214 | 19 | 9% | 1 | 0% |
| Zirconium (Zr) | XRF | 0.0008 | 0.0013 | 0.0021 | 214 | 103 | 48% | 49 | 23% |
| Molybdenum (Mo) | XRF | 0.0013 | 0.0026 | 0.0039 | 214 | 21 | 10% | 0 | 0% |
| Palladium (Pd) | XRF | 0.0053 | 0.0068 | 0.0107 | 214 | 0 | 0% | 0 | 0% |
| Silver (Ag) | XRF | 0.0058 | 0.0080 | 0.0127 | 214 | 5 | 2% | 0 | 0% |
| Cadmium (Cd) | XRF | 0.0058 | 0.0081 | 0.0133 | 214 | 29 | 14% | 12 | 6% |
| Indium (In) | XRF | 0.0062 | 0.0094 | 0.0147 | 214 | 3 | 1% | 0 | 0% |
| Tin (Sn) | XRF | 0.0081 | 0.0123 | 0.0193 | 214 | 5 | 2% | 0 | 0% |
| Antimony (Sb) | XRF | 0.0086 | 0.0145 | 0.0227 | 214 | 18 | 8% | 1 | 0% |
| Barium (Ba) | XRF | 0.0249 | 0.0545 | 0.0867 | 214 | 94 | 44% | 21 | 10% |

**Table 3-4.** (continued)

| Species | Analysis Method[a] | MDL[b] (μg/m$^3$) | RMS[c] (μg/m$^3$) | LQL[d] (μg/m$^3$) | No. of Values[e] | No. > MDL | % > MDL | No. > LQL | % > LQL |
|---|---|---|---|---|---|---|---|---|---|
| Lanthanum (La) | XRF | 0.0297 | 0.0787 | 0.1182 | 214 | 24 | 11% | 0 | 0% |
| Gold (Au) | XRF | 0.0015 | 0.0027 | 0.0039 | 214 | 0 | 0% | 0 | 0% |
| Mercury (Hg) | XRF | 0.0012 | 0.0020 | 0.0032 | 214 | 0 | 0% | 0 | 0% |
| Thallium (Tl) | XRF | 0.0012 | 0.0020 | 0.0031 | 214 | 5 | 2% | 0 | 0% |
| Lead (Pb) | XRF | 0.0014 | 0.0025 | 0.0044 | 214 | 127 | 59% | 57 | 27% |
| Uranium (U) | XRF | 0.0011 | 0.0021 | 0.0032 | 214 | 2 | 1% | 0 | 0% |
| Ammonia ($NH_3$) | AC | 0.0521 | 0.3205 | 0.0852 | 214 | 212 | 99% | 212 | 99% |

[a] IC=ion chromatography. AC=automated colorimetry. AAS=atomic absorption spectrophotometry. TOR= thermal/optical reflectance. XRF=x-ray fluorescence.

[b] Minimum detectable limit (MDL) is the concentration at which instrument response equals three times the standard deviation of the response to a known concentration of zero. Typical sample volumes are 28.8 m$^3$.

[c] Root mean squared precision (RMS) is the square root of the sum of the squared uncertainties of the observations divided by the number of observations.

[d] Lower quantifiable limit (LQL) is two times the uncertainty of the field blank. LQL is expressed here in terms of mass per cubic meter after dividing by 28.8 m$^3$ for SGS samplers.

[e] Number of non-void values (with -99) reported.

of the averaged squared uncertainties. The LQL is defined as a concentration corresponding to two times the precision of the dynamic field blank. The LQLs in Table 3-4 were divided by 28.8 m$^3$ for the SGS samplers. This is the nominal sample volume for 24-hour samples. Actual volumes varied from sample to sample, typically within ±5% of the pre-set volume. The LQLs should always be equal to or larger than the analytical MDLs because they include the standard deviation of the field blank and flow rate precision (Watson et al., 1995). This was the case for most of the chemical compounds noted in Table 3-4. This table also indicates that the RMS precisions were comparable in magnitude to the LQLs for most species.

The number of reported (nonvoid, nonmissing) concentrations for each species and the number of reported concentrations greater than the MDLs and LQLs are also summarized in Table 3-4. For the study samples, mass, ions (e.g., nonvolatilized nitrate, sulfate, ammonium, soluble sodium, and soluble potassium), organic and elemental carbon, and sulfur, were detected in almost all samples. Chloride and volatilized nitrate were detected in 43% and 74% of the samples, respectively. Several transition metals (e.g., Cr, Ga, Y, Mo, Pd, Ag, In, Sn, Sb, La, Au, Tl, U) were not detected in most of the samples. This is typical for urban sites in most regions. Other transition metals, such as titanium (Ti), zirconium (Zr), barium (Ba), and cobalt (Co), were detected in 80%, 48%, 44%, and 34% of the samples and were above the LQLs in 20%, 23%, 10%, and 17% of the samples, respectively. Residual-oil-related species, such as nickel (Ni), were detected in 31% of the samples, and vanadium (V) was detected in 28% of the samples. Industrial-source-related toxic species

such as mercury (Hg) was not detected in any of the samples. Cadmium (Cd), arsenic (As), and selenium (Se), however, were found above the MDLs in 14%, 20%, and 2% of the samples, respectively. The maximum arsenic (As) concentration of 0.0076 $\mu g/m^3$ was far below those levels that might be hazardous to human health. Crustal-related species such as aluminum (Al), silicon (Si), potassium (K), calcium (Ca), manganese (Mn), iron (Fe), and zinc (Zn) were found above the MDLs in all of the samples and above the LQLs in more than 90% of the samples. Copper (Cu), manganese (Mn), and strontium (Sr) were found above the MDLs in more than 80% of the samples, and above the LQLs in more than 60% of the samples. Motor-vehicle-related species such as bromine (Br) and lead (Pb) were detected in 82% and 27% of the samples, respectively. Gaseous ammonia was detected in almost all of the samples and chlorine was detected in nearly half of the samples.

These analytical specifications imply that $PM_{2.5}$ and $PM_{10}$ samples acquired during the study possess adequate sample loading for chemical analysis of those species that are expected from sources in the region. In addition, the MDLs of the selected chemical analysis methods were sufficiently low to establish valid measurements with acceptable precisions.

## 3.3 Quality Assurance

Quality control (QC) and quality auditing establish the precision, accuracy, and validity of measured values. Quality assurance integrates quality control, quality auditing, measurement method validation, and sample validation into the measurement process. The results of quality assurance are data values with specified precisions, accuracies, and validities.

Field blanks were acquired and replicate analyses were performed for ~10% of all ambient samples. Quality audits of sample flow rates were conducted at the beginning, middle, and end of the study period, and these audits determined that flow rates were within ±10% of specifications. Data were submitted to three levels of data validation (Chow et al., 1994, Watson et al., 2001a). Detailed data validation processes are documented in the following subsections.

## 3.4 Data Validation

Data acquired from the study was submitted to three data validation levels:

- Level 0 sample validation designates data as they come off the instrument. This process ascertains that the field or laboratory instrument is functioning properly.

- Level I sample validation: 1) flags samples when significant deviations from measurement assumptions have occurred, 2) verifies computer file entries against data sheets, 3) eliminates values for measurements that are known to be invalid because of instrument malfunctions, 4) replaces data from a backup data acquisition system in the event of failure of the primary system, and 5) adjusts values for quantifiable calibration or interference biases.

- Level II sample validation applies consistency tests to the assembled data based on known physical relationships between variables.

- Level III sample validation is part of the data interpretation process. The first assumption upon finding a measurement which is inconsistent with physical expectations is that the unusual value is due to a measurement error. If, upon tracing the path of the measurement nothing unusual is found, the value can be assumed to be a valid result of an environmental cause. Unusual values are identified during the data interpretation process as: 1) extreme values, 2) values which would otherwise normally track the values of other variables in a time series, and 3) values for observables which would normally follow a qualitatively predictable spatial or temporal pattern.

Level I validation flags and comments are included with each data record in the data base as documented in Section 3.1. Level II validation tests and results are described in the following subsections.

Level II tests evaluate the chemical data for internal consistency. In this study, Level II data validations were made for: 1) sum of chemical species versus $PM_{10}$ or $PM_{2.5}$ mass, 2) physical consistency, 3) anion and cation balance, 4) nitrate volatilization, 5) reconstructed versus measured mass, and 5) collocated comparison of gaseous ammonia. Correlations and linear regression statistics were computed and scatter plots prepared to examine the data.

### 3.4.1 Sum of Chemical Species versus Mass

The sum of the individual chemical concentrations for $PM_{10}$ or $PM_{2.5}$ should be less than or equal to the corresponding gravimetrically measured mass concentrations. This sum includes chemicals quantified on the front Teflon-membrane and front quartz-fiber filters. Total sulfur (S), soluble chloride ($Cl^-$), and soluble potassium ($K^+$) are excluded from the sum to avoid double counting since sulfate ($SO_4^=$), chlorine (Cl), and total potassium (K) are included in the sum. Elemental sodium (Na) and magnesium (Mg) have low atomic numbers and require detailed particle size distributions in order to completely correct for particle x-ray absorption effects, so these concentrations are also excluded from the calculation. Measured concentrations do not account for unmeasured metal oxides in crustal material, unmeasured cations, or hydrogen and oxygen associated with organic carbon.

Figure 3-2 shows scatter plots of the $PM_{10}$ sum of species versus mass at the East Charleston site and $PM_{2.5}$ sum of species versus mass at all three sites. Each plot contains a dashed line indicating the slope with intercept and a solid one-to-one line. Measurement uncertainties associated with the x- and y-axes are shown for comparison. Regression statistics with mass as the independent variable (X) and sum of species as the dependent variable (Y) are also calculated. The average ratio of Y over X is also shown for comparison. As intercepts are low compared to the measured concentrations, the slope closely represents the ratio of Y over X. Suspect data were examined, flagged, and removed from further statistical analysis when sampling or analytical anomalies were identified.

As shown in Figure 3-2a, all of the sums are less than the corresponding $PM_{10}$ or $PM_{2.5}$ mass within the reported precisions. An excellent relationship was found between the sum of species and $PM_{10}$ mass with correlation coefficients exceeding 0.98 for the East Charleston measurements. Approximately 60% to 70% of the $PM_{10}$ mass was explained by the chemical species measured during the study. Geological material was a major component of coarse particles. Unmeasured metal oxides in geological material constituted a major portion of the unaccounted mass.

a)

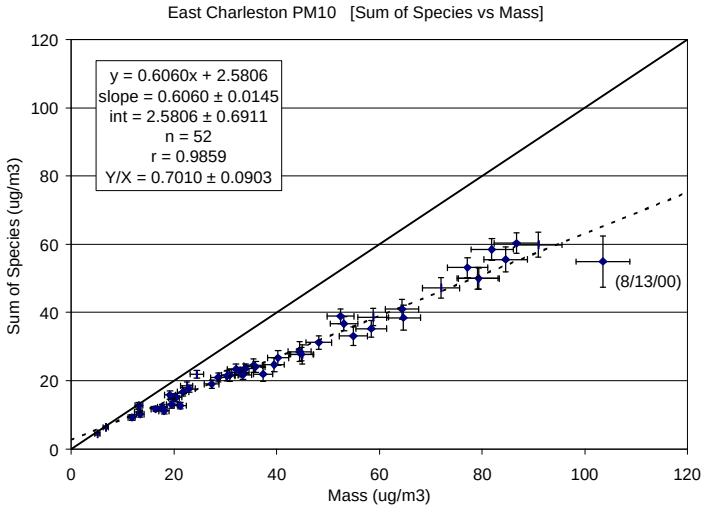


b)

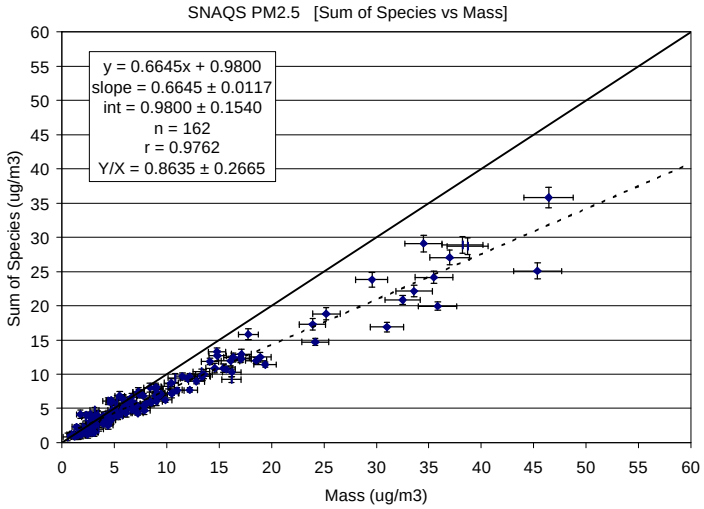


**Figure 3-2.** Scatter plots of sum of species versus mass measurements from: a) $PM_{10}$ data acquired at the East Charleston site; and b) $PM_{2.5}$ data acquired at the East Charleston, Palo Verde, and Jean sites.

Similar comparisons were made among $PM_{2.5}$ measurements at the three sites. Figure 3-2b shows that almost all $PM_{2.5}$ measurements are below the one-to-one line within measurement uncertainties with high correlation (r=0.98). The $PM_{2.5}$ comparison in Figure 3-2b is similar to the $PM_{10}$ comparison but with a ~17% higher sum-of-species-to-mass ratio. When $PM_{2.5}$ mass was low, the sum of species was much closer to $PM_{2.5}$ mass. Since organic carbon is often a large portion of $PM_{2.5}$ mass, the elevated sum of species was affected by high carbon mass.

### 3.4.2 Physical Consistency

The composition of chemical species concentrations measured by different chemical analysis methods was examined. Physical consistency was tested for: 1) sulfate versus total sulfur, 2) chloride versus chlorine, and 3) soluble potassium versus total potassium.

### 3.4.2.1 Sulfate versus Total Sulfur

Water-soluble sulfate ($SO_4^=$) was measured by ion chromatography (IC) analysis on quartz-fiber filters, and total sulfur (S) was measured by x-ray fluorescence (XRF) analysis on Teflon-membrane filters. The ratio of sulfate to total sulfur should equal "3" if all of the sulfur were present as soluble sulfate. Figure 3-3a shows scatter plots of sulfate versus sulfur concentrations at the East Charleston site. A good correlation (r>0.95) was found among $PM_{10}$ sulfur/sulfate measurements with an average ratio of 3.09±0.43.

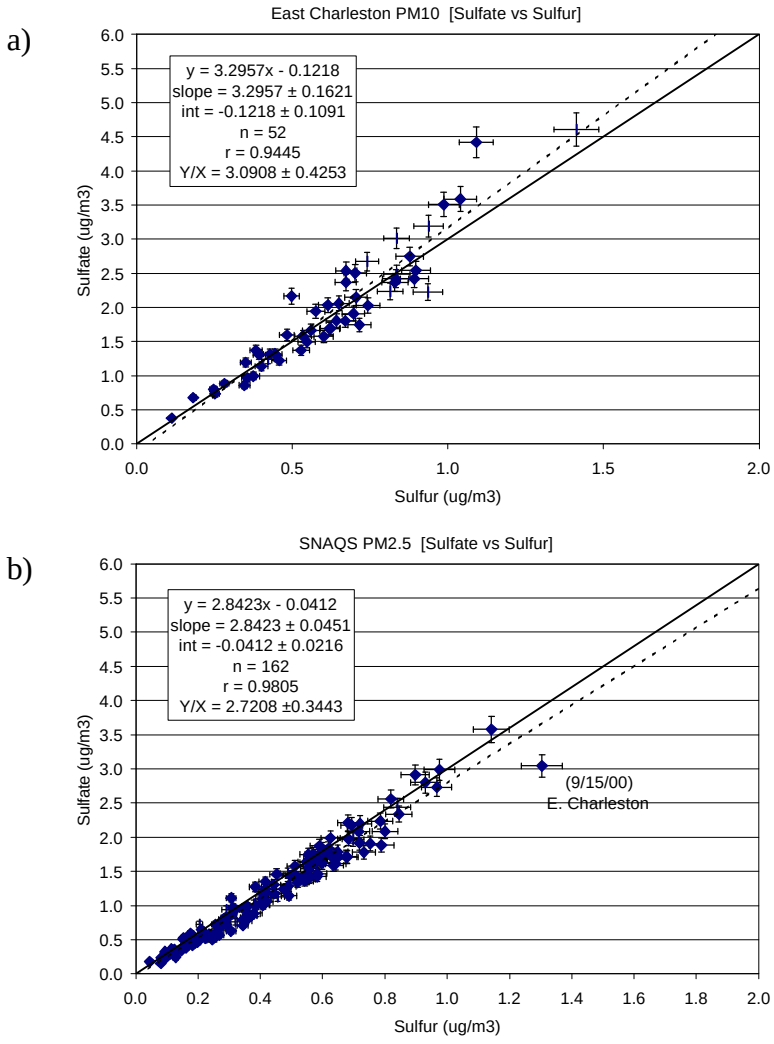


**Figure 3-3.** Scatter plots of sulfate versus sulfur measurements from: a) $PM_{10}$ data acquired at the East Charleston site; and b) $PM_{2.5}$ data acquired at the East Charleston, Palo Verde, and Jean sites.

Higher correlations (r=0.98) were found for $PM_{2.5}$ sulfate/sulfur comparisons among the three sites. For the $PM_{2.5}$ samples, Figure 3-3b shows that all but a few of the 162 data pairs fell beyond the three-to-one line. The regression statistics give a slope of 2.84±0.05 with negligible intercept (–0.041±0.02 $\mu g/m^3$). The only data pair with a low $SO_4^=/S$ ratios beyond the regression line was from East Charleston on 09/15/00. This sample was reanalyzed with consistent results. Overall, the sulfate and total sulfur comparisons in this study support the contentions that more than 90% of sulfur was present as soluble sulfate in the atmosphere and that both XRF and IC measurements are valid.

### 3.4.2.2 Chloride versus Chlorine

Chloride ($Cl^-$) was measured by IC on quartz-fiber filters, and chlorine (Cl) was measured by XRF on Teflon-membrane filters. Because chloride is the water-soluble portion of chlorine, the chloride-to-chlorine ratio is expected to be less than unity. Figure 3-4a shows that high correlations (r=0.98) were found between $PM_{10}$ chloride and chlorine measurements, with a slope close to unity and low intercept at the East Charleston site.

Similar comparisons were made for $PM_{2.5}$ chloride/chlorine measurements. Figure 3-4b shows that most of the $PM_{2.5}$ chloride concentrations were low (below 0.3 $\mu g/m^3$) with high relative uncertainties, but that there was good correlation (r>0.93) between chloride and chlorine measurements. The uncertainties of chloride measurements were higher at low concentrations because chloride's elution peak in ion chromatographic analysis is close to the distilled water dip which, in turn, shifts the baseline of the chromatogram (Chow and Watson, 1999). In addition, chlorine collected on the Teflon filter may be lost through volatilization because XRF analysis is conducted in a vacuum chamber. Such losses are especially apparent when chlorine concentrations are low.

a)

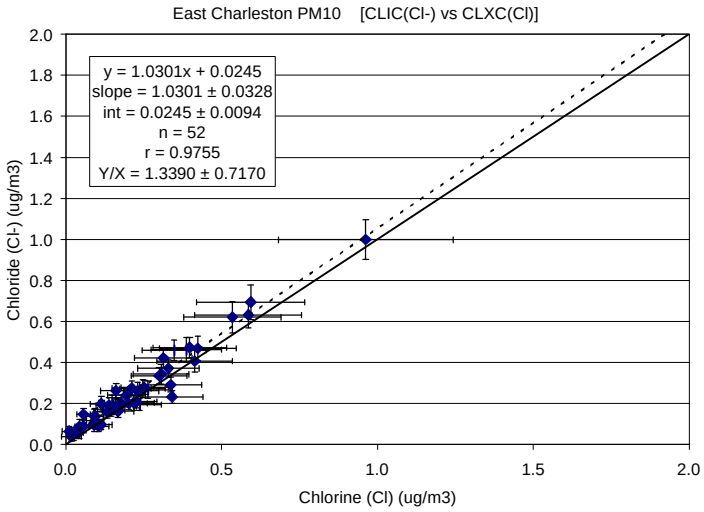


b)

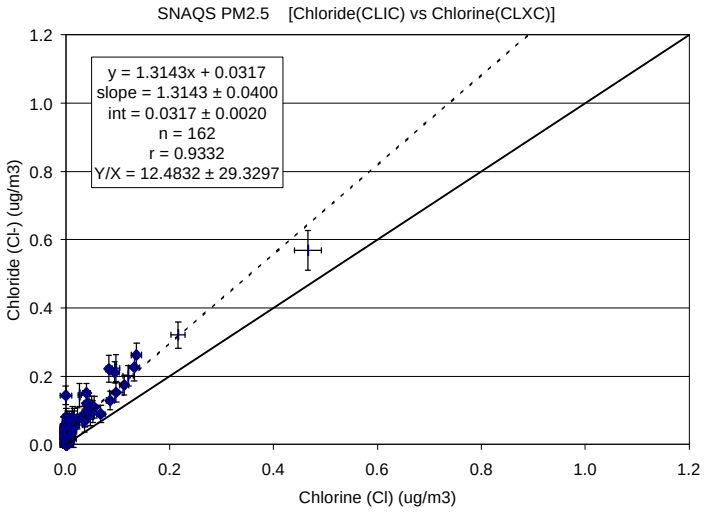


**Figure 3-4.** Scatter plots of chloride versus chlorine measurements from: a) $PM_{10}$ data acquired at the East Charleston site; and b) $PM_{2.5}$ data acquired at the East Charleston, Palo Verde, and Jean sites.

### 3.4.2.3 Soluble Potassium versus Total Potassium

Soluble potassium ($K^+$) was measured by atomic absorption spectrophotometry (AAS) analysis on quartz-fiber filters, and total potassium (K) was measured by XRF analysis on Teflon-membrane filters. Figure 3-5 displays the scatter plot of soluble potassium versus total potassium concentrations. Large uncertainty intervals associated with total potassium measurements reflected the uncertainty of light element particle corrections in x-ray fluorescence analysis.

The data pairs were scattered at low concentrations, but they were well within the measurement uncertainties. It is apparent that some of the $K^+/K$ ratios were quite low, especially when potassium concentrations were below 1 $\mu g/m^3$. The average y/x ratio of $K^+/K$ was 0.32±0.12. These figures show that approximately one-third of $PM_{10}$ total potassium was in its soluble state during the study. The average soluble potassium to total potassium ratio was about 25% higher in the $PM_{2.5}$ fraction as compared to the $PM_{10}$ fraction, indicating an enrichment of soluble potassium in the fine particle fraction.

a)

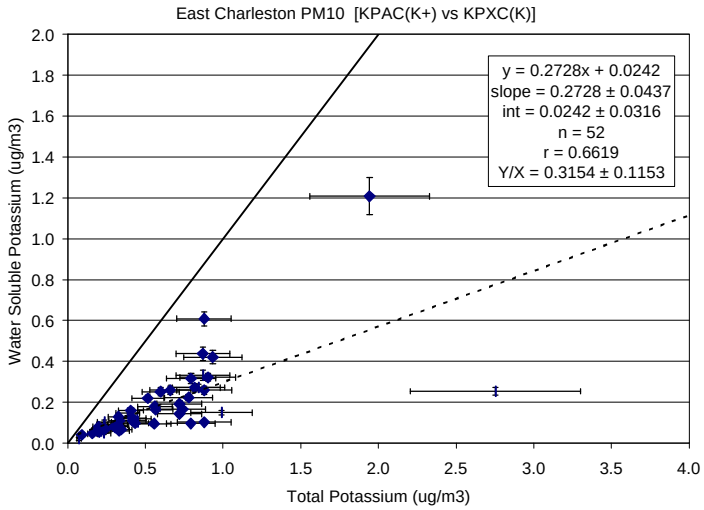


b)

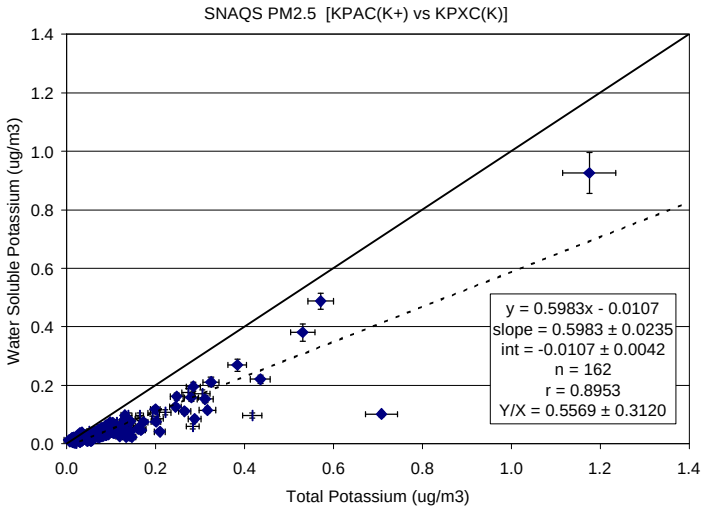


**Figure 3-5.** Scatter plots of soluble potassium versus total potassium measurements from: a) $PM_{10}$ data acquired at the East Charleston site; and b) $PM_{2.5}$ data acquired at the East Charleston, Palo Verde, and Jean sites.

### 3.4.3 Anion and Cation Balance

Ammonium nitrate ($NH_4NO_3$), ammonium sulfate ($[NH_4]_2SO_4$), and ammonium bisulfate ($NH_4HSO_4$), are the most likely nitrate and sulfate compounds to be found in central California. Some sodium nitrate ($NaNO_3$) and sodium sulfate ($Na_2SO_4$) may be attributable to transport by prevailing winds from the Pacific Ocean to the Las Vegas Valley, especially during summer. In the coarse particle fraction, some of the sulfate may also be present as gypsum ($CaSO_4$). Ammonium ($NH_4^+$) can be calculated based on the stoichiometric ratios of the different compounds and compared with that which was measured. In Figure 3-6, ammonium is calculated from nitrate and sulfate, assuming that all nitrate was in the form of ammonium nitrate and all sulfate was in the form of either ammonium sulfate (i.e., calculated ammonium = 0.38 × sulfate + 0.29 × nitrate). These calculated values were compared with the measured values (acquired from quartz filter samples by automated colorimetry) for ammonium. Figure 3-6 shows a higher correlation (r=0.84) was found between calculated and measured ammonium when ammonium bisulfate rather than ammonium sulfate was assumed. Study measurements indicate there was abundant ammonia in the atmosphere to neutralize nitrate and sulfate, so the higher correlation implies that other cations were associated with ammonium.

a)

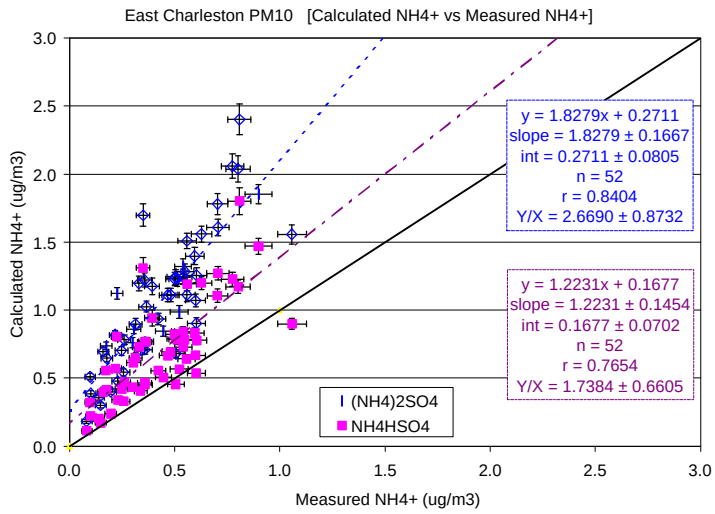


b)

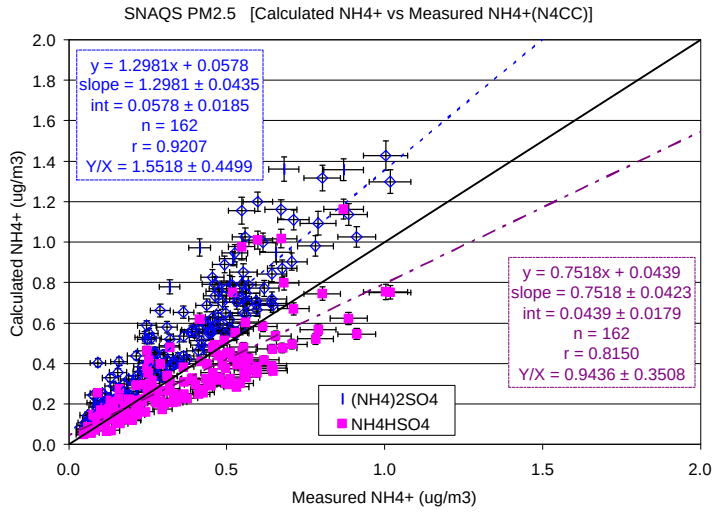


**Figure 3-6.** Scatter plots of calculated ammonium versus measured ammonium from: a) $PM_{10}$ data acquired at the East Charleston site; and b) $PM_{2.5}$ data acquired at the East Charleston, Palo Verde, and Jean sites.

When all sulfate and nitrate are assumed to be fully neutralized, calculated ammonium exceeds measured ammonium. This phenomenon is more pronounced in the $PM_{10}$ fraction than in the $PM_{2.5}$ fraction, indicating the presence of coarse-particle sulfate and/or nitrate salts that might be associated with water-soluble $Ca^{++}$ or

a)

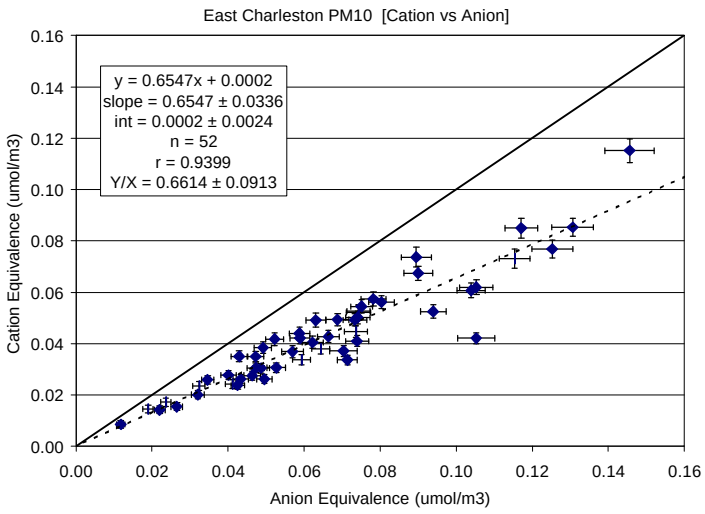


b)

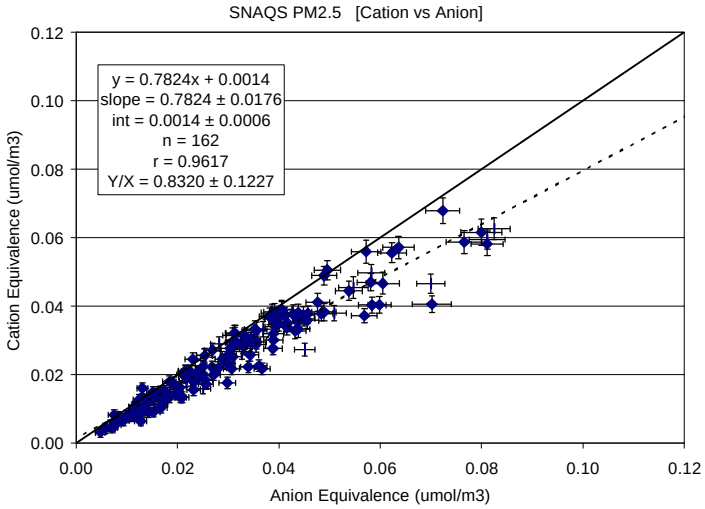


**Figure 3-7.** Scatter plots of cation versus anion measurements from: a) $PM_{10}$ data acquired at the East Charleston site; and b) $PM_{2.5}$ data acquired at the East Charleston, Palo Verde, and Jean sites.

$Na^+$ ions. The chromatograms from ion chromatography analysis for nitrate and sulfate and graphs from automated colorimetry analysis for ammonium were examined, but no anomalies were found. The anion and cation balance in Figure 3-7 also shows a deficiency in cations that is not accounted for by measured anions. The correlations are high ($r>0.94$) for both $PM_{2.5}$ and $PM_{10}$ size fractions. Figure 3-7a shows that unaccounted $PM_{10}$ cations could be as high as 35%, which is consistent with comparisons between calculated and measured ammonium, and which confirms the presence of coarse-particle sulfate and/or nitrate salts that are not in the form of ammonium sulfate and/or ammonium nitrate.

### 3.4.4 Nitrate Volatilization

The quartz-fiber/sodium-chloride-impregnated cellulose-fiber filter pack (shown in Figure 2-3), preceded by anodized aluminum nitric acid denuders, measures $PM_{2.5}$ nitrate (i.e., nonvolatilized nitrate) from the front quartz-fiber filter and captures the volatilized particulate nitrate dissociated from the front quartz-fiber filter with a backup sodium-chloride-impregnated cellulose-fiber filter. Equivalent sampling configurations were used for $PM_{10}$ nitrate. The sum of these two nitrate measurements in this filter pack gives total PM particulate nitrate. The nitric-acid-denuded total PM particulate nitrate should be greater than or equal to the PM nonvolatilized nitrate, depending on the extent of nitrate volatilization.

Figure 3-8a displays scatter plots of $PM_{10}$ nonvolatilized particulate nitrate versus nitric-acid-denuded total $PM_{10}$ particulate nitrate. Secondary ammonium nitrate is not a stable compound (Watson et al., 1994c). Its equilibrium with gaseous ammonia and nitric acid is strongly influenced by temperature and relative humidity. The dissociation of particulate nitrate from the front quartz-fiber filter is expected to be more prevalent when temperatures are higher. Figure 3-8a yields a slope of 0.80±0.02 for $PM_{10}$ measurements with negligible intercept and high correlation (r>0.98). On average, approximately 20% of the $PM_{10}$ particulate nitrate from the front quartz-fiber filters volatilized during the study period. The $PM_{2.5}$ nitrate comparison is more scattered (r=0.93) with ~2% higher volatilization found.

a)

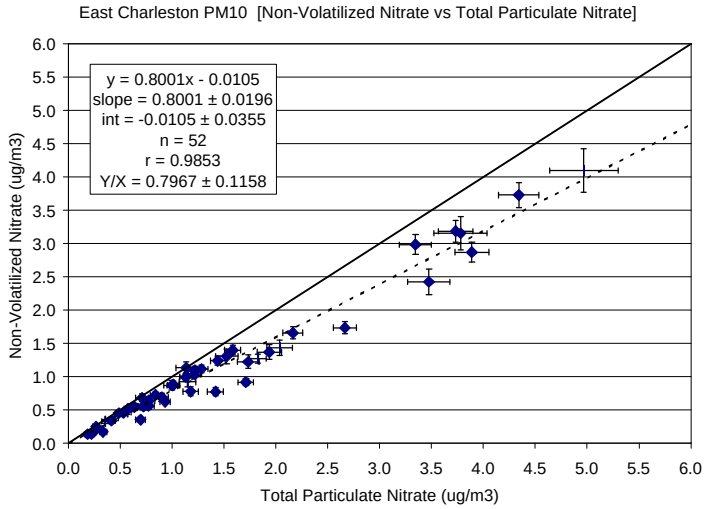


b)

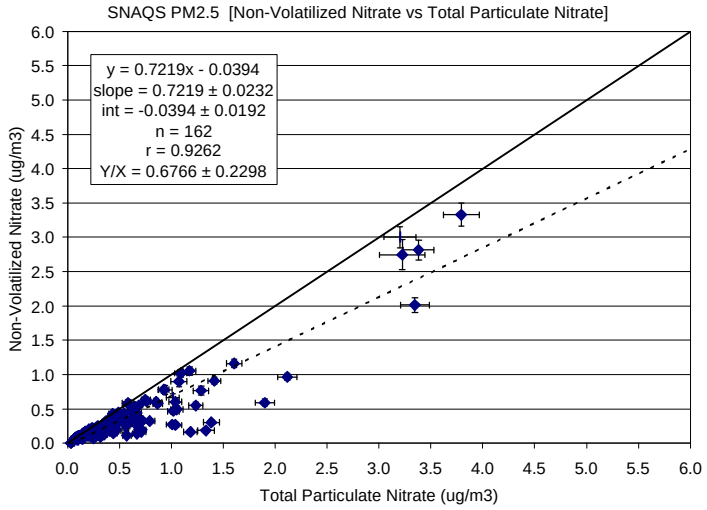


**Figure 3-8.** Scatter plots of nonvolatilized nitrate versus total particulate nitrate measurements from: a) $PM_{10}$ data acquired at the East Charleston site; and b) $PM_{2.5}$ data acquired at the East Charleston, Palo Verde, and Jean sites.

Nitric acid deposits on just about any type of surface (except for PFA Teflon) at a rate which is 10 times faster than particle deposition. In an ammonia-rich environment, much of the nitrate may be in the particle phase, similar to the situation in Rubidoux, CA (Chow et al., 1992). Any positive artifact resulting from nitric acid absorption is expected to be insignificant.

These comparisons demonstrate that nitrate volatilization was significant (in the range of 20% to 25%) during the study. Nitrate volatilization was found in several other studies (e.g., Chow et al., 1996; Hering and Cass, 1999; Chow et al., 2002). Volatilized nitrate was not part of the measured $PM_{10}$ or $PM_{2.5}$ mass, so this loss does not show up in the sum of species comparison shown in Figure 3-2 and represents an underestimation of actual PM mass present in the atmosphere.

### 3.4.5 Reconstructed versus Measured Mass

Major PM components can be used to reconstruct PM mass. The major components include: 1) geological material (estimated as 1.89×Al + 2.14×Si + 1.4×Ca + 1.43×Fe to account for unmeasured oxides), 2) organic matter (1.4×organic carbon to account for unmeasured hydrogen and oxygen), 3) soot (elemental carbon), 4) sulfate, 5) nitrate, 6) ammonium, 7) noncrustal trace elements (sum of other-than-geological elements listed in Section 2.2 excluding Al, Si, Ca, Fe, Cl, and S), and 8) unidentified mass (difference between measured mass and the sum of the major components).

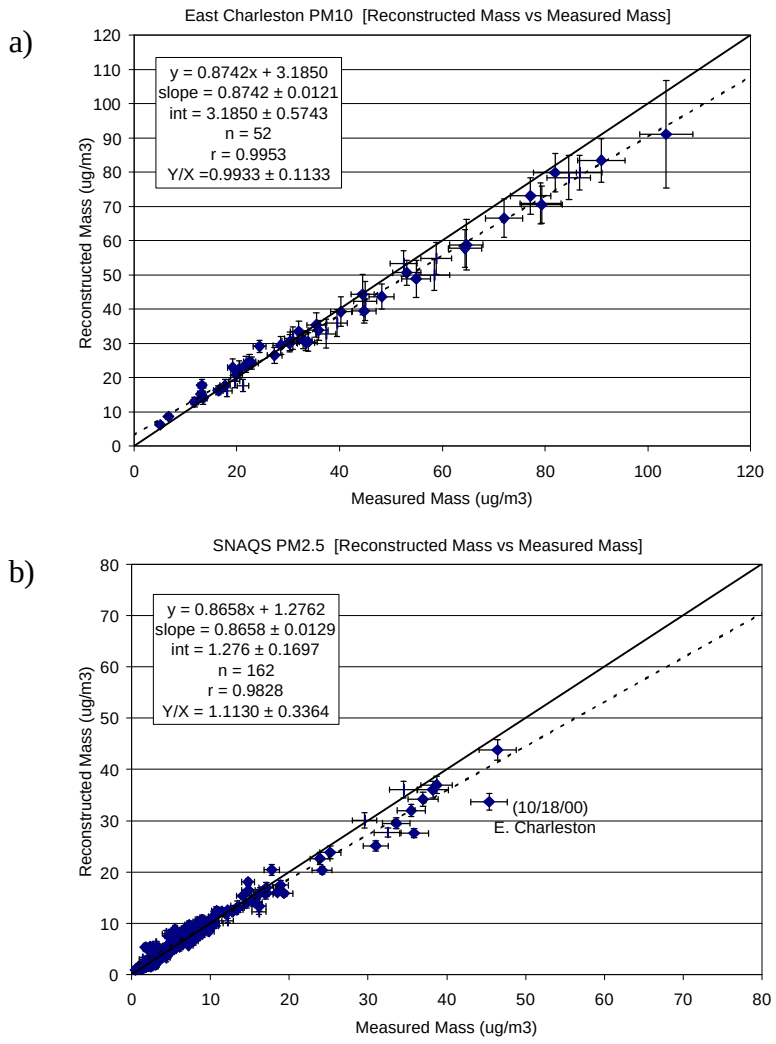


**Figure 3-9.** Scatter plots of reconstructed mass versus measured mass from: a) $PM_{10}$ data acquired at the East Charleston site; and b) $PM_{2.5}$ data acquired at the East Charleston, Palo Verde, and Jean sites.

Figure 3-9 shows that high correlations ($r>0.98$) were found between reconstructed and measured mass. Most of the reconstructed $PM_{10}$ mass was within ±10% of measured mass. Figure 3-9b shows good agreement between $PM_{2.5}$ reconstructed and measured mass, with the exception of $PM_{2.5}$ samples obtained on 05/25/01 at the Jean site.

In contrast to the sum-of-species-versus-mass comparison in Figure 3-2, unaccounted mass in Figure 3-9 was largely eliminated when unmeasured oxygen and hydrogen were factored in. These comparisons confirm the validity of gravimetric and chemical measurements.

### 3.4.6 Collocated Comparison for Gaseous Ammonia

Ammonia ($NH_3$) was acquired by placing a citric-acid-impregnated cellulose-fiber filter behind the Teflon-membrane filter in each $PM_{2.5}$ and $PM_{10}$ SGS (see Figure 2-3). At the East Charleston site, ammonia was acquired in both the $PM_{2.5}$ and $PM_{10}$ channels as part

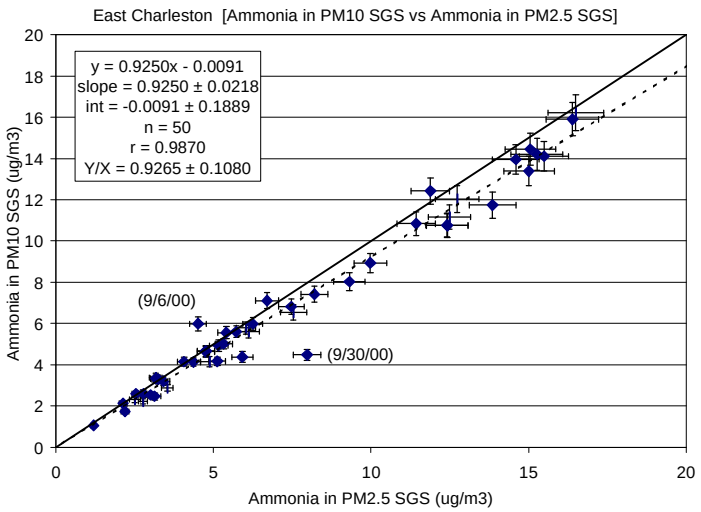


**Figure 3-10.** Scatter plot of $PM_{10}$ ammonia versus $PM_{2.5}$ ammonia measurements from the East Charleston site.

of the quality assurance checks so that coarse-particle chemistry could be derived at the East Charleston site based on the difference between $PM_{10}$ and $PM_{2.5}$ measurements.

As shown in Figure 3-10, high correlations (r=0.99) were found between the two sampling systems with two exceptions on 09/06/00 and 09/30/00. These samples were reanalyzed.

## 3.5 Data Comparability

### 3.5.1 SGS vs. FRM $PM_{2.5}$ Mass

At the East Charleston and Palo Verde sites, the CCDAQM operated Thermo Andersen Federal Reference Method $PM_{2.5}$ samplers. Comparisons between $PM_{2.5}$ mass concentrations measured on these filters and mass concentrations from the DRI SGS are shown in this section. The comparison between measurements made at the East Charleston site is shown in Figure 3-11. The correlation is surprisingly poor, with a correlation coefficient of only 0.65. The average concentration from the SGS sampler is 48% greater than the average concentration from the FRM. The reason for these differences is unknown, but we can speculate they are partially due to differences in removing particles larger than $PM_{2.5}$ from the air stream. The SGS uses a cyclone to remove particles greater than 2.5 microns in diameter. The cut-point is not sharp for cyclones and would allow for some particles larger than 2.5 microns to pass through and be collected on the filter. In a very dusty area such as Las Vegas, there may be significant PM mass near the size of cut-point, especially on the larger side of the cut-point. In contrast, the FRM sampler

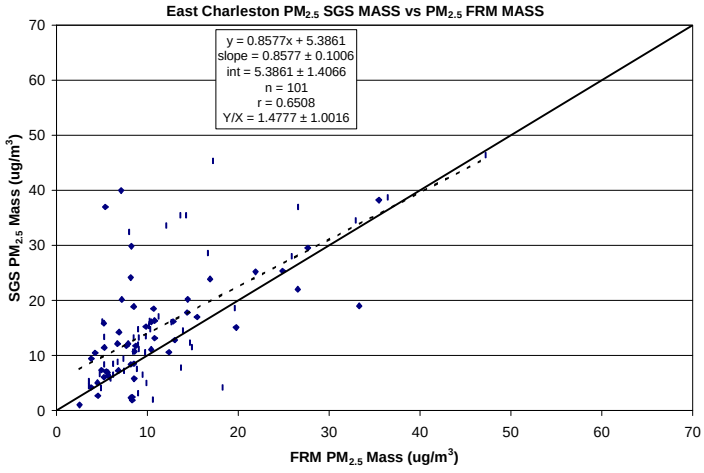


**Figure 3-11.** Comparison between SGS $PM_{2.5}$ mass and FRM $PM_{2.5}$ mass at the East Charleston site for all days.

includes a size-selective inlet for $PM_{10}$, followed by an impactor for $PM_{2.5}$. Impactors have much sharper cut-points than cyclones and would result in less crustal mass being sampled. An issue regarding the FRM's has been raised (Vanderpool et al., 2001) that demonstrated that material could build up on the impactors and potentially lower the cut-point. The regulations require frequent cleaning of the impactors, but it is conceivable that in an area as dusty as Las Vegas, frequent cleaning alone may not fully prevent potential buildup effect. This should be investigated further for the Las Vegas area.

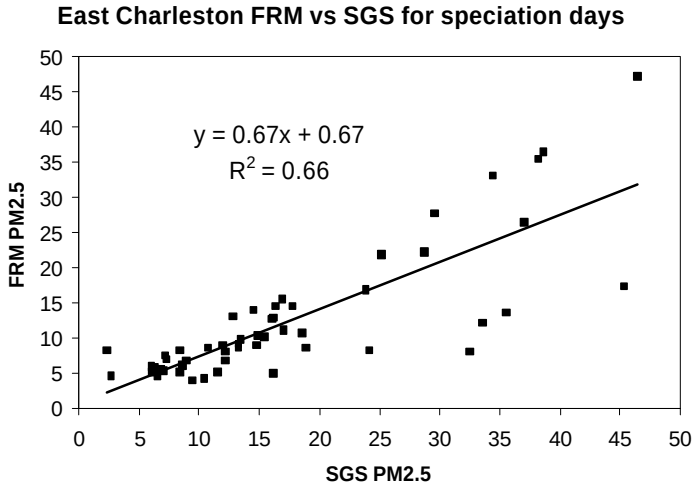


**Figure 3-12.** Comparison between SGS $PM_{2.5}$ mass concentration and FRM $PM_{2.5}$ mass concentration at the East Charleston site for days with chemical speciation.

The comparison for days for which chemical speciation of the SGS samples was performed is shown in Figure 3-12. The relationship is better for these days than for the entire study year. For these days, calculated $PM_{2.5}$ soil was subtracted from SGS mass and the resultant concentration compared to the FRM mass. These are compared in Figure 3-13. The correlation improves between the two samplers, and the slope of the regression line is near one, indicating little bias. This seems to suggest that although the SGS sampler is probably measuring too much fine soil, the FRM sampler is capturing virtually no fine soil. This could occur if the cut-point is biased low for the FRM sample as suggested above.

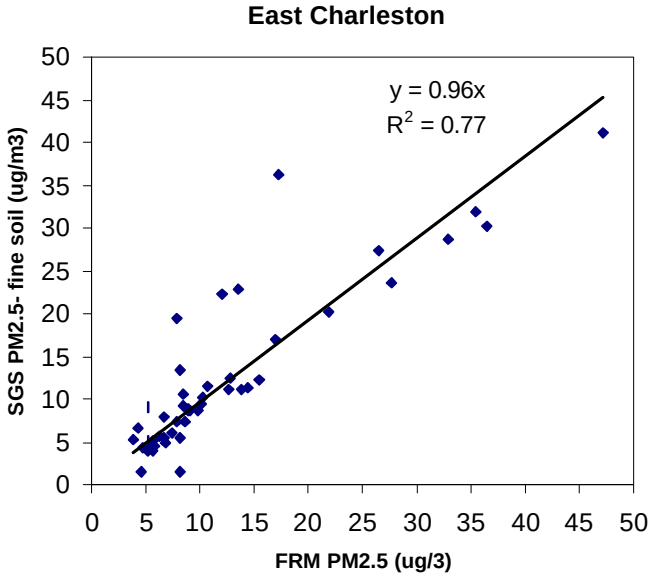


**Figure 3-13.** Comparison of SGS $PM_{2.5}$ mass minus calculated fine soil and FRM $PM_{2.5}$ mass at East Charleston.

The comparison between the SGS and FRM $PM_{2.5}$ concentrations at Jean are shown in Figure 3-14. The correlation is poor, although the average ratio is near one. The concentrations are low, with maximum $PM_{2.5}$ of less than 12 $\mu g/m^3$ for both samplers.

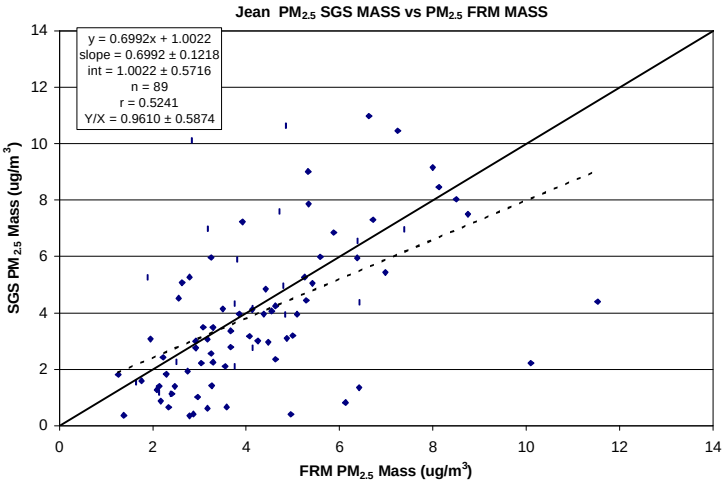


**Figure 3-14.** Comparison between SGS $PM_{2.5}$ mass concentration and FRM $PM_{2.5}$ mass concentration at the Jean site for all days.

### 3.5.2 SGS vs. BAM $PM_{10}$

At the East Charleston site, the CCDAQM monitors $PM_{10}$ with a beta attenuation monitor. Concentrations from this monitor can be compared to the SGS $PM_{10}$ concentration. It should be noted that the CCDAQM beta attenuation monitor is located immediately adjacent to East Charleston road, while the SGS $PM_{10}$ sampler is located about 50 m north of the road. Thus, the CCDAQM site is likely to be more impacted by dust and vehicle exhaust from East Charleston. The concentrations for all SGS sample days are compared in Figure 3-15. The correlation is 0.82 and the average SGS concentration is 92% of the average BAM concentration. The comparison for chemical analysis days is shown in Figure 3-16. The overall relationship is very good with a correlation coefficient of 0.88.

### 3.5.3 Nephelometer Intercomparison

There were three nephelometers at the East Charleston site during the last few months of the study (mainly April-July 2001). This included the Optec NGN-2 nephelometer (also present at Jean and Palo Verde), a Radiance Research M903 nephelometer, and an additional Radiance Research M903 nephelometer with a $PM_{2.5}$ size-cut cyclone. The $PM_{2.5}$ size-cut nephelometer was used to help determine fine and coarse particle

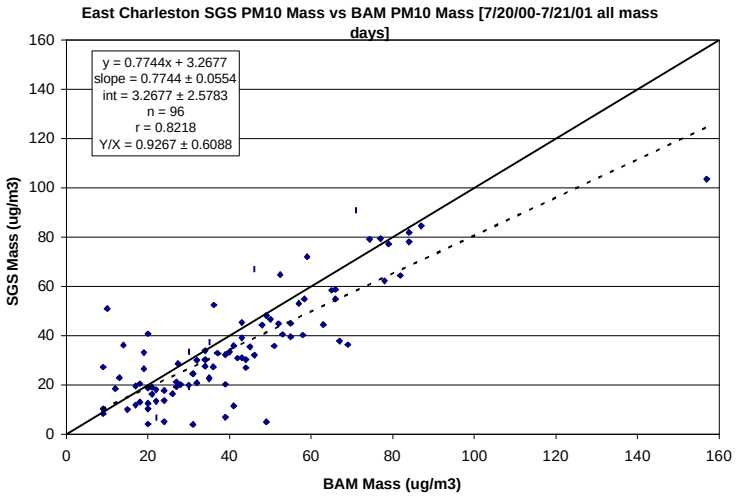


**Figure 3-15.** SGS $PM_{10}$ mass concentration versus BAM $PM_{10}$ mass concentration at East Charleston for all SGS sample days.

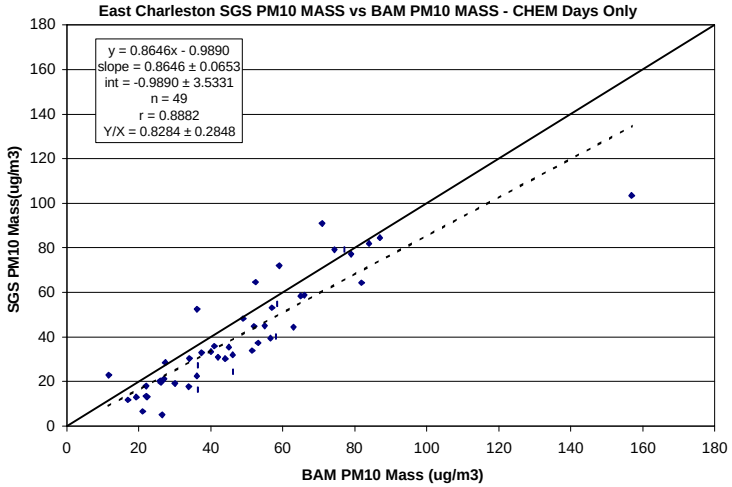


**Figure 3-16.** SGS $PM_{10}$ mass concentration versus BAM $PM_{10}$ mass concentration at East Charleston for SGS sample days with chemical speciation.

scattering. This is important because we expect most of the fine particle scattering to be caused by combustion products and most of the coarse particle scattering to be caused by crustal components. Thus, it has implications regarding the importance of different source types to haze.

While the Optec NGN-2 has a completely open-air design (the door is open throughout operation), the Radiance nephelometers were mounted inside small wooden boxes, with inlets on the bottom. This somewhat more circuitous route would inhibit very large particles from entering the nephelometer chamber where light scattering measurements are made. The Radiance nephelometers were also fitted with heaters that dry the air when the humidity is greater than 70%, a condition that did not occur with much frequency during the study. Perhaps more importantly, the integration angle of the Radiance nephelometers was 10-165 degrees, compared to 5-175 degrees for the Optec nephelometers. The effect of the smaller integration angle of the Radiance nephelometers is to miss more of the coarse particle scattering (e.g., by dust) than the Optec's do (Molenar, 1997). This effect (called "truncation error") would have much less effect upon the Radiance nephelometer with the $PM_{2.5}$ size-cut.

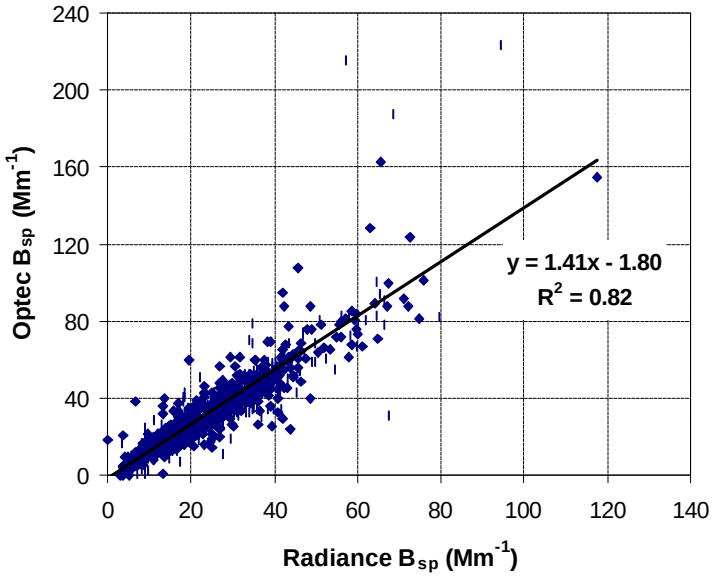


**Figure 3-17.** Comparison of Optec and Radiance no-cut nephelometers at East Charleston.

A scatterplot of hourly averaged particle light scattering ($B_{sp}$) for the Optec and Radiance no-cut nephelometers is shown in Figure 3-17. There is good correlation between the nephelometers ($r^2$=0.82). However, the Optec nephelometer's $B_{sp}$ is generally considerably higher. The slope of the regression line is 1.41, implying the Optec nephelometer is measuring about 40% more scattering. An analysis of the hourly ratios of the Optec to Radiance

nephelometers shows a median ratio of 1.26. Over all hours with data for both instruments, the average Optec $B_{sp}$ was 1.32 times the average Radiance $B_{sp}$. As the RH was nearly always less than required for Radiance nephelometer's heater to come on, we can conclude from the difference between the Optec and Radiance nephelometers that the Radiance nephelometer is missing a large fraction of coarse-particle scattering. This can be confirmed by considering the periods when the ratio of Optec to Radiance nephelometer readings are highest. These periods corresponded to high winds and large values of $PM_{10}$ concentration.

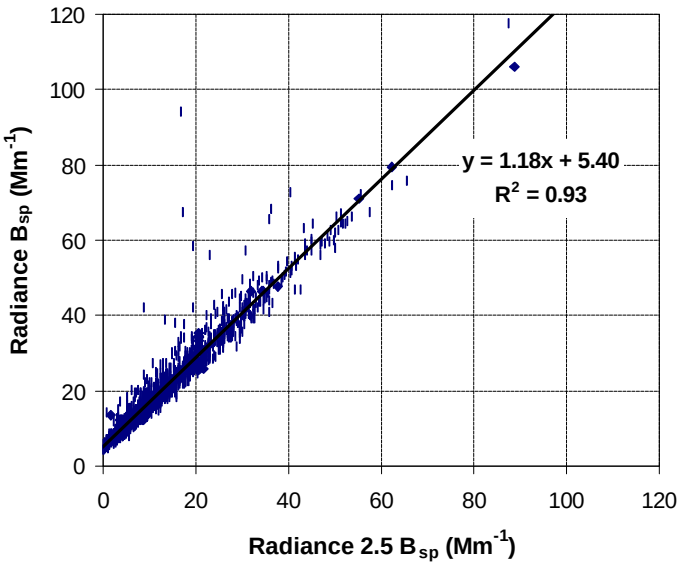


**Figure 3-18.** Comparison of Radiance Research M903 nephelometers with and without $PM_{2.5}$ size-cut cyclones.

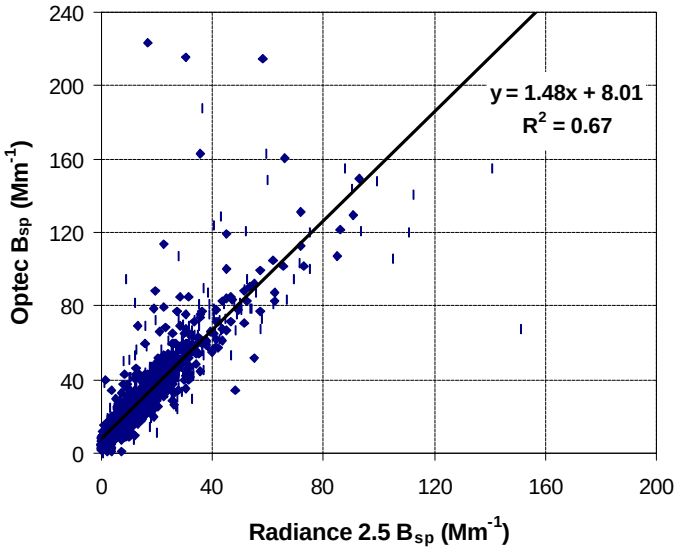


**Figure 3-19.** Comparison of Optec NGN-2 and $PM_{2.5}$ size-cut Radiance M903 nephelometers at East Charleston.

The two Radiance nephelometers (one with $PM_{2.5}$ size-cut) are compared in Figure 3-18. The correlation among the Radiance nephelometers is very high ($r^2$=0.93). The slope is 1.18, but the intercept is not insignificant at 5 $Mm^{-1}$. Either there is a calibration problem with one of the nephelometers or there are periods with almost no fine-particle scattering, but still scattering from coarse particles. Examination of weather maps for periods with near-zero scattering by the $PM_{2.5}$ size-cut nephelometer showed that these cases were associated with flow from the northwest after passage of a cold-front (04/12/01, 05/03/01, and 06/14/01). These meteorological conditions are usually very clean, associated with airflow from the "Clean Air Corridor" (Green and Gebhart, 1997). The hours with the no-cut $B_{sp}$ values significantly above the regression line were periods of high BAM $PM_{10}$.

The Optec nephelometer and the Radiance $PM_{2.5}$ size-cut nephelometers are compared in Figure 3-19. The slope of the regression line is 1.48. There is a substantial intercept of 8 $Mm^{-1}$. The correlation coefficient between Optec total scattering and Radiance $PM_{2.5}$ scattering is not particularly high; this is reasonable because

periods with high Optec scattering and low Radiance $PM_{2.5}$ scattering correspond to windy periods when we would expect a greater fraction of the scattering to be by coarse, wind-raised particles. The median value of the ratio of Optec total to Radiance $PM_{2.5}$ nephelometer is 2.03. If the Optec is a good representation of total scattering (we know it underestimates coarse-particle scattering), and the Radiance $PM_{2.5}$ nephelometer represents fine-particle scattering, then these results suggest about one-third to one-half of the scattering is due to coarse particles, mainly crustal material. Since even the Optec nephelometer misses some of the coarse-particle scattering, this suggests a major contribution of crustal material to the light scattering budget. This is true not only for windy periods, but nearly all hours with data. Component contributions to the light scattering and extinction budget are addressed in detail in Section 6.

### 3.5.4 Optical Particle Counter Area vs. Nephelometer Scattering

The Climet Optical Particle Counter (OPC) uses light scattering information to estimate the size of each individual particle sampled. The validity of the OPC and nephelometer measurements can be examined by comparison of data from the OPC and nepehlometers. Except for near the wavelength of light, where scattering is enhanced, the scattering of a particle is proportional to its cross-sectional area. The cross-sectional area of the particles measured by the OPC can be estimated by assuming spherical particles and multiplying the number of particles in each of the 16 size bins by the mass median particle radius squared times π. This area can then be plotted against nephelometer-derived light scattering. The results from using hourly averaged data for the month of December 2000 are shown in Figure 3-20. While the relationship is quite good ($r^2$=0.9), there are some outliers with very high OPC area, but moderate $b_{scat}$ values. Inspection of the data showed these hours to be periods with high winds and very high values of $PM_{10}$ measured from the CCDAQM beta attenuation monitor at East Charleston. As discussed in Section 3.5.3, the Optec nephelometer misses a portion of the coarse-particle scattering (and the Radiance nephelometer misses even more). It appears that the OPC is able to detect the large particles, but the Optec nephelometer only detects some of the scattering from these particles. The correlation between cross-sectional area and Optec NGN-2 $b_{scat}$ was found to be greatest when the area of particles up to 4 µm was used. This relationship is shown in Figure 3-21. The relationship is excellent, with an $r^2$ of 0.97. These results confirm

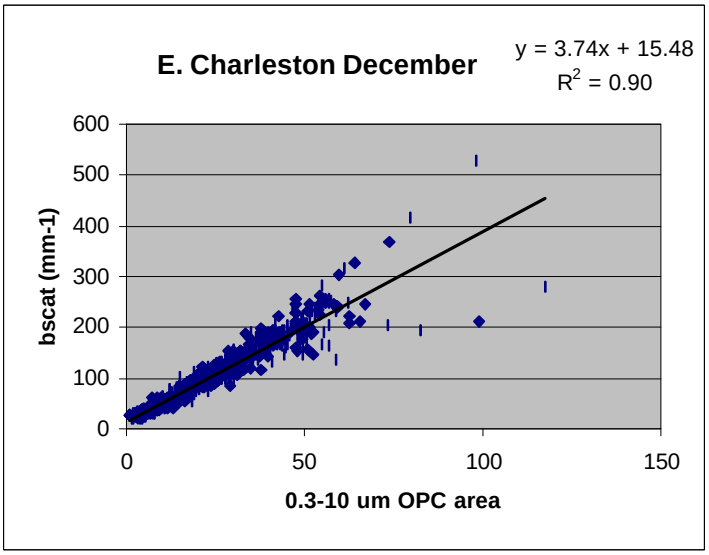


**Figure 3-20.** Optical particle counter derived cross-sectional area versus Optec NGN-2 nephelometer light scattering at East Charleston. The OPC area is for all particle with optical diameter mess than 10 µm. The Nephelometer $b_{scat}$ includes Rayleigh scattering of 10.98 $Mm^{-1}$.

the basic validity of the nephelometer and OPC measurements and demonstrate that the Optec nephelometer misses a portion of the coarse-particle scattering, which is expected by theory.

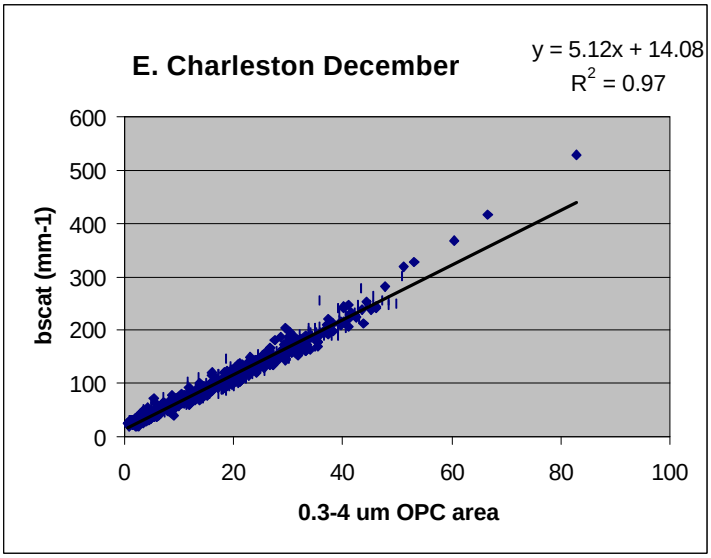


**Figure 3-21.** OPC area for particles less than 4 µm optical diameter versus Optec NGN-2 nephelometer scattering for December 2000 at East Charleston.

# 4. MASS AND CHEMICAL SPECIATION OF PARTICULATE FILTER SAMPLES

A total of 105 sets of 24-hour-average $PM_{2.5}$ and $PM_{10}$ samples were acquired over the yearlong sampling period between 07/20/00 and 07/21/01 on an every-third-day sampling schedule. Mass concentrations along with meteorological and optical data were examined, and approximately 50% of the samples were selected for detailed chemical speciation. The prerequisites for sample selection were that valid corresponding samples were obtained from all three sites and in both $PM_{2.5}$ and $PM_{10}$ size fractions at the East Charleston site.

## 4.1 Statistical Summary of $PM_{2.5}$ and $PM_{10}$ Chemical Concentrations

Tables 4-1 and 4-2 summarize maximum, minimum, and average 24-hour concentrations of $PM_{2.5}$ and $PM_{10}$ and their chemical constituents at each site. $PM_{2.5}$ and $PM_{10}$ mass concentrations for the entire data set are also listed for comparison. During the study period, the highest 24-hour $PM_{10}$ concentration at the East Charleston site was 103.5±5.2 μg/m$^3$ observed on 08/13/00. This is ~50% below the 24-hour $PM_{10}$ National Ambient Air Quality Standard (NAAQS) of 150 μg/m$^3$. The highest 24-hour $PM_{2.5}$ concentrations were 46.4±2.4 μg/m$^3$ on 01/01/01 at the East Charleston site, 19.4 ±1.1 μg/m$^3$ on 04/01/01 at the Palo Verde site, and 11.0±0.7 μg/m$^3$ on 05/10/01 at the Jean site. These levels are well below the 24-hour $PM_{2.5}$ NAAQS of 65 μg/m$^3$.

At the East Charleston site, the annual-average $PM_{10}$ concentration of 34.9±22.2 μg/m$^3$ was well below the annual $PM_{10}$ NAAQS of 50 μg/m$^3$, but the annual-average $PM_{2.5}$ concentration of 15.7±10.8 μg/m$^3$ (15.6 ±4.0 μg/m$^3$ if averaged by calendar quarter) was higher than the annual $PM_{2.5}$ NAAQS of 15 μg/m$^3$. The $PM_{2.5}$ compliance monitoring network requires three years of monitoring to determine compliance with annual standards.

Tables 4-1 and 4-2 show that the mass concentrations from the subset of samples selected for chemical speciation were ~15% higher, ~17% higher, and ~5% higher, respectively, than the annual averages of all samples at the East Charleston, Palo Verde, and Jean sites. Averages of chemical components in the selected subset of samples would be positively biased by ~5% to ~17% if compared to averages for the entire sample set. The most abundant (>0.5 μg/m$^3$) chemical components found were organic carbon (OC), elemental carbon (EC), nitrate ($NO_3^-$), sulfate ($SO_4^=$), ammonium ($NH_4^+$), in both $PM_{2.5}$ and $PM_{10}$ size fractions, and also geological elements (Al, Si, K, Ca, and Fe) in the $PM_{10}$ size fraction.

At the East Charleston site, the OC/TC ratios were 0.68 in $PM_{2.5}$ and 0.74 in $PM_{10}$, which are similar to OC/TC ratios in vehicle exhaust profiles (e.g., Watson et al., 1994a, 1994b, 2001b; Watson and Chow, 2001a) but lower than ratios found for woodburning (0.81 to 0.93) and meat cooking (0.95 to 0.97) (McDonald et al., 2000; Watson and Chow, 2001b; Watson et al., 2001b).

**Table 4-1.** Statistical summary of $PM_{10}$ mass and chemistry acquired at the East Charleston site.

| | East Charleston PM10 | | | | | | |
|---|---|---|---|---|---|---|---|
| | Average | ± | Std Dev | Nbr in Avg | Minimum | Maximum | Date of Maximum |
| Mass (all days) | | ± | | | | | |
| Mass (chem analysis days) | 40.7681 | ± | 24.7988 | 52 | 5.0818 | 103.5354 | 08/13/00 |
| Volatilized Nitrate (NO3-) | 0.2910 | ± | 0.2813 | 52 | 0.0000 | 1.0500 | 02/03/01 |
| Chloride (Cl-) | 0.2575 | ± | 0.1849 | 52 | 0.0395 | 0.9987 | 01/01/01 |
| Nonvolatilized Nitrate (NO3 | 1.1122 | ± | 0.9389 | 52 | 0.1367 | 4.0983 | 04/04/01 |
| Sulfate (SO4=) | 1.9343 | ± | 0.8917 | 52 | 0.3777 | 4.6047 | 09/15/00 |
| Ammonium (NH4+) | 0.4302 | ± | 0.2214 | 52 | 0.0819 | 1.0577 | 05/10/01 |
| Soluble Sodium (Na+) | 0.3352 | ± | 0.2175 | 52 | 0.0791 | 1.5461 | 04/04/01 |
| Soluble Potassium (K+) | 0.1794 | ± | 0.1866 | 52 | 0.0223 | 1.2076 | 01/01/01 |
| Organic Carbon (OC) | 8.0663 | ± | 5.7812 | 52 | 1.5107 | 24.4386 | 01/01/01 |
| Elemental Carbon (EC) | 2.8365 | ± | 2.2456 | 52 | 0.4996 | 9.7659 | 01/01/01 |
| Total Carbon (TC) | 10.8949 | ± | 7.9457 | 52 | 2.0058 | 34.1937 | 01/01/01 |
| Sodium (Na) | 0.0945 | ± | 0.2047 | 52 | 0.0000 | 1.2748 | 04/04/01 |
| Magnesium (Mg) | 0.4217 | ± | 0.2771 | 52 | 0.0317 | 1.0731 | 12/20/00 |
| Aluminum (Al) | 1.0807 | ± | 1.0812 | 52 | 0.1714 | 7.8537 | 08/13/00 |
| Silicon (Si) | 4.6423 | ± | 3.3428 | 52 | 0.6789 | 22.2477 | 08/13/00 |
| Phosphorus (P) | 0.0059 | ± | 0.0124 | 52 | 0.0000 | 0.0581 | 08/13/00 |
| Sulfur (S) | 0.6238 | ± | 0.2556 | 52 | 0.1125 | 1.4127 | 09/15/00 |
| Chlorine (Cl) | 0.2262 | ± | 0.1751 | 52 | 0.0113 | 0.9625 | 01/01/01 |
| Patassium (K) | 0.5686 | ± | 0.4527 | 52 | 0.0715 | 2.7534 | 08/13/00 |
| Calcium (Ca) | 4.6799 | ± | 3.0151 | 52 | 0.5755 | 12.1393 | 12/20/00 |
| Titanium (Ti) | 0.0663 | ± | 0.0591 | 52 | 0.0147 | 0.4182 | 08/13/00 |
| Vanadium (V) | 0.0012 | ± | 0.0022 | 52 | 0.0000 | 0.0118 | 08/13/00 |
| Chromium (Cr) | 0.0016 | ± | 0.0016 | 52 | 0.0000 | 0.0071 | 01/04/01 |
| Manganese (Mn) | 0.0194 | ± | 0.0158 | 52 | 0.0029 | 0.1093 | 08/13/00 |
| Iron (Fe) | 1.0837 | ± | 0.7545 | 52 | 0.1627 | 4.4260 | 08/13/00 |
| Cobalt (Co) | 0.0017 | ± | 0.0023 | 52 | 0.0000 | 0.0086 | 01/04/01 |
| Nickel (Ni) | 0.0009 | ± | 0.0007 | 52 | 0.0000 | 0.0031 | 01/04/01 |
| Copper (Cu) | 0.0186 | ± | 0.0136 | 52 | 0.0032 | 0.0624 | 11/20/00 |
| Zinc (Zn) | 0.0366 | ± | 0.0264 | 52 | 0.0040 | 0.1123 | 11/20/00 |
| Gallium (Ga) | 0.0001 | ± | 0.0002 | 52 | 0.0000 | 0.0008 | 08/13/00 |
| Arsenic (As) | 0.0010 | ± | 0.0011 | 52 | 0.0000 | 0.0073 | 01/01/01 |
| Selenium (Se) | 0.0002 | ± | 0.0002 | 52 | 0.0000 | 0.0008 | 07/06/01 |
| Bromine (Br) | 0.0051 | ± | 0.0025 | 52 | 0.0010 | 0.0127 | 02/18/01 |
| Rubidium (Rb) | 0.0019 | ± | 0.0016 | 52 | 0.0004 | 0.0111 | 08/13/00 |
| Strontium (Sr) | 0.0231 | ± | 0.0132 | 52 | 0.0028 | 0.0515 | 12/20/00 |
| Yttrium (Y) | 0.0006 | ± | 0.0006 | 52 | 0.0000 | 0.0035 | 08/13/00 |
| Zirconium (Zr) | 0.0039 | ± | 0.0024 | 52 | 0.0006 | 0.0117 | 08/13/00 |
| Molybdenum (Mo) | 0.0011 | ± | 0.0009 | 52 | 0.0000 | 0.0030 | 12/23/00 |
| Palladium (Pd) | 0.0007 | ± | 0.0011 | 52 | 0.0000 | 0.0039 | 11/26/00 |
| Silver (Ag) | 0.0010 | ± | 0.0015 | 52 | 0.0000 | 0.0063 | 09/12/00 |
| Cadmium (Cd) | 0.0009 | ± | 0.0011 | 52 | 0.0000 | 0.0048 | 08/04/00 |
| Indium (In) | 0.0020 | ± | 0.0015 | 52 | 0.0000 | 0.0055 | 08/04/00 |
| Tin (Sn) | 0.0028 | ± | 0.0031 | 52 | 0.0000 | 0.0130 | 10/06/00 |
| Antimony (Sb) | 0.0048 | ± | 0.0058 | 52 | 0.0000 | 0.0230 | 01/01/01 |
| Barium (Ba) | 0.0708 | ± | 0.0555 | 52 | 0.0000 | 0.2056 | 01/01/01 |
| Lanthanum (La) | 0.0079 | ± | 0.0117 | 52 | 0.0000 | 0.0434 | 08/19/00 |
| Gold (Au) | 0.0001 | ± | 0.0002 | 52 | 0.0000 | 0.0014 | 11/20/00 |
| Mercury (Hg) | 0.0001 | ± | 0.0002 | 52 | 0.0000 | 0.0007 | 01/04/01 |
| Thallium (Tl) | 0.0005 | ± | 0.0004 | 52 | 0.0000 | 0.0016 | 11/26/00 |
| Lead (Pb) | 0.0083 | ± | 0.0098 | 52 | 0.0000 | 0.0622 | 01/01/01 |
| Uranium (U) | 0.0004 | ± | 0.0004 | 52 | 0.0000 | 0.0014 | 10/06/00 |
| Sum of Species | 27.2857 | ± | 15.2421 | 52 | 4.4412 | 60.2658 | 01/01/01 |
| Ammonia (NH3) | 6.9585 | ± | 4.3299 | 52 | 1.0511 | 16.2254 | 01/01/01 |

**Table 4-2.** Statistical summary of $PM_{2.5}$ mass and chemistry acquired at the East Charleston, Palo Verde, and Jean sites.

| | East Charleston PM2.5 | | | | | Palo Verde PM2.5 | | | | | Jean PM2.5 | | | | |
|---|---|---|---|---|---|---|---|---|---|---|---|---|---|---|---|
| | Average ± Std Dev | Nbr in Avg | Minimum | Maximum | Date of Maximum | Average ± Std Dev | Nbr in Avg | Minimum | Maximum | Date of Maximum | Average ± Std Dev | Nbr in Avg | Minimum | Maximum | Date of Maximum |
| Mass (all days) | 15.6782 ± 10.7915 | 102 | 1.0560 | 46.4271 | 01/01/01 | 5.5340 ± 3.8229 | 94 | 0.8364 | 19.3770 | 04/01/01 | 3.8776 ± 2.6028 | 102 | 0.3489 | 10.9737 | 05/10/01 |
| Mass (chem analysis days) | 17.8787 ± 11.4980 | 53 | 2.3293 | 46.4271 | 01/01/01 | 6.3014 ± 4.0368 | 54 | 1.5649 | 19.3770 | 04/01/01 | 4.2160 ± 2.6102 | 55 | 0.5168 | 10.9737 | 05/10/01 |
| Volatilized Nitrate (NO3-) | 0.2340 ± 0.2580 | 53 | 0.0212 | 1.3358 | 11/20/00 | 0.2183 ± 0.2955 | 54 | 0.0000 | 1.3091 | 02/03/01 | 0.1155 ± 0.1937 | 55 | 0.0000 | 1.0817 | 11/26/00 |
| Chloride (Cl-) | 0.1037 ± 0.0938 | 53 | 0.0162 | 0.5690 | 01/01/01 | 0.0313 ± 0.0195 | 54 | 0.0000 | 0.1175 | 06/15/01 | 0.0255 ± 0.0249 | 55 | 0.0000 | 0.1436 | 08/13/01 |
| Nonvolatilized Nitrate (NO3-) | 0.6347 ± 0.7457 | 53 | 0.0863 | 3.3286 | 12/23/00 | 0.2756 ± 0.2250 | 54 | 0.0000 | 1.0530 | 12/23/00 | 0.1419 ± 0.1088 | 55 | 0.0000 | 0.5835 | 01/25/01 |
| Sulfate (SO4=) | 1.3308 ± 0.6858 | 53 | 0.3020 | 3.0427 | 09/15/00 | 1.1051 ± 0.7319 | 54 | 0.2393 | 3.5769 | 09/15/00 | 0.9837 ± 0.6198 | 55 | 0.1539 | 2.8000 | 09/15/00 |
| Ammonium (NH4+) | 0.3999 ± 0.2160 | 53 | 0.0596 | 0.8856 | 05/10/01 | 0.3615 ± 0.2242 | 54 | 0.0676 | 1.0176 | 05/10/01 | 0.3384 ± 0.2048 | 55 | 0.0472 | 0.9117 | 05/10/01 |
| Soluble Sodium (Na+) | 0.1350 ± 0.0680 | 53 | 0.0406 | 0.3703 | 06/15/01 | 0.0714 ± 0.0497 | 54 | 0.0136 | 0.2407 | 04/04/01 | 0.0565 ± 0.0428 | 55 | 0.0080 | 0.2446 | 04/04/01 |
| Soluble Potassium (K+) | 0.1126 ± 0.1449 | 53 | 0.0172 | 0.9264 | 01/01/01 | 0.0319 ± 0.0240 | 54 | 0.0027 | 0.1184 | 06/15/01 | 0.0262 ± 0.0183 | 55 | 0.0031 | 0.1058 | 06/15/01 |
| Organic Carbon (OC) | 5.0772 ± 3.8144 | 53 | 1.4022 | 18.2829 | 01/01/01 | 1.4462 ± 0.9276 | 54 | 0.0000 | 3.4892 | 08/04/00 | 0.9317 ± 0.8512 | 55 | 0.0000 | 3.5014 | 05/13/01 |
| Elemental Carbon (EC) | 2.3749 ± 2.0355 | 53 | 0.3209 | 8.4667 | 01/01/01 | 0.8555 ± 0.4834 | 54 | 0.1329 | 2.0038 | 03/20/01 | 0.4072 ± 0.2054 | 55 | 0.1275 | 0.9042 | 07/26/00 |
| Total Carbon (TC) | 7.4439 ± 5.7457 | 53 | 2.1872 | 26.7420 | 01/01/01 | 2.2911 ± 1.2555 | 54 | 0.0000 | 5.0642 | 06/15/01 | 1.3030 ± 1.0360 | 55 | 0.0000 | 3.9259 | 05/13/01 |
| Sodium (Na) | 0.0401 ± 0.0480 | 53 | 0.0000 | 0.1981 | 04/04/01 | 0.0459 ± 0.0650 | 54 | 0.0000 | 0.3245 | 06/12/01 | 0.0394 ± 0.0657 | 55 | 0.0000 | 0.3794 | 06/12/01 |
| Magnesium (Mg) | 0.1658 ± 0.1087 | 53 | 0.0174 | 0.4950 | 09/15/00 | 0.0542 ± 0.0489 | 54 | 0.0000 | 0.2445 | 08/13/00 | 0.0197 ± 0.0170 | 55 | 0.0000 | 0.0758 | 10/09/00 |
| Aluminum (Al) | 0.1880 ± 0.1756 | 53 | 0.0426 | 1.2489 | 08/13/00 | 0.0937 ± 0.0875 | 54 | 0.0060 | 0.4736 | 04/01/01 | 0.0782 ± 0.0622 | 55 | 0.0009 | 0.2524 | 10/09/00 |
| Silicon (Si) | 0.8624 ± 0.6824 | 53 | 0.1448 | 4.1798 | 08/13/00 | 0.3624 ± 0.3412 | 54 | 0.0629 | 1.8539 | 04/01/01 | 0.2412 ± 0.2097 | 55 | 0.0263 | 0.8572 | 10/09/00 |
| Phosphorus (P) | 0.0022 ± 0.0035 | 53 | 0.0000 | 0.0127 | 11/20/00 | 0.0006 ± 0.0013 | 54 | 0.0000 | 0.0045 | 12/29/00 | 0.0006 ± 0.0013 | 55 | 0.0000 | 0.0071 | 09/12/00 |
| Sulfur (S) | 0.4921 ± 0.2440 | 53 | 0.0958 | 1.3043 | 09/15/00 | 0.3788 ± 0.2393 | 54 | 0.0939 | 1.1423 | 09/15/00 | 0.3755 ± 0.2174 | 55 | 0.0448 | 0.9294 | 09/15/00 |
| Chlorine (Cl) | 0.0459 ± 0.0744 | 53 | 0.0000 | 0.4663 | 01/01/01 | 0.0027 ± 0.0071 | 54 | 0.0000 | 0.0449 | 06/15/01 | 0.0008 ± 0.0025 | 55 | 0.0000 | 0.0151 | 01/01/01 |
| Patassium (K) | 0.2168 ± 0.1953 | 53 | 0.0312 | 1.1757 | 01/01/01 | 0.0679 ± 0.0567 | 54 | 0.0055 | 0.2837 | 04/01/01 | 0.0544 ± 0.0406 | 55 | 0.0077 | 0.1928 | 06/15/01 |
| Calcium (Ca) | 1.2120 ± 0.8194 | 53 | 0.1777 | 3.3029 | 09/15/00 | 0.4939 ± 0.3852 | 54 | 0.0930 | 1.7061 | 06/15/01 | 0.1196 ± 0.0890 | 55 | 0.0081 | 0.4654 | 06/15/01 |
| Titanium (Ti) | 0.0210 ± 0.0202 | 53 | 0.0000 | 0.1318 | 08/13/00 | 0.0067 ± 0.0099 | 54 | 0.0000 | 0.0558 | 04/01/01 | 0.0049 ± 0.0048 | 55 | 0.0000 | 0.0210 | 06/15/01 |
| Vanadium (V) | 0.0010 ± 0.0014 | 53 | 0.0000 | 0.0066 | 08/13/00 | 0.0007 ± 0.0009 | 54 | 0.0000 | 0.0035 | 04/01/01 | 0.0007 ± 0.0008 | 55 | 0.0000 | 0.0025 | 06/15/01 |
| Chromium (Cr) | 0.0005 ± 0.0008 | 53 | 0.0000 | 0.0031 | 04/01/01 | 0.0002 ± 0.0003 | 54 | 0.0000 | 0.0015 | 04/01/01 | 0.0001 ± 0.0002 | 55 | 0.0000 | 0.0007 | 06/15/01 |
| Manganese (Mn) | 0.0075 ± 0.0060 | 53 | 0.0006 | 0.0373 | 08/13/00 | 0.0025 ± 0.0023 | 54 | 0.0000 | 0.0126 | 04/01/01 | 0.0019 ± 0.0014 | 55 | 0.0002 | 0.0064 | 06/15/01 |
| Iron (Fe) | 0.4194 ± 0.2711 | 53 | 0.0730 | 1.4136 | 08/13/00 | 0.1091 ± 0.0955 | 54 | 0.0234 | 0.5560 | 04/01/01 | 0.0746 ± 0.0568 | 55 | 0.0141 | 0.2543 | 09/21/00 |
| Cobalt (Co) | 0.0008 ± 0.0013 | 53 | 0.0000 | 0.0056 | 04/01/01 | 0.0004 ± 0.0006 | 54 | 0.0000 | 0.0038 | 04/01/01 | 0.0002 ± 0.0003 | 55 | 0.0000 | 0.0011 | 04/22/01 |
| Nickel (Ni) | 0.0003 ± 0.0004 | 53 | 0.0000 | 0.0014 | 03/20/01 | 0.0002 ± 0.0002 | 54 | 0.0000 | 0.0005 | 04/01/01 | 0.0002 ± 0.0002 | 55 | 0.0000 | 0.0010 | 12/29/00 |
| Copper (Cu) | 0.0090 ± 0.0063 | 53 | 0.0014 | 0.0273 | 11/20/00 | 0.0017 ± 0.0014 | 54 | 0.0000 | 0.0079 | 07/26/00 | 0.0008 ± 0.0008 | 55 | 0.0000 | 0.0034 | 07/20/00 |
| Zinc (Zn) | 0.0199 ± 0.0142 | 53 | 0.0025 | 0.0552 | 11/20/00 | 0.0049 ± 0.0026 | 54 | 0.0007 | 0.0122 | 07/26/00 | 0.0027 ± 0.0016 | 55 | 0.0004 | 0.0091 | 09/15/00 |
| Gallium (Ga) | 0.0001 ± 0.0002 | 53 | 0.0000 | 0.0007 | 12/23/00 | 0.0001 ± 0.0002 | 54 | 0.0000 | 0.0006 | 02/15/01 | 0.0001 ± 0.0002 | 55 | 0.0000 | 0.0009 | 07/20/00 |
| Arsenic (As) | 0.0007 ± 0.0011 | 53 | 0.0000 | 0.0076 | 01/01/01 | 0.0003 ± 0.0003 | 54 | 0.0000 | 0.0012 | 09/27/00 | 0.0003 ± 0.0003 | 55 | 0.0000 | 0.0012 | 07/03/01 |
| Selenium (Se) | 0.0002 ± 0.0002 | 53 | 0.0000 | 0.0007 | 08/31/00 | 0.0002 ± 0.0002 | 54 | 0.0000 | 0.0009 | 09/21/00 | 0.0002 ± 0.0002 | 55 | 0.0000 | 0.0005 | 02/18/01 |
| Bromine (Br) | 0.0042 ± 0.0020 | 53 | 0.0005 | 0.0101 | 01/01/01 | 0.0027 ± 0.0017 | 54 | 0.0004 | 0.0078 | 05/10/01 | 0.0024 ± 0.0015 | 55 | 0.0004 | 0.0066 | 05/10/01 |
| Rubidium (Rb) | 0.0007 ± 0.0006 | 53 | 0.0000 | 0.0036 | 08/13/00 | 0.0003 ± 0.0003 | 54 | 0.0000 | 0.0013 | 04/01/01 | 0.0003 ± 0.0002 | 55 | 0.0000 | 0.0010 | 06/15/01 |
| Strontium (Sr) | 0.0086 ± 0.0061 | 53 | 0.0014 | 0.0283 | 08/19/00 | 0.0018 ± 0.0015 | 54 | 0.0002 | 0.0072 | 04/01/01 | 0.0009 ± 0.0007 | 55 | 0.0000 | 0.0033 | 06/15/01 |
| Yttrium (Y) | 0.0002 ± 0.0002 | 53 | 0.0000 | 0.0007 | 11/20/00 | 0.0001 ± 0.0002 | 54 | 0.0000 | 0.0006 | 04/01/01 | 0.0001 ± 0.0002 | 55 | 0.0000 | 0.0006 | 09/06/00 |
| Zirconium (Zr) | 0.0015 ± 0.0010 | 53 | 0.0001 | 0.0040 | 04/01/01 | 0.0004 ± 0.0005 | 54 | 0.0000 | 0.0021 | 04/01/01 | 0.0004 ± 0.0003 | 55 | 0.0000 | 0.0010 | 05/13/01 |
| Molybdenum (Mo) | 0.0003 ± 0.0004 | 53 | 0.0000 | 0.0018 | 04/01/01 | 0.0001 ± 0.0003 | 54 | 0.0000 | 0.0012 | 03/20/01 | 0.0001 ± 0.0002 | 55 | 0.0000 | 0.0009 | 08/10/00 |
| Palladium (Pd) | 0.0006 ± 0.0010 | 53 | 0.0000 | 0.0043 | 11/23/00 | 0.0005 ± 0.0009 | 54 | 0.0000 | 0.0031 | 07/26/00 | 0.0007 ± 0.0009 | 55 | 0.0000 | 0.0029 | 02/15/01 |
| Silver (Ag) | 0.0017 ± 0.0017 | 53 | 0.0000 | 0.0080 | 09/15/00 | 0.0011 ± 0.0016 | 54 | 0.0000 | 0.0066 | 07/26/00 | 0.0016 ± 0.0015 | 55 | 0.0000 | 0.0060 | 12/29/00 |
| Cadmium (Cd) | 0.0030 ± 0.0040 | 53 | 0.0000 | 0.0170 | 10/18/00 | 0.0068 ± 0.0150 | 54 | 0.0000 | 0.0827 | 07/20/00 | 0.0027 ± 0.0050 | 55 | 0.0000 | 0.0292 | 08/04/00 |
| Indium (In) | 0.0016 ± 0.0019 | 53 | 0.0000 | 0.0071 | 09/06/00 | 0.0011 ± 0.0016 | 54 | 0.0000 | 0.0057 | 07/20/00 | 0.0012 ± 0.0015 | 55 | 0.0000 | 0.0070 | 09/27/00 |
| Tin (Sn) | 0.0014 ± 0.0017 | 53 | 0.0000 | 0.0062 | 01/04/01 | 0.0013 ± 0.0021 | 54 | 0.0000 | 0.0114 | 04/01/01 | 0.0014 ± 0.0018 | 55 | 0.0000 | 0.0062 | 07/03/01 |
| Antimony (Sb) | 0.0039 ± 0.0052 | 53 | 0.0000 | 0.0209 | 08/19/00 | 0.0018 ± 0.0023 | 54 | 0.0000 | 0.0092 | 08/19/00 | 0.0022 ± 0.0026 | 55 | 0.0000 | 0.0083 | 11/08/00 |
| Barium (Ba) | 0.0316 ± 0.0291 | 53 | 0.0000 | 0.1032 | 06/15/01 | 0.0150 ± 0.0137 | 54 | 0.0000 | 0.0510 | 09/06/00 | 0.0084 ± 0.0105 | 55 | 0.0000 | 0.0361 | 07/15/01 |
| Lanthanum (La) | 0.0105 ± 0.0160 | 53 | 0.0000 | 0.0747 | 10/18/00 | 0.0102 ± 0.0139 | 54 | 0.0000 | 0.0499 | 12/20/00 | 0.0083 ± 0.0116 | 55 | 0.0000 | 0.0373 | 05/13/01 |
| Gold (Au) | 0.0001 ± 0.0002 | 53 | 0.0000 | 0.0008 | 11/26/00 | 0.0001 ± 0.0002 | 54 | 0.0000 | 0.0011 | 10/09/00 | 0.0001 ± 0.0002 | 55 | 0.0000 | 0.0010 | 11/17/00 |
| Mercury (Hg) | 0.0001 ± 0.0002 | 53 | 0.0000 | 0.0006 | 05/13/01 | 0.0002 ± 0.0002 | 54 | 0.0000 | 0.0008 | 09/21/00 | 0.0001 ± 0.0002 | 55 | 0.0000 | 0.0009 | 08/10/00 |
| Thallium (Tl) | 0.0003 ± 0.0003 | 53 | 0.0000 | 0.0012 | 08/10/00 | 0.0003 ± 0.0003 | 54 | 0.0000 | 0.0017 | 09/30/00 | 0.0002 ± 0.0003 | 55 | 0.0000 | 0.0011 | 11/23/00 |
| Lead (Pb) | 0.0053 ± 0.0072 | 53 | 0.0002 | 0.0449 | 01/01/01 | 0.0015 ± 0.0013 | 54 | 0.0000 | 0.0059 | 01/01/01 | 0.0010 ± 0.0009 | 55 | 0.0000 | 0.0041 | 11/26/00 |
| Uranium (U) | 0.0002 ± 0.0003 | 53 | 0.0000 | 0.0011 | 03/20/01 | 0.0004 ± 0.0003 | 54 | 0.0000 | 0.0010 | 09/21/01 | 0.0003 ± 0.0003 | 55 | 0.0000 | 0.0010 | 04/07/01 |
| Sum of Species | 13.0361 ± 7.7238 | 53 | 4.0429 | 35.8108 | 01/01/01 | 5.3091 ± 2.6623 | 54 | 1.2235 | 12.4657 | 09/15/00 | 3.4732 ± 1.9589 | 55 | 0.8258 | 8.2337 | 06/15/01 |
| Ammonia (NH3) | 7.2783 ± 4.5115 | 53 | 1.1907 | 16.4956 | 01/01/01 | 1.8116 ± 1.5186 | 54 | 0.0000 | 9.2160 | 07/06/01 | 0.8276 ± 0.9122 | 55 | 0.0228 | 5.6760 | 07/06/01 |

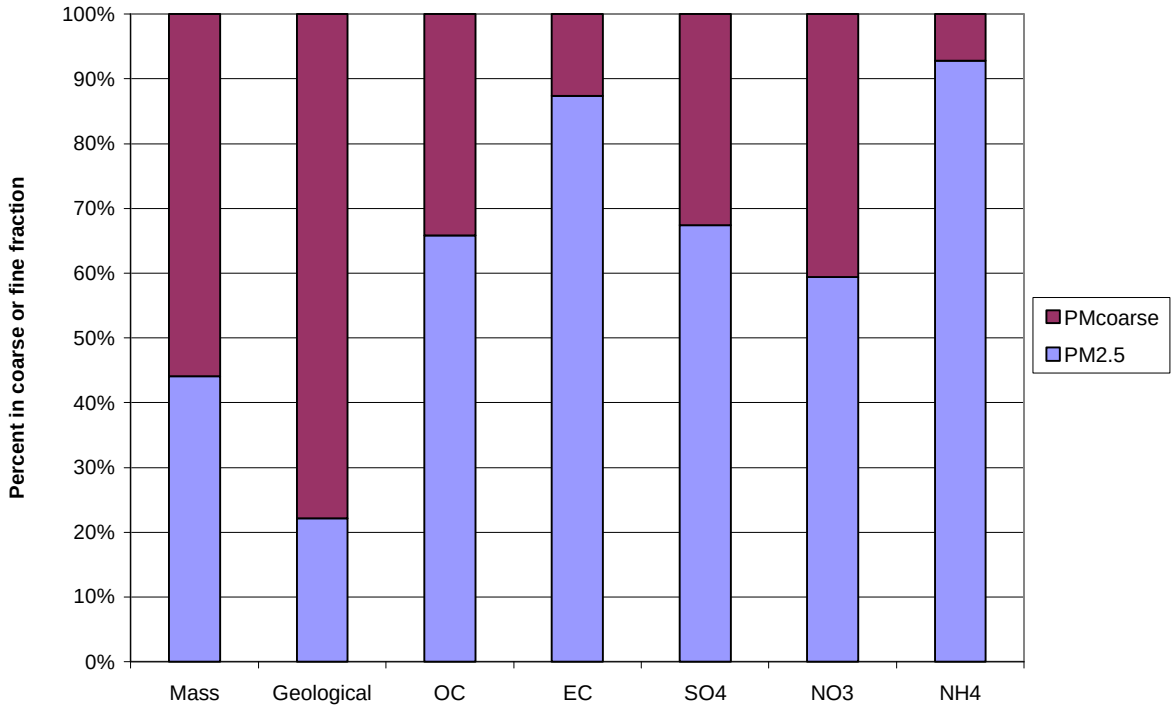


**Figure 4-1.** Percent distribution between $PM_{2.5}$ and $PM_{coarse}$ ($PM_{10}$ minus $PM_{2.5}$) fractions for samples acquired every third day between 07/20/00 and 07/21/01 at the East Charleston site.

Approximately 45% of $PM_{10}$ was in the $PM_{2.5}$ fraction. Figure 4-1 shows that ~80% of geological material resided in the $PM_{coarse}$ ($PM_{10}$ minus $PM_{2.5}$) fraction and that almost all of the ammonium, >90% of EC, and >65% of OC were in the $PM_{2.5}$ fraction. Approximately 30% to 35% of the $NO_3^-$ and $SO_4^=$ was allocated to the coarse particle fraction, which is consistent with the ammonium balance and anion/cation balance in Section 3.4. Some of the $SO_4^=$ may have been present as $Na_2SO_4$ or $CaSO_4$ at all sites. Ammonium concentrations at all three sites were not usually high enough to fully neutralize fine sulfate. There was also significant coarse sulfate (no coarse ammonium) at East Charleston. Due to the pervasive extent of gypsum ($CaSO_4$) in soils in the Las Vegas Valley (USDA, 1985) and nearby gypsum mines), it is expected that much of the non-neutralized fine and coarse sulfate is crustal-related in the form of $CaSO_4$.

As shown in Table 4-3, the highest $PM_{2.5}$ mass, OC, EC, $Cl^-$, $K^+$, Cl, K, As, Br, Pb, and $NH_3$ were found on 01/01/01 at the East Charleston site. The 24-hour-average $PM_{10}$ concentration on 01/01/01 was elevated (86.7±4.3 µg/m$^3$, which is 2.5 times higher than the annual average of 34.9±22.2 µg/m$^3$). The maximum $PM_{10}$ OC, EC, $Cl^-$, $K^+$, Cl, K, As, and Pb concentrations were also found on 01/01/01. $PM_{2.5}$ mass concentrations were low (2.1±0.41 µg/m$^3$ and 0.52±0.4 µg/m$^3$, respectively) at the Palo Verde and Jean sites. Compared to annual averages, organic, elemental, and total carbon increased by three- to

**Table 4-3.** $PM_{2.5}$ and $PM_{10}$ mass and chemical components acquired on 01/01/01.

| | East Charleston PM10 | East Charleston PM2.5 | Palo Verde PM2.5 | Jean PM2.5 |
|---|---|---|---|---|
| Mass (chem analysis days) | 86.6895 ± 4.3529 | 46.4271 ± 2.3540 | 2.1000 ± 0.4083 | 0.5168 ± 0.3956 |
| Volatilized Nitrate (NO3-) | 0.5453 ± 0.0388 | 0.5685 ± 0.0402 | 0.0069 ± 0.0164 | 0.0000 ± 0.0161 |
| Chloride (Cl-) | 0.9987 ± 0.0967 | 0.5690 ± 0.0586 | 0.0235 ± 0.0243 | 0.0161 ± 0.0238 |
| Nonvolatilized Nitrate (NO3-) | 3.1867 ± 0.1625 | 2.8143 ± 0.1440 | 0.4285 ± 0.0324 | 0.0883 ± 0.0241 |
| Sulfate (SO4=) | 1.8036 ± 0.0989 | 1.0101 ± 0.0589 | 0.2434 ± 0.0274 | 0.1777 ± 0.0255 |
| Ammonium (NH4+) | 0.7060 ± 0.0523 | 0.5977 ± 0.0464 | 0.1022 ± 0.0253 | 0.0493 ± 0.0241 |
| Soluble Sodium (Na+) | 0.3442 ± 0.0206 | 0.1343 ± 0.0119 | 0.015 ± 0.0095 | 0.008 ± 0.0093 |
| Soluble Potassium (K+) | 1.2076 ± 0.0912 | 0.9264 ± 0.0700 | 0.0980 ± 0.0084 | 0.0389 ± 0.0048 |
| Organic Carbon (OC) | 24.4386 ± 1.7793 | 18.2829 ± 1.3935 | 0.4691 ± 0.5593 | 0.0000 ± 0.5449 |
| Elemental Carbon (EC) | 9.7659 ± 0.6329 | 8.4667 ± 0.5488 | 0.2966 ± 0.0459 | 0.2677 ± 0.0446 |
| Total Carbon (TC) | 34.1937 ± 2.2933 | 26.7420 ± 1.8399 | 0.7546 ± 0.5806 | 0.0580 ± 0.5648 |
| Sodium (Na) | 0.0000 ± 0.0751 | 0.0246 ± 0.0479 | 0.0088 ± 0.0236 | 0.0003 ± 0.0209 |
| Magnesium (Mg) | 0.8546 ± 0.0478 | 0.2032 ± 0.0162 | 0.0413 ± 0.0086 | 0.0227 ± 0.0074 |
| Aluminum (Al) | 1.3347 ± 0.3974 | 0.1616 ± 0.0124 | 0.0352 ± 0.0078 | 0.0220 ± 0.0074 |
| Silicon (Si) | 5.6248 ± 1.7805 | 0.6123 ± 0.0375 | 0.1071 ± 0.0216 | 0.0490 ± 0.0210 |
| Phosphorus (P) | 0.0318 ± 0.0151 | 0.0044 ± 0.0083 | 0.0021 ± 0.0043 | 0.0025 ± 0.0037 |
| Sulfur (S) | 0.6696 ± 0.0341 | 0.4090 ± 0.0211 | 0.0941 ± 0.0056 | 0.0448 ± 0.0035 |
| Chlorine (Cl) | 0.9625 ± 0.2802 | 0.4663 ± 0.0255 | 0.0021 ± 0.0073 | 0.0151 ± 0.0050 |
| Patassium (K) | 1.9430 ± 0.3867 | 1.1757 ± 0.0596 | 0.1311 ± 0.0086 | 0.0346 ± 0.0051 |
| Calcium (Ca) | 7.5714 ± 1.2730 | 1.2323 ± 0.0632 | 0.2165 ± 0.0157 | 0.0447 ± 0.0113 |
| Titanium (Ti) | 0.0822 ± 0.0216 | 0.0197 ± 0.0286 | 0.0000 ± 0.0248 | 0.0022 ± 0.0239 |
| Vanadium (V) | 0.0006 ± 0.0160 | 0.0014 ± 0.0124 | 0.0000 ± 0.0135 | 0.0009 ± 0.0106 |
| Chromium (Cr) | 0.0014 ± 0.0042 | 0.0000 ± 0.0032 | 0.0000 ± 0.0040 | 0.0000 ± 0.0028 |
| Manganese (Mn) | 0.0242 ± 0.0022 | 0.0067 ± 0.0015 | 0.0003 ± 0.0020 | 0.0004 ± 0.0017 |
| Iron (Fe) | 1.9302 ± 0.0967 | 0.5439 ± 0.0276 | 0.0330 ± 0.0042 | 0.0180 ± 0.0039 |
| Cobalt (Co) | 0.0000 ± 0.0287 | 0.0000 ± 0.0083 | 0.0000 ± 0.0012 | 0.0000 ± 0.0011 |
| Nickel (Ni) | 0.0012 ± 0.0008 | 0.0003 ± 0.0011 | 0.0000 ± 0.0009 | 0.0000 ± 0.0010 |
| Copper (Cu) | 0.0511 ± 0.0028 | 0.0227 ± 0.0015 | 0.0040 ± 0.0009 | 0.0008 ± 0.0009 |
| Zinc (Zn) | 0.0882 ± 0.0046 | 0.0483 ± 0.0026 | 0.0034 ± 0.0009 | 0.0007 ± 0.0012 |
| Gallium (Ga) | 0.0000 ± 0.0022 | 0.0000 ± 0.0021 | 0.0002 ± 0.0017 | 0.0004 ± 0.0017 |
| Arsenic (As) | 0.0073 ± 0.0099 | 0.0076 ± 0.0028 | 0.0005 ± 0.0023 | 0.0000 ± 0.0021 |
| Selenium (Se) | 0.0000 ± 0.0013 | 0.0000 ± 0.0013 | 0.0000 ± 0.0011 | 0.0001 ± 0.0011 |
| Bromine (Br) | 0.0113 ± 0.0011 | 0.0101 ± 0.0010 | 0.0014 ± 0.0008 | 0.0006 ± 0.0010 |
| Rubidium (Rb) | 0.0023 ± 0.0008 | 0.0014 ± 0.0007 | 0.0002 ± 0.0009 | 0.0002 ± 0.0009 |
| Strontium (Sr) | 0.0467 ± 0.0025 | 0.0177 ± 0.0012 | 0.0058 ± 0.0009 | 0.0017 ± 0.0008 |
| Yttrium (Y) | 0.0009 ± 0.0016 | 0.0000 ± 0.0015 | 0.0000 ± 0.0012 | 0.0002 ± 0.0012 |
| Zirconium (Zr) | 0.0071 ± 0.0014 | 0.0019 ± 0.0012 | 0.0001 ± 0.0015 | 0.0001 ± 0.0015 |
| Molybdenum (Mo) | 0.0030 ± 0.0022 | 0.0005 ± 0.0030 | 0.0000 ± 0.0026 | 0.0005 ± 0.0026 |
| Palladium (Pd) | 0.0000 ± 0.0095 | 0.0000 ± 0.0089 | 0.0000 ± 0.0078 | 0.0014 ± 0.0078 |
| Silver (Ag) | 0.0000 ± 0.0110 | 0.0010 ± 0.0102 | 0.0019 ± 0.0092 | 0.0041 ± 0.0092 |
| Cadmium (Cd) | 0.0000 ± 0.0117 | 0.0125 ± 0.0078 | 0.0215 ± 0.0078 | 0.0000 ± 0.0100 |
| Indium (In) | 0.0000 ± 0.0130 | 0.0000 ± 0.0121 | 0.0057 ± 0.0111 | 0.0000 ± 0.0110 |
| Tin (Sn) | 0.0038 ± 0.0167 | 0.0032 ± 0.0155 | 0.0011 ± 0.0141 | 0.0000 ± 0.0141 |
| Antimony (Sb) | 0.0230 ± 0.0134 | 0.0196 ± 0.0130 | 0.0005 ± 0.0166 | 0.0060 ± 0.0166 |
| Barium (Ba) | 0.2056 ± 0.0500 | 0.0879 ± 0.0476 | 0.0134 ± 0.0598 | 0.0112 ± 0.0605 |
| Lanthanum (La) | 0.0000 ± 0.0919 | 0.0000 ± 0.0904 | 0.0306 ± 0.0820 | 0.0139 ± 0.0823 |
| Gold (Au) | 0.0000 ± 0.0045 | 0.0000 ± 0.0036 | 0.0005 ± 0.0028 | 0.0006 ± 0.0028 |
| Mercury (Hg) | 0.0000 ± 0.0028 | 0.0000 ± 0.0027 | 0.0000 ± 0.0023 | 0.0001 ± 0.0024 |
| Thallium (Tl) | 0.0000 ± 0.0033 | 0.0000 ± 0.0030 | 0.0005 ± 0.0023 | 0.0003 ± 0.0023 |
| Lead (Pb) | 0.0622 ± 0.0042 | 0.0449 ± 0.0035 | 0.0059 ± 0.0025 | 0.0023 ± 0.0024 |
| Uranium (U) | 0.0001 ± 0.0026 | 0.0007 ± 0.0025 | 0.0003 ± 0.0022 | 0.0002 ± 0.0022 |
| Sum of Species | 60.2658 ± 2.9675 | 35.8108 ± 1.5141 | 2.1798 ± 0.5747 | 0.8258 ± 0.5599 |
| Ammonia (NH3) | 16.2254 ± 0.8673 | 16.4956 ± 0.8811 | 0.9499 ± 0.0702 | 0.2807 ± 0.0405 |

fourfold on 01/01/01 in both $PM_{2.5}$ and $PM_{10}$ size fractions. $PM_{2.5}$ and $PM_{10}$ $K^+$ were six- and 3.5-fold higher on 01/01/01 than the corresponding annual averages at the East Charleston site. New Year's Eve celebrations on the Las Vegas Strip and Downtown Las Vegas brought large crowds and heavy vehicle traffic that continued into the early morning hours of New Year's Day. Nighttime drainage flows from these areas would transport emissions toward the East Charleston site. Residential wood combustion also may have contributed to the elevated concentrations.

The highest $PM_{10}$ concentration was found on 08/13/00 (103.5±5.2 $\mu g/m^3$). Elevated $PM_{2.5}$ mass concentrations were found at all three sites on this date with 31.0±1.6 $\mu g/m^3$ at East Charleston, 8.9±0.6 $\mu g/m^3$ at Palo Verde, and 9.2±0.6 $\mu g/m^3$ at Jean. On this day, during the early evening, a dust cloud resulting from a thunderstorm complex in northwestern Arizona, moved into and across the Las Vegas Valley. This cloud could be tracked across the valley by the Clark County DAQM beta-attenuation hourly $PM_{10}$ data, which showed values in excess of 1,000 $\mu g/m^3$. While carbonaceous material and secondary aerosol components remained similar to the annual averages, the geological component was elevated. $PM_{10}$ aluminum, silicon, and iron concentrations were 7.9±2.3 $\mu g/m^3$, 22.3±7 $\mu g/m^3$, and 4.4±0.22 $\mu g/m^3$, respectively, on 08/13/00. These levels are 4 to 7 times higher than the corresponding annual averages at the site. Table 4-4 shows that elevated Al, Si, and Fe concentrations were found in $PM_{2.5}$ at all sites compared to the annual averages shown in Table 4-2. $PM_{2.5}$ geological material concentrations recorded on 08/13/00 were 3 to 7 times higher than the corresponding averages.

## 4.2 Temporal and Spatial Variations of Major PM Components

Material balance was conducted to include the major PM components listed in Section 3.4.5. Figure 4-2 shows that large differences in source attributions were found among the three size fractions at the East Charleston site. The largest contributors to $PM_{2.5}$ mass were organic material (accounting for 40.4% of $PM_{2.5}$) followed by 24.8% geological matter and 13.6% soot. Source attributions were quite different for the $PM_{coarse}$ fraction with 69% attributed to geological, 17.6% to organic matter, and 2.8% to sulfate and 1.9% nitrate. Geological material was the largest contributor to both $PM_{coarse}$ and $PM_{10}$ fractions. Figure 4-3 shows that $PM_{10}$ aerosol consisted of 49.3% geological material and 27.8% organic matter. Figure 4-3 also shows that large spatial variations were found for $PM_{2.5}$ mass and major chemical components, with organic matter and geological material being the two largest contributors. The Palo Verde and Jean sites were somewhat more similar to each other than either was to the East Charleston site. The largest difference was the elevated organic matter at the urban East Charleston site (which was ~11% to 12% on a fractional basis higher than at the other two sites). Secondary sulfate was higher on a fractional basis (22%) at the background/transport Jean site as compared to the urban East Charleston site (7%). However, on a mass basis, $PM_{2.5}$ sulfate at Jean was somewhat lower, on average, than at East Charleston.

**Table 4-4.** $PM_{2.5}$ and $PM_{10}$ mass and chemical components acquired on 08/13/00.

| | East Charleston PM10 | East Charleston PM2.5 | Palo Verde PM2.5 | Jean PM2.5 |
|---|---|---|---|---|
| Mass (chem analysis days) | 103.5354 ± 5.1900 | 31.0018 ± 1.5952 | 8.9172 ± 0.5802 | 9.1559 ± 0.5870 |
| Volatilized Nitrate (NO3-) | 0.1823 ± 0.0198 | 0.1173 ± 0.0179 | 0.0981 ± 0.0174 | 0.0946 ± 0.0171 |
| Chloride (Cl-) | 0.2622 ± 0.0341 | 0.0759 ± 0.0249 | 0.0243 ± 0.0240 | 0.1436 ± 0.0271 |
| Nonvolatilized Nitrate (NO3-) | 1.4015 ± 0.0745 | 0.6345 ± 0.0399 | 0.2834 ± 0.0278 | 0.2933 ± 0.0278 |
| Sulfate (SO4=) | 2.1651 ± 0.1176 | 1.6041 ± 0.0886 | 1.1891 ± 0.0676 | 1.2409 ± 0.0701 |
| Ammonium (NH4+) | 0.4994 ± 0.0407 | 0.4621 ± 0.0390 | 0.3643 ± 0.0342 | 0.3885 ± 0.0351 |
| Soluble Sodium (Na+) | 0.4672 ± 0.0266 | 0.222 ± 0.0151 | 0.0975 ± 0.0107 | 0.1714 ± 0.013 |
| Soluble Potassium (K+) | 0.2544 ± 0.0197 | 0.1020 ± 0.0087 | 0.0513 ± 0.0055 | 0.0529 ± 0.0055 |
| Organic Carbon (OC) | 6.5544 ± 0.7264 | 3.4868 ± 0.6155 | 1.6719 ± 0.5704 | 2.6587 ± 0.5848 |
| Elemental Carbon (EC) | 0.6645 ± 0.0599 | 0.8569 ± 0.0706 | 0.7388 ± 0.0649 | 0.7548 ± 0.0647 |
| Total Carbon (TC) | 7.2081 ± 0.7481 | 4.3327 ± 0.6481 | 2.3997 ± 0.5987 | 3.4026 ± 0.6148 |
| Sodium (Na) | 0.1419 ± 0.0322 | 0.0915 ± 0.0246 | 0.0537 ± 0.0185 | 0.0685 ± 0.0172 |
| Magnesium (Mg) | 0.7354 ± 0.0441 | 0.3426 ± 0.0244 | 0.2445 ± 0.0175 | 0.0398 ± 0.0098 |
| Aluminum (Al) | 7.8537 ± 2.3327 | 1.2489 ± 0.0646 | 0.2824 ± 0.0173 | 0.2368 ± 0.0151 |
| Silicon (Si) | 22.2477 ± 7.0411 | 4.1798 ± 0.2106 | 1.1434 ± 0.0612 | 0.7920 ± 0.0449 |
| Phosphorus (P) | 0.0581 ± 0.0263 | 0.0062 ± 0.0106 | 0.0000 ± 0.0071 | 0.0000 ± 0.0066 |
| Sulfur (S) | 0.4978 ± 0.0254 | 0.5664 ± 0.0288 | 0.4171 ± 0.0213 | 0.4747 ± 0.0242 |
| Chlorine (Cl) | 0.1614 ± 0.0500 | 0.0368 ± 0.0082 | 0.0000 ± 0.0117 | 0.0000 ± 0.0113 |
| Patassium (K) | 2.7534 ± 0.5475 | 0.7084 ± 0.0365 | 0.1686 ± 0.0103 | 0.1611 ± 0.0097 |
| Calcium (Ca) | 5.0302 ± 0.8459 | 1.7788 ± 0.0900 | 0.5426 ± 0.0295 | 0.1929 ± 0.0145 |
| Titanium (Ti) | 0.4182 ± 0.0283 | 0.1318 ± 0.0197 | 0.0142 ± 0.0245 | 0.0162 ± 0.0179 |
| Vanadium (V) | 0.0118 ± 0.0188 | 0.0066 ± 0.0120 | 0.0000 ± 0.0108 | 0.0000 ± 0.0103 |
| Chromium (Cr) | 0.0008 ± 0.0062 | 0.0003 ± 0.0034 | 0.0000 ± 0.0028 | 0.0000 ± 0.0027 |
| Manganese (Mn) | 0.1093 ± 0.0061 | 0.0373 ± 0.0025 | 0.0064 ± 0.0014 | 0.0054 ± 0.0014 |
| Iron (Fe) | 4.4260 ± 0.2215 | 1.4136 ± 0.0709 | 0.2675 ± 0.0140 | 0.2250 ± 0.0119 |
| Cobalt (Co) | 0.0000 ± 0.0656 | 0.0000 ± 0.0211 | 0.0000 ± 0.0042 | 0.0000 ± 0.0036 |
| Nickel (Ni) | 0.0024 ± 0.0009 | 0.0009 ± 0.0012 | 0.0004 ± 0.0010 | 0.0002 ± 0.0009 |
| Copper (Cu) | 0.0115 ± 0.0011 | 0.0097 ± 0.0010 | 0.0030 ± 0.0009 | 0.0018 ± 0.0008 |
| Zinc (Zn) | 0.0240 ± 0.0015 | 0.0150 ± 0.0012 | 0.0065 ± 0.0010 | 0.0039 ± 0.0009 |
| Gallium (Ga) | 0.0008 ± 0.0020 | 0.0006 ± 0.0018 | 0.0000 ± 0.0018 | 0.0000 ± 0.0017 |
| Arsenic (As) | 0.0005 ± 0.0026 | 0.0007 ± 0.0023 | 0.0006 ± 0.0021 | 0.0001 ± 0.0020 |
| Selenium (Se) | 0.0003 ± 0.0013 | 0.0002 ± 0.0011 | 0.0000 ± 0.0012 | 0.0001 ± 0.0011 |
| Bromine (Br) | 0.0079 ± 0.0009 | 0.0079 ± 0.0009 | 0.0051 ± 0.0008 | 0.0058 ± 0.0008 |
| Rubidium (Rb) | 0.0111 ± 0.0009 | 0.0036 ± 0.0007 | 0.0004 ± 0.0010 | 0.0006 ± 0.0009 |
| Strontium (Sr) | 0.0291 ± 0.0017 | 0.0123 ± 0.0010 | 0.0019 ± 0.0008 | 0.0019 ± 0.0008 |
| Yttrium (Y) | 0.0035 ± 0.0010 | 0.0007 ± 0.0013 | 0.0001 ± 0.0013 | 0.0002 ± 0.0012 |
| Zirconium (Zr) | 0.0117 ± 0.0014 | 0.0039 ± 0.0012 | 0.0008 ± 0.0016 | 0.0005 ± 0.0014 |
| Molybdenum (Mo) | 0.0006 ± 0.0030 | 0.0009 ± 0.0027 | 0.0000 ± 0.0028 | 0.0000 ± 0.0025 |
| Palladium (Pd) | 0.0014 ± 0.0099 | 0.0000 ± 0.0086 | 0.0000 ± 0.0081 | 0.0003 ± 0.0078 |
| Silver (Ag) | 0.0000 ± 0.0113 | 0.0007 ± 0.0101 | 0.0039 ± 0.0095 | 0.0011 ± 0.0091 |
| Cadmium (Cd) | 0.0000 ± 0.0119 | 0.0099 ± 0.0077 | 0.0143 ± 0.0076 | 0.0050 ± 0.0098 |
| Indium (In) | 0.0044 ± 0.0130 | 0.0014 ± 0.0116 | 0.0028 ± 0.0112 | 0.0000 ± 0.0106 |
| Tin (Sn) | 0.0000 ± 0.0164 | 0.0039 ± 0.0149 | 0.0000 ± 0.0144 | 0.0000 ± 0.0137 |
| Antimony (Sb) | 0.0000 ± 0.0189 | 0.0019 ± 0.0175 | 0.0021 ± 0.0170 | 0.0000 ± 0.0160 |
| Barium (Ba) | 0.0000 ± 0.0669 | 0.0061 ± 0.0624 | 0.0212 ± 0.0616 | 0.0155 ± 0.0586 |
| Lanthanum (La) | 0.0031 ± 0.0897 | 0.0000 ± 0.0847 | 0.0177 ± 0.0845 | 0.0000 ± 0.0794 |
| Gold (Au) | 0.0000 ± 0.0033 | 0.0000 ± 0.0030 | 0.0000 ± 0.0030 | 0.0000 ± 0.0027 |
| Mercury (Hg) | 0.0006 ± 0.0027 | 0.0000 ± 0.0024 | 0.0000 ± 0.0025 | 0.0003 ± 0.0023 |
| Thallium (Tl) | 0.0011 ± 0.0027 | 0.0002 ± 0.0024 | 0.0000 ± 0.0024 | 0.0004 ± 0.0022 |
| Lead (Pb) | 0.0063 ± 0.0025 | 0.0044 ± 0.0024 | 0.0009 ± 0.0033 | 0.0016 ± 0.0030 |
| Uranium (U) | 0.0006 ± 0.0029 | 0.0005 ± 0.0024 | 0.0004 ± 0.0023 | 0.0000 ± 0.0021 |
| Sum of Species | 54.9438 ± 7.5271 | 16.9001 ± 0.6865 | 6.8523 ± 0.5952 | 7.1761 ± 0.6059 |
| Ammonia (NH3) | 3.1950 ± 0.2023 | 3.4067 ± 0.2127 | 1.7557 ± 0.1046 | 1.0593 ± 0.0670 |

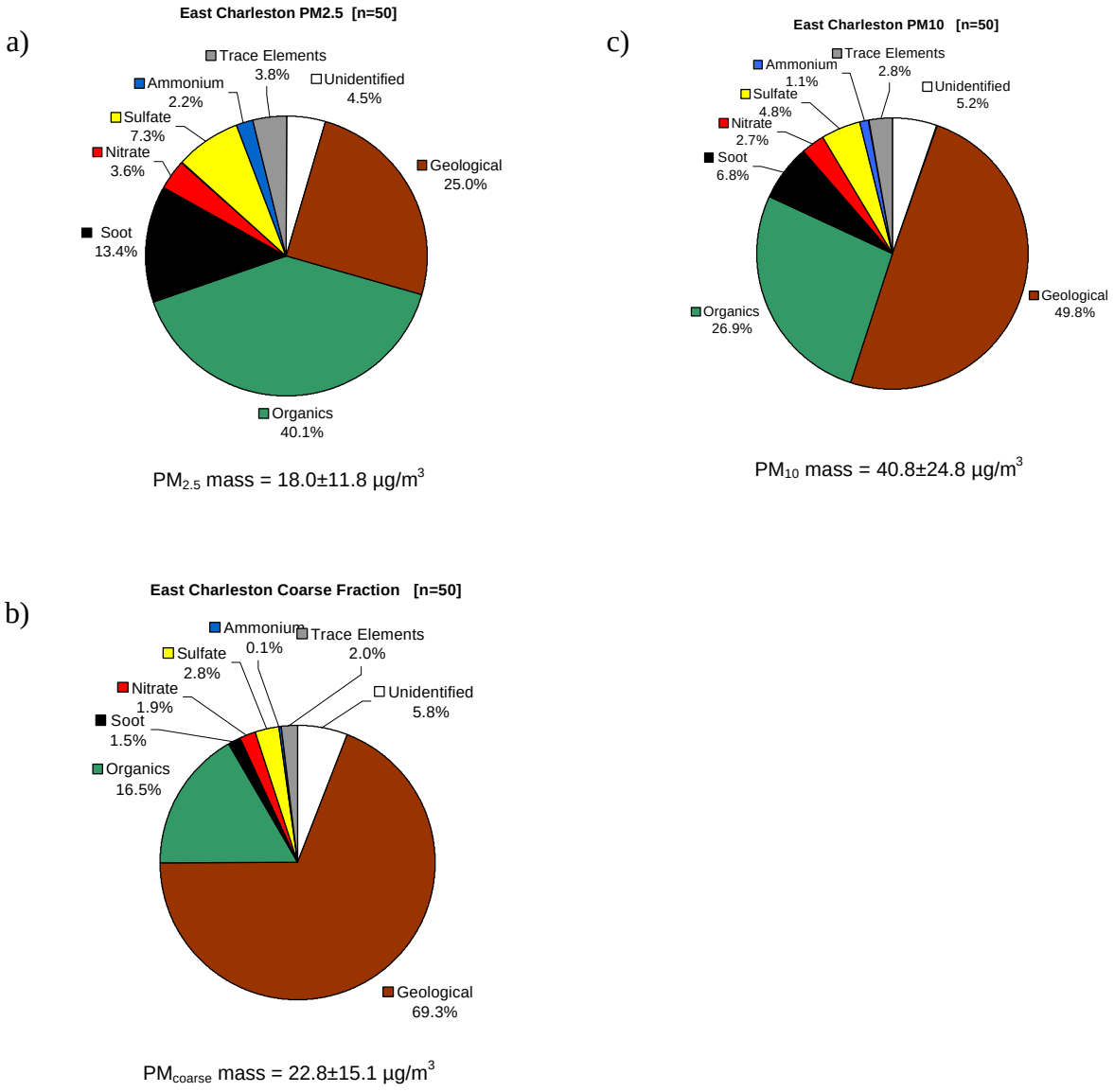


**Figure 4-2.** Material balance of $PM_{2.5}$, $PM_{coarse}$, and $PM_{10}$ for samples acquired at the East Charleston site. The major components of reconstructed mass include: 1) geological material (estimated as 1.89×Al + 2.14×Si + 1.4×Ca + 1.43×Fe to account for unmeasured oxides), 2) organic matter (1.4×organic carbon to account for unmeasured hydrogen and oxygen), 3) soot (elemental carbon), 4) sulfate, 5) nitrate, 6) ammonium, 7) noncrustal trace elements (sum of other-than-geological elements listed in Table 4-1 excluding Al, Si, Ca, Fe, Cl, and S), and 7) unidentified mass (difference between measured mass and the sum of the major components).

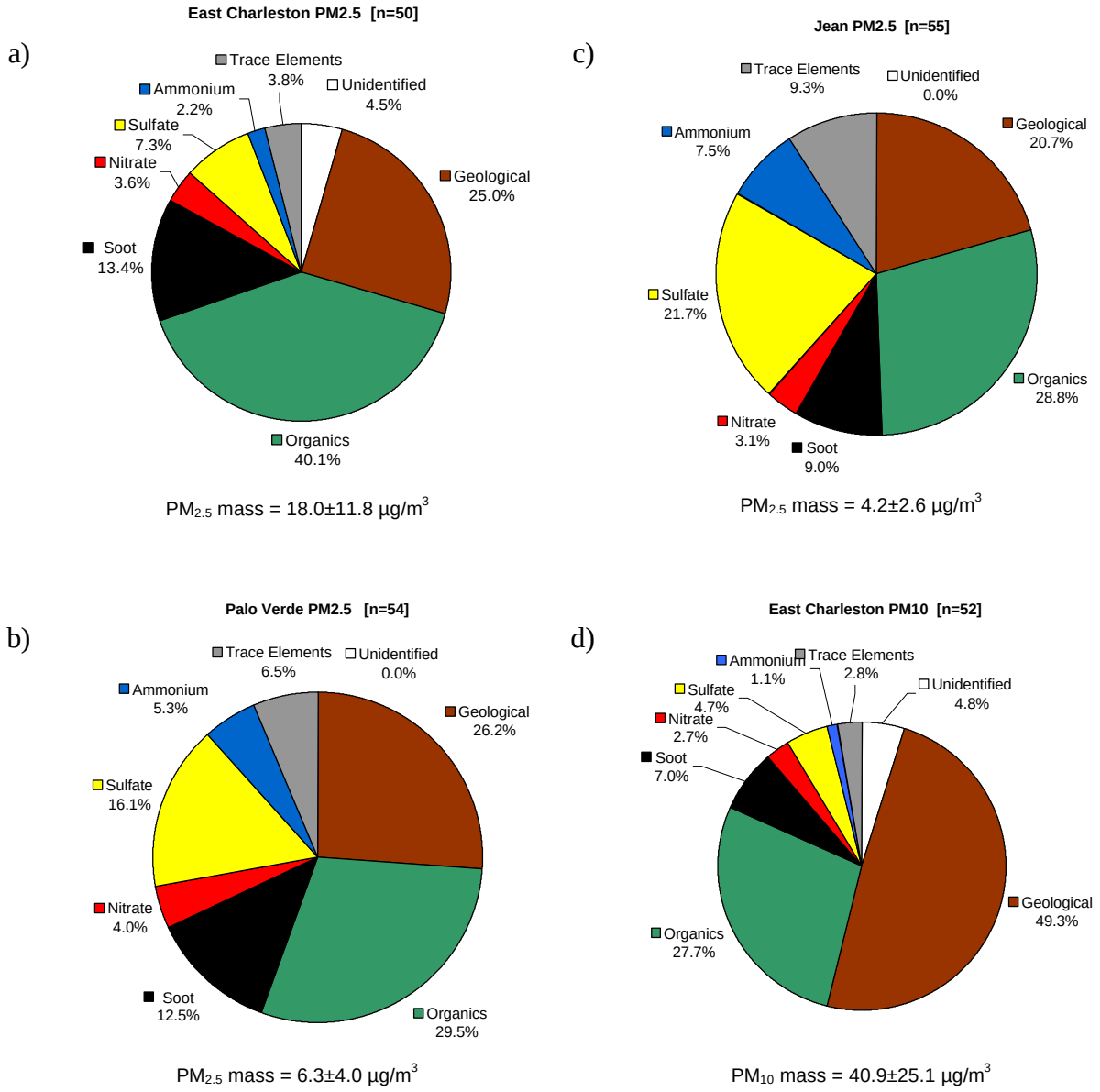


**Figure 4-3.** Material balance of $PM_{2.5}$ and $PM_{10}$ for samples acquired at the East Charleston, Palo Verde, and Jean sites. The major components of reconstructed mass include: 1) geological material (estimated as 1.89×Al + 2.14×Si + 1.4×Ca + 1.43×Fe to account for unmeasured oxides), 2) organic matter (1.4×organic carbon to account for unmeasured hydrogen and oxygen), 3) soot (elemental carbon), 4) sulfate, 5) nitrate, 6) ammonium, 7) noncrustal trace elements (sum of other-than-geological elements listed in Table 4-1 excluding Al, Si, Ca, Fe, Cl, and S), and 7) unidentified mass (difference between measured mass and the sum of the major components).

Next we consider the variations in concentrations of the major components throughout the study year (July 2000-July 2001). Figures 4-4a to 4-4g show time series of $PM_{2.5}$ and $PM_{10}$ concentration, organic mass, elemental carbon, sulfate, nitrate, ammonium, and fine soil for each site. The ratio of $PM_{10}$ to $PM_{2.5}$ is fairly consistent at East Charleston, most often between 2 and 2.5, with a median of 2.26. The $PM_{2.5}$ mass at East Charleston is typically much higher than the other sites, particularly in the winter months.

The organic mass (OMC- Figure 4-4b) is much higher at East Charleston than at the other sites, particularly in winter. Most of the organic mass is in the $PM_{2.5}$ size range at East Charleston. Elemental carbon (Figure 4-4c) is also far higher at East Charleston than at the other sites, especially in winter. There are a few cases (e.g., 09/15/00, 03/20/01, 06/15/01) when elemental carbon rises at all three sites, suggesting a regional component.

Fine ($PM_{2.5}$) sulfate (Figure 4-4d) is well correlated at the three sites, and similar in magnitude at the sites. This suggests that fine sulfate is due to regional rather than local sources. These "regional" sources are likely to include sources in much of the southwestern United States and northwestern Mexico. Figure 4-5 contains scatterplots of sulfate for each pair of sites and illustrates the high correlations for sulfate. Fine nitrate (Figure 4-4e) is low except for a few winter cases at East Charleston and Palo Verde. There is often 0.5 $\mu g/m^3$ or so of coarse particulate nitrate at the East Charleston site. Ammonium (Figure 4-4f) is well correlated at the sites, but it is less correlated in winter when much of it is likely to be in the form of ammonium nitrate. At warmer temperatures, ammonium concentrations are very well correlated and nearly equal at the sites, as the ammonium is expected to be mainly ammonium sulfate (regional).

Fine soil (Figure 4-4g) is highest at East Charleston, then Palo Verde. It is somewhat correlated among the sites at warmer temperatures, most likely due to windy conditions. The higher concentrations at the urban and suburban sites are a consequence of enhanced surface disturbance (such as construction activity, disturbed vacant land, road dust, etc.) in these areas.

Figure 4-6 shows the day-by-day contributions of each major component to $PM_{2.5}$ at each site. Note that the axes are different for each site. Figure 4-7 shows the fractional contribution of each major chemical component each day to $PM_{2.5}$. The contributions of organic mass for several late fall and winter days at Jean was zero because the organic carbon concentrations were lower than the lower detectable limit. Although nitrate is usually a small fraction of fine mass, it was the greatest single component on two rather clean days during winter at Palo Verde.

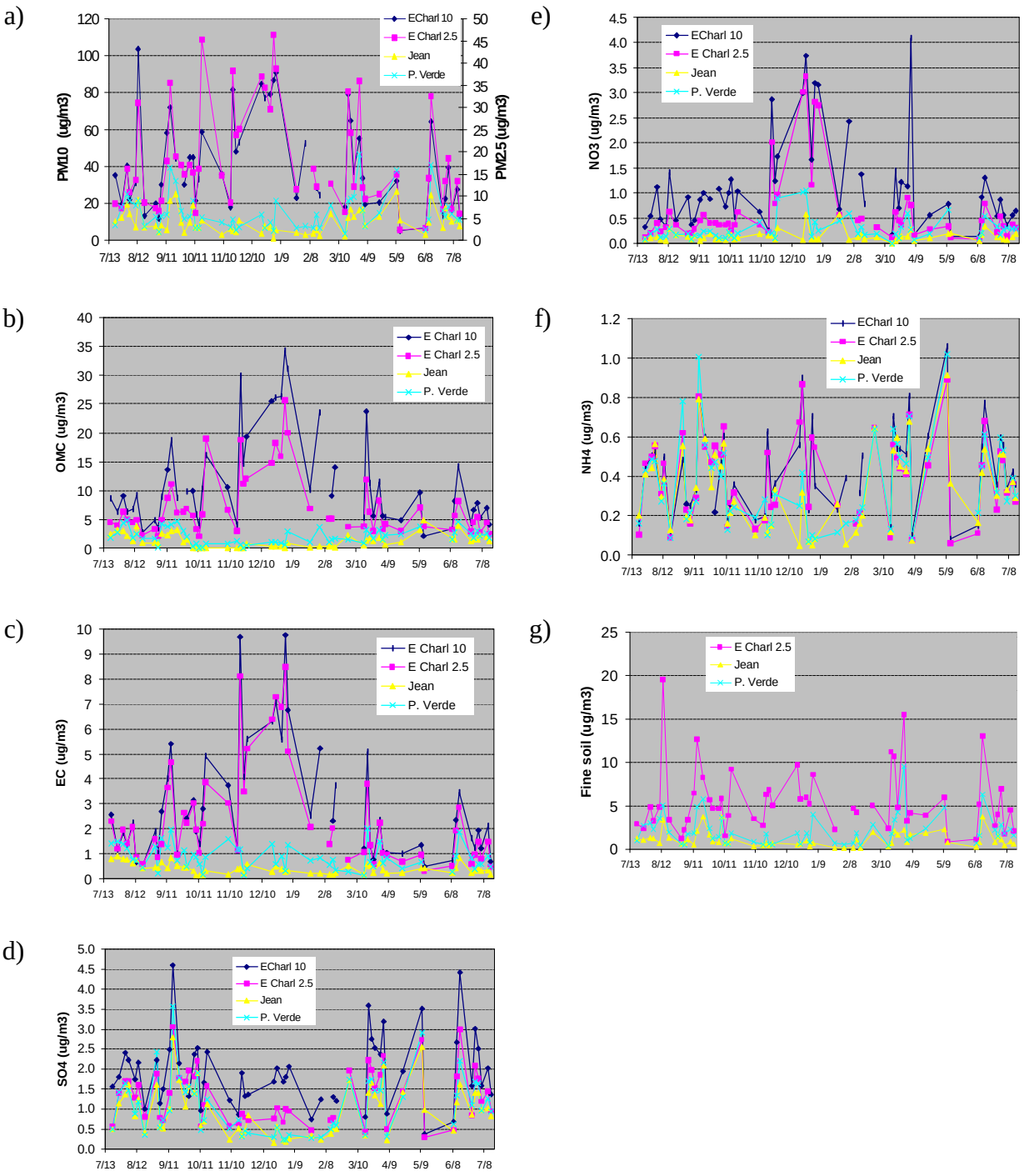


**Figure 4-4.** Time series of major chemical components at each site: a) $PM_{2.5}$ at all sites and $PM_{10}$ at East Charleston; b) organic mass; c) elemental carbon; d) sulfate; e) nitrate; f) ammonium; and g) fine soil.

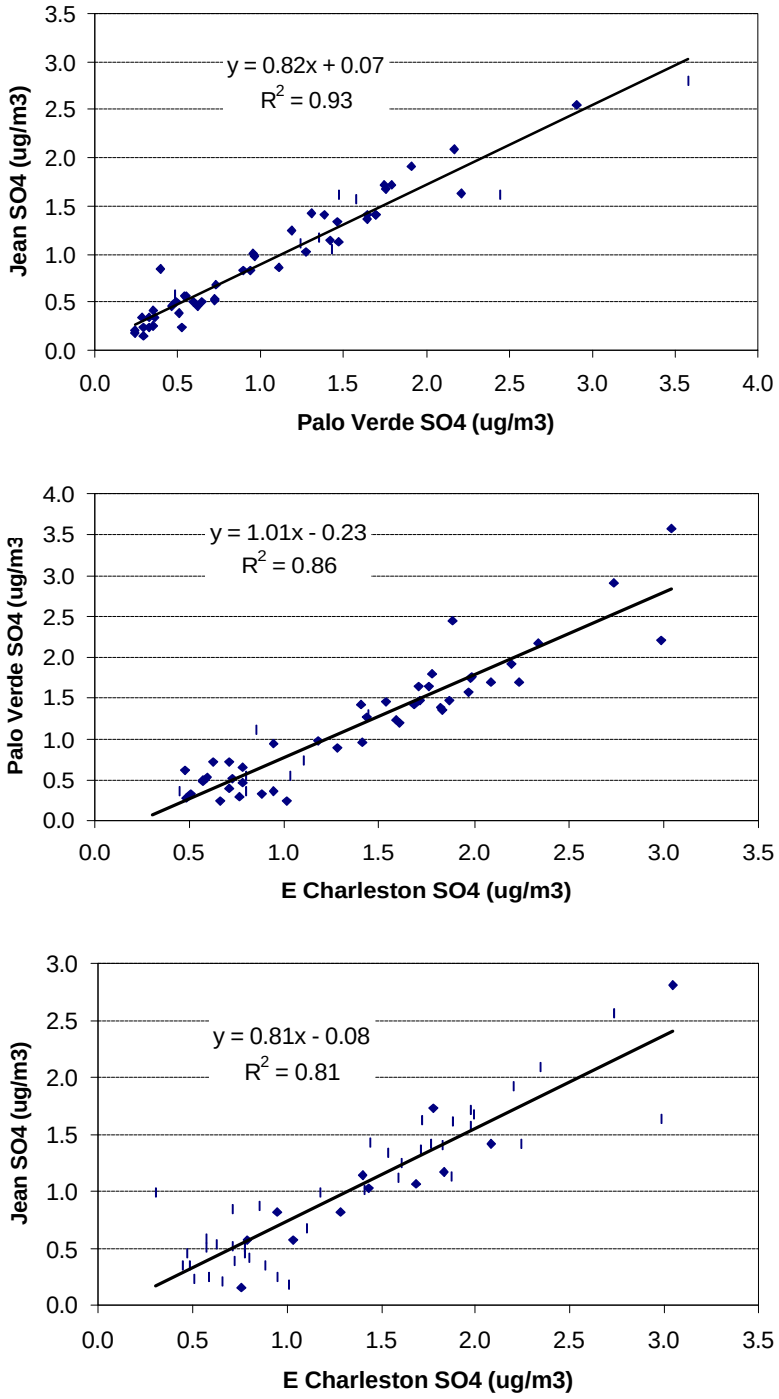


**Figure 4-5.** Scatterplots of fine sulfate for each pair of sites: a) Jean vs. Palo Verde; b) Jean vs. East Charleston; and c) Palo Verde vs. East Charleston.

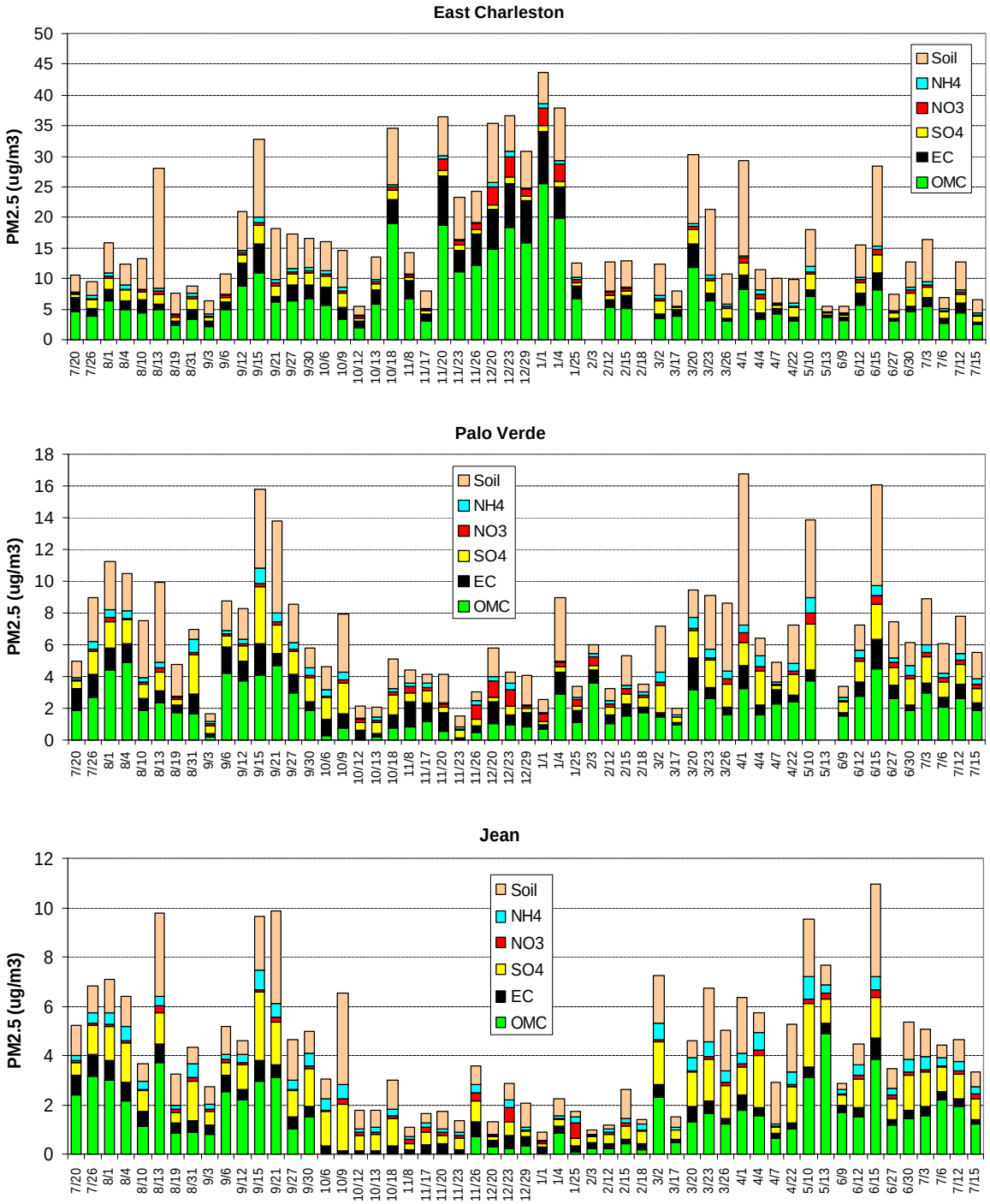


**Figure 4-6.** Time series plots of contribution of each major chemical component to $PM_{2.5}$ mass: a) East Charleston; b) Palo Verde; and c) Jean.

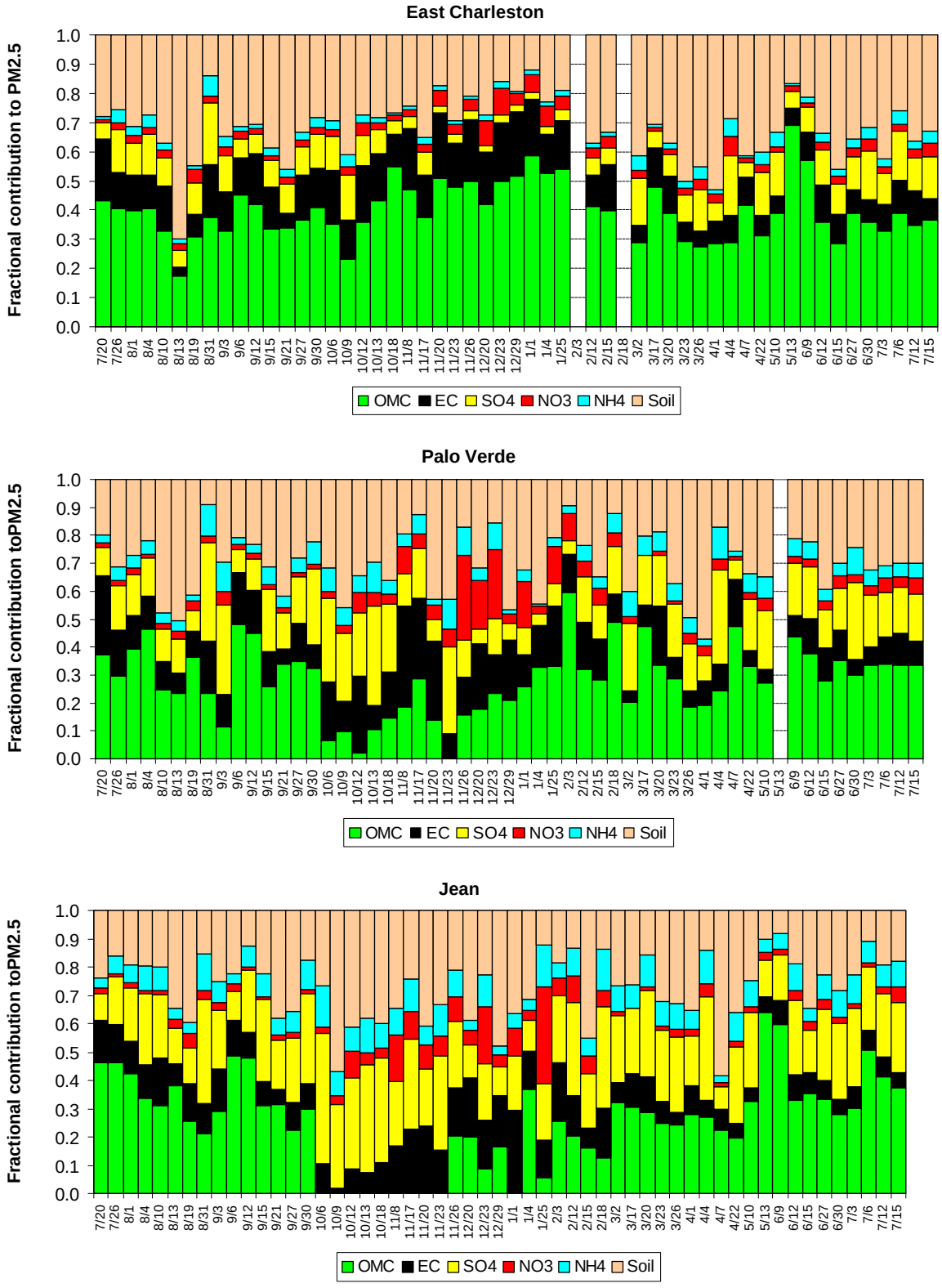


**Figure 4-7.** Time series plots of fractional contribution of each major chemical component to $PM_{2.5}$ mass: a) East Charleston; b) Palo Verde; and c) Jean.

# 5. SPATIAL AND TEMPORAL PATTERNS OF LIGHT SCATTERING AND ABSORPTION

## 5.1 Seasonal Patterns in Haze by Site

The differences and similarities of patterns of measured light scattering and light absorption are analyzed in this section. In Section 6, we look at "reconstructed" light scattering and absorption obtained from the speciated particulate data. The 12 months of the study have been grouped into Cold Season months and Warm Season months. A representative group of months from each category was chosen to characterize the patterns of haze. The months that were chosen to show the Warm Season patterns are April-01, May-01, June-01, and July-01. The months that were selected for demonstration of the Cold Season patterns are October-00, November-00, December-00, and January-01. Five-minute aethalometer data and 2-minute nephelometer data were used to calculate hourly averages. The 50$^{th}$ percentile of the hourly averages was used to show the fractional contributions of light absorption ($b_{abs}$), light scattering by particles ($b_{sp}$), and light scattering by gases (natural Rayleigh scattering, $b_{sg}$). At the East Charleston site, $b_{abs}$ and $b_{sp}$ decrease from cold season to warm season (Figures 5-1 and 5-2). Elevation of $b_{abs}$ is observed at the beginning and end of the day at this site. This will be further discussed later in this section.

Conversely, the percentage of $b_{ext}$ from $b_{sp}$ declines at the Jean site during the cold season. The $b_{abs}$ increases only by 1%, and $b_{sg}$ increases. This is due to the location of these two sites. Where East Charleston is in the urban center of the city, Jean is a background site. At East Charleston, buildup of pollutants is greater in winter than summer due to decreased

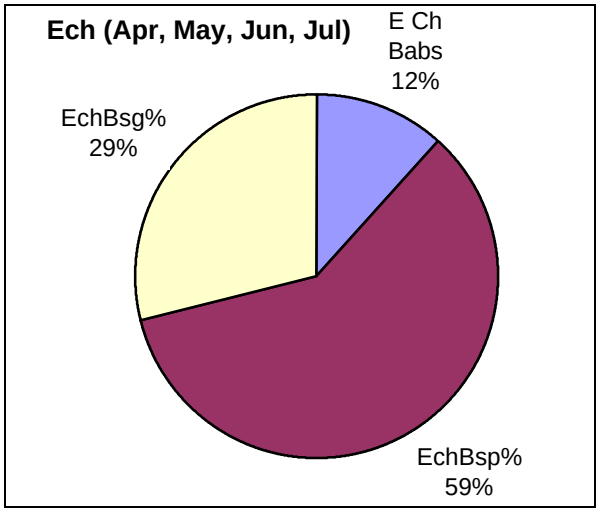


**Figure 5-1.** Fractional contribution to light extinction coefficient bext from absorption ($b_{abs}$), particle scattering ($b_{sp}$), and scattering by gases (Rayleigh or $b_{sg}$) for the warm season at East Charleston.

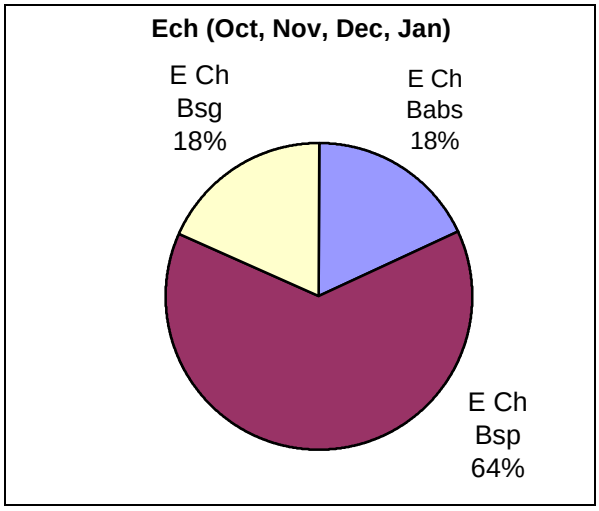


**Figure 5-2.** Fractional contribution to light extinction coefficient bext from absorption ($b_{abs}$), particle scattering ($b_{sp}$), and scattering by gases (Rayleigh or $b_{sg}$) for the cold season at East Charleston.

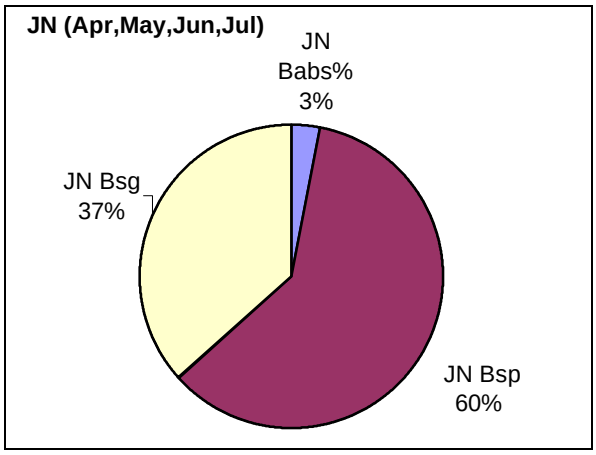


**Figure 5-3.** Fractional contribution to light extinction coefficient $b_{ext}$ from absorption ($b_{abs}$), particle scattering ($b_{sp}$), and scattering by gases (Rayleigh or $b_{sg}$) for the warm season at Jean.

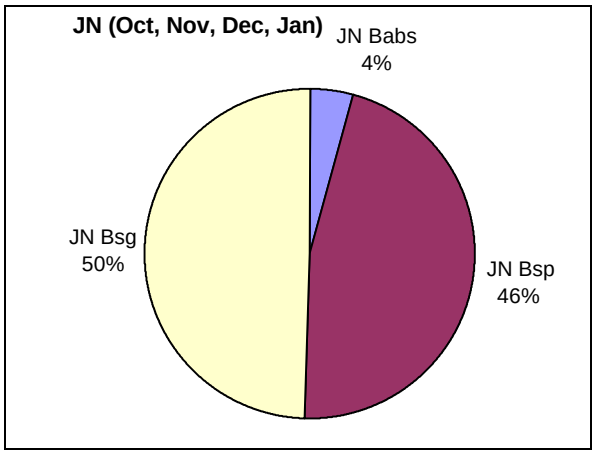


**Figure 5-4.** Fractional contribution to light extinction coefficient $b_{ext}$ from absorption ($b_{abs}$), particle scattering ($b_{sp}$), and scattering by gases (Rayleigh or $b_{sg}$) for the cold season at Jean.

vertical mixing of pollutants. Jean is located distant from urban sources and is rather clean in winter. In summer, transport of pollutants from other areas such as southern California is more frequent, leading to a greater fractional contribution to $b_{ext}$ from particle scattering (Figures 5-3 and 5-4).

Table 5-1 displays the percentages of contributions to $b_{ext}$ from $b_{abs}$, $b_{sp}$ and $b_{sg}$ at each site for the cold and warm season. The table also contains the total light extinction values for each site.

**Table 5-1.** Total light extinction coefficient and percentage contribution of each component ($b_{abs}$, $b_{sg}$, and $b_{sp}$) to the extinction coefficient during warm and cold seasons at each site.

| | Warm Season | | | | Cold Season | | | |
|---|---|---|---|---|---|---|---|---|
| Site | $b_{ext}$ ($Mm^{-1}$) | $b_{abs}$ (%) | $b_{sp}$ (%) | $b_{sg}$ (%) | $b_{ext}$ ($Mm^{-1}$) | $b_{abs}$ (%) | $b_{sp}$ (%) | $b_{sg}$ (%) |
| East Charleston | 40.3 | 11.6 | 59.5 | 28.9 | 74.6 | 18.0 | 63.6 | 18.3 |
| Jean | 29.5 | 2.9 | 60.5 | 36.6 | 21.6 | 4.3 | 46.3 | 49.5 |
| Palo Verde | 30.6 | 18.6 | 46.6 | 34.8 | 27.16 | 15.9 | 41.5 | 42.5 |

## 5.2 Comparison of Sites by Season

In this section, the patterns of scattering coefficient ($b_{scat}$) and absorption coefficient ($b_{abs}$) for the warm and cold seasons are compared at the three sites. At the East Charleston site, a distinct diurnal pattern is present for $b_{abs}$ during the cold season. This pattern is very visible at the 90$^{th}$ percentile (Figure 5-5). Overall, $b_{abs}$ values are higher during the cold season. A special point of interest is at midday when $b_{abs}$ values decrease at the East Charleston site. For a few hours around midday, $b_{abs}$ values are lower at the East Charleston site compared to the Palo Verde site during the cold season. This is due to good heating and mixing conditions at the East Charleston site at this time of the day.

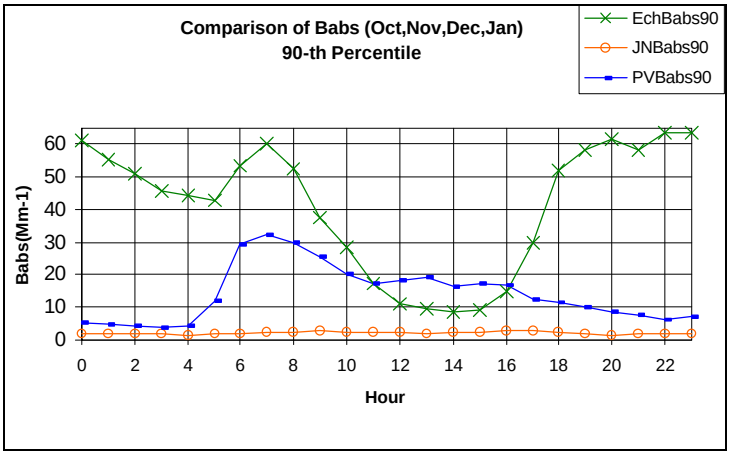


**Figure 5-5.** Cold season diurnal patterns in 90$^{th}$ percentile particle light absorption ($b_{abs}$) at the three sites.

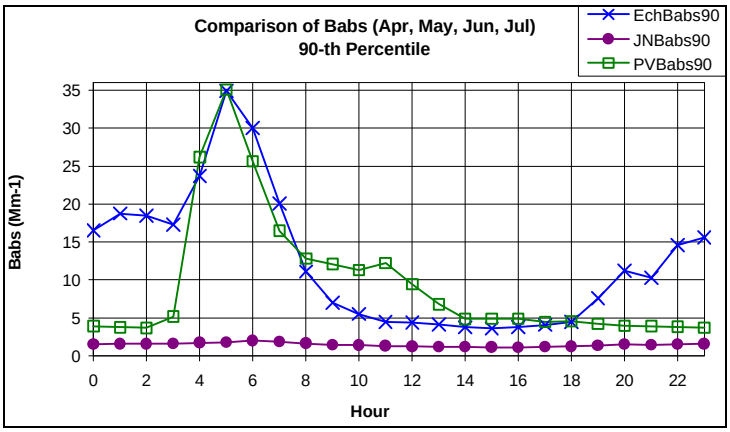


**Figure 5-6.** Warm season diurnal patterns in 90$^{th}$ percentile particle light absorption ($b_{abs}$) at the three sites.

After midday, $b_{abs}$ values at the East Charleston site increase and stay high through the night until the next day. $b_{abs}$ values are stable and low during both cold and warm seasons at the Jean site even at the 90$^{th}$ percentile. $b_{abs}$ values increase during morning at the Palo Verde site. There is a very small secondary peak present near midday. This peak is more noticeable during the warm season. The diurnal pattern at the East Charleston site is not present during the warm season, and East Charleston and Palo Verde show the same patterns of distribution for $b_{abs}$ values (Figure 5-6). $b_{abs}$ values peak early in the morning at the East Charleston and Palo Verde sites. The peak is sharper at the East Charleston site than at the Palo Verde site, and a secondary peak is visible near midday at the Palo Verde site. $b_{abs}$ values stay high through the night at the East Charleston site until the next day when they peak early in the morning.

$b_{scat}$ values follow a diurnal pattern similar to $b_{abs}$ values during the cold season. $b_{scat}$ values at the East Charleston site have a distinct diurnal pattern even at the 50th percentile (Figure 5-7). The Jean site does not show any diurnal patterns during cold or warm seasons even at the 90th percentile. $b_{scat}$ values at the Palo Verde site are closer to those at the Jean site than at the East Charleston site during both cold and warm seasons.

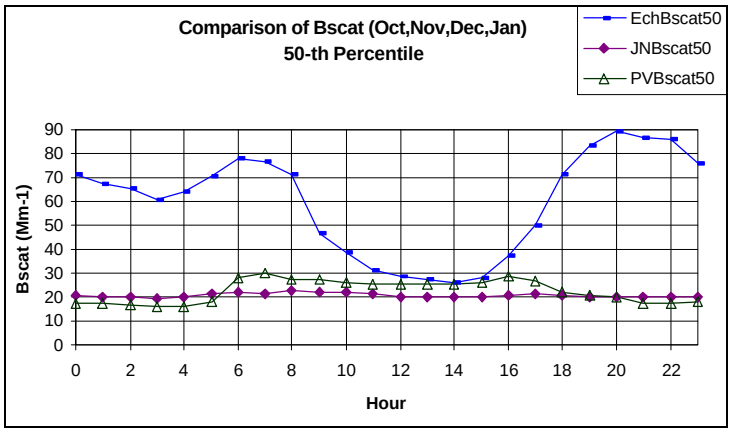


**Figure 5-7.** Cold season diurnal patterns in 90th percentile light scattering ($b_{scat}$) values at the East Charleston (Ech), Jean (JN), and Palo Verde (PV) sites.

## 5.3 Hourly Patterns of Haze for the Entire Study

In this section, patterns of haze at all three sites for the entire duration of the study are compared. $b_{abs}$ values at the Jean site are lower than at the other two sites during the entire study. The East Charleston site has very high $b_{abs}$ values. The ratios of $b_{abs}$ values at the East Charleston site to those at the Palo Verde site increase during the beginning and the end of each day. However, during midday, $b_{abs}$ values are higher at the Palo Verde site than at the East Charleston site. This is observable in the 10th, 50th, and 90th percentiles of the data (Figures 5-8 to 5-10). $b_{abs}$ values show a diurnal pattern at the East Charleston site, but at the Palo Verde site, they peak early in the morning and decrease by the end of the day. The tail of this peak is what causes the $b_{abs}$ values to be higher at the Palo Verde site than at the East Charleston site at midday. $b_{abs}$ values for Jean are stable. An early morning peak is barely present at this site in the 10th percentile, but it is not observable in the 50th or 90th percentiles.

A diurnal pattern is once again visible in $b_{scat}$ values at the East Charleston site. These values are very close at Jean and Palo Verde near midday in the 50th percentile (Figure 5-11).

The difference between East Charleston and Jean is evident when looking at Figure 5-12. For almost all hours except a few during midday, $b_{abs}$ 10th percentile values at East Charleston are higher than $b_{abs}$ 90th percentile values at Jean. Thus, even "clean" days at East Charleston have higher light absorption than "dirty" days at Jean.

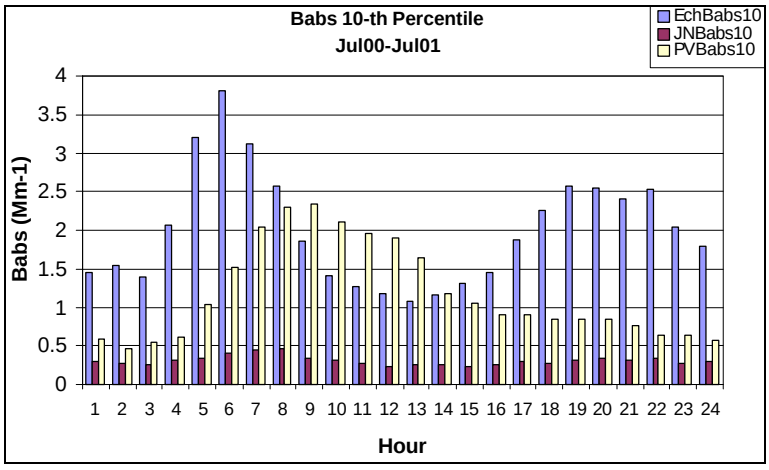


**Figure 5-8.** Comparison of 10th percentile absorption coefficient ($b_{abs}$) values from July 2000 to July 2001 at the East Charleston (Ech), Jean (JN), and Palo Verde (PV) sites.

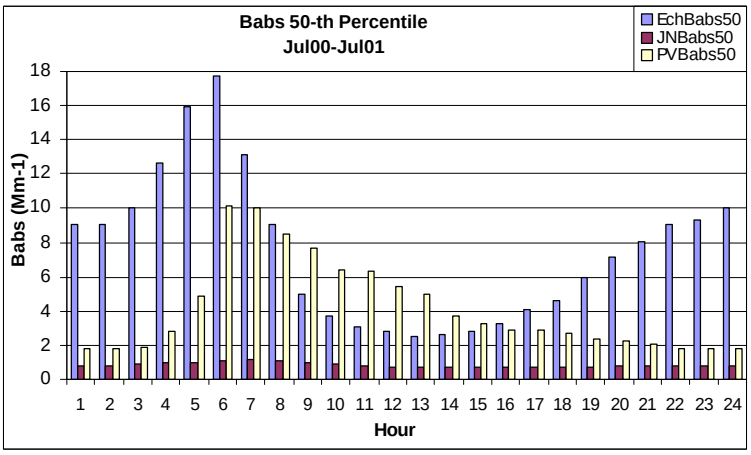


**Figure 5-9.** Comparison of 50th percentile absorption coefficient ($b_{abs}$) values at the East Charleston (Ech), Jean (JN), and Palo Verde (PV) sites (July 2000 – July 2001).

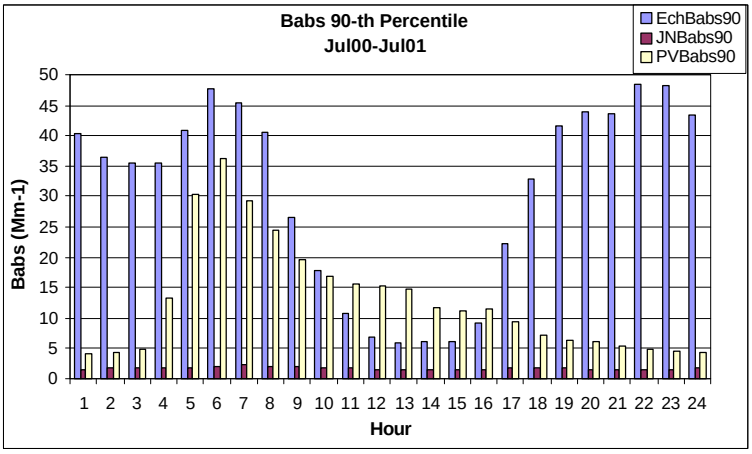


**Figure 5-10.** Comparison of 90th percentile absorption coefficient ($b_{abs}$) values at the East Charleston (Ech), Jean (JN), and Palo Verde (PV) sites (July 2000 – July 2001).

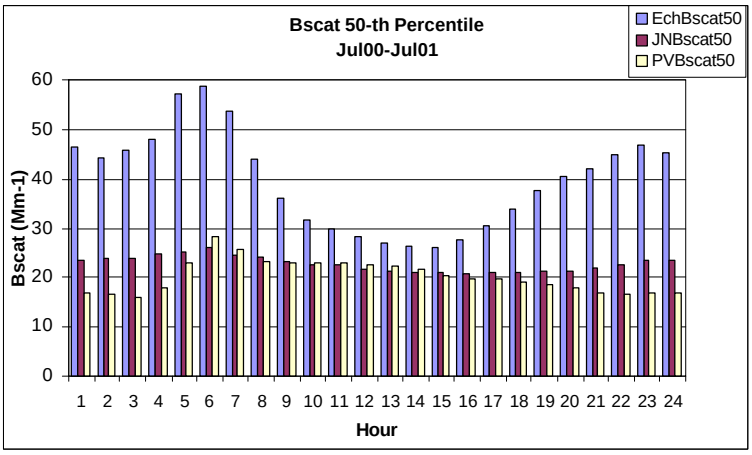


**Figure 5-11.** Comparison of 50$^{th}$ percentile light scattering ($b_{scat}$) values at the East Charleston (Ech), Jean (JN), and Palo Verde (PV) sites (July 2000 – July 2001).

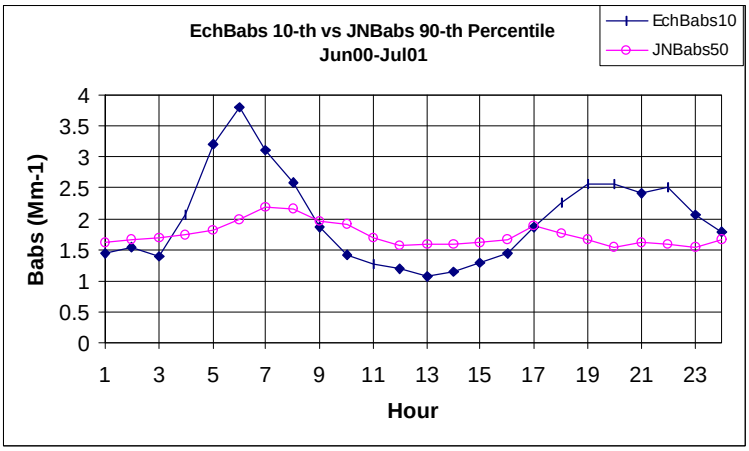


**Figure 5-12.** Comparison of 10$^{th}$ percentile absorption coefficient ($b_{abs}$) values at East Charleston (Ech) to 90$^{th}$ percentile $b_{abs}$ values at Jean (June 2000 – July 2001).

## 5.4 Diesel Impacts at Palo Verde

In Sections 5.2 and 5.3, it was shown that particle light absorption ($b_{abs}$) was typically highest at Palo Verde in the morning hours. Especially rapid increases in $b_{abs}$ in early morning were observed in August 2000. These were periods when school was not in session, but construction was occurring on the I-215 beltway immediately west of the high school grounds and less than 1 km from the monitoring site. Very large, rapid increases in $b_{abs}$ occurred often at about sunrise. Values peaked typically about 6 am PDT and then began decreasing. Hourly average $b_{abs}$ data at Palo Verde for one week in August are shown in Figure 5-13. Seven days are shown – the first five days with high values are Monday through Friday, and the last two days with much lower concentrations are Saturday and

Sunday. Wind data showed light downslope winds from the west during the early morning hours and then changing and becoming more upslope during late morning. These typical early morning downslope winds would transport emissions from the construction site toward the monitoring site under stable condition, with little vertical mixing. Later in the morning, greater mixing and changing wind directions would substantially reduce the impacts of emissions from the construction. Light scattering increased about the same absolute magnitude as light absorption, but much less as a percentage basis. The fraction of non-Rayleigh light extinction from absorption ($b_{abs}$) is shown in Figure 5-14. During periods without fresh diesel exhaust impacting the site, light absorption is only about 10% on the non-Rayleigh extinction, with scattering by particles ($b_{sp}$) being the remaining 90%. When diesel exhaust does influence the site, absorption and scattering by particles are about equal.

The magnitude of this impact and the large number of construction sites around the Las Vegas Valley suggest that construction-related diesel equipment may make a significant contribution to haze in the valley.

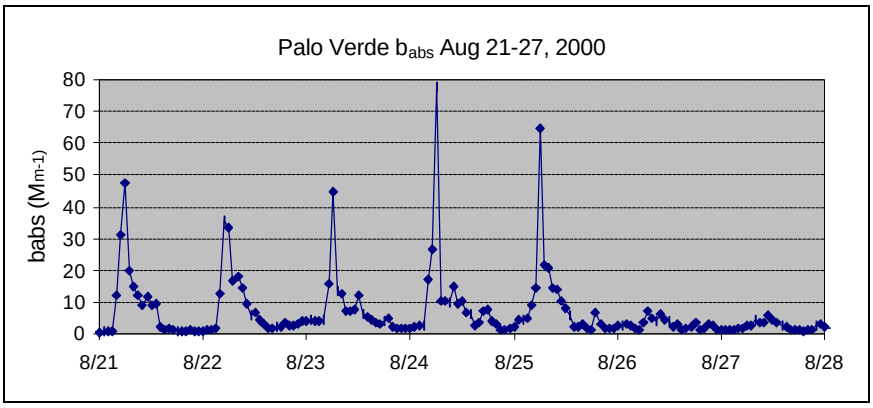


**Figure 5-13.** Hourly averaged particle light absorption ($b_{abs}$) at the Palo Verde site (August 21-27, 2000).

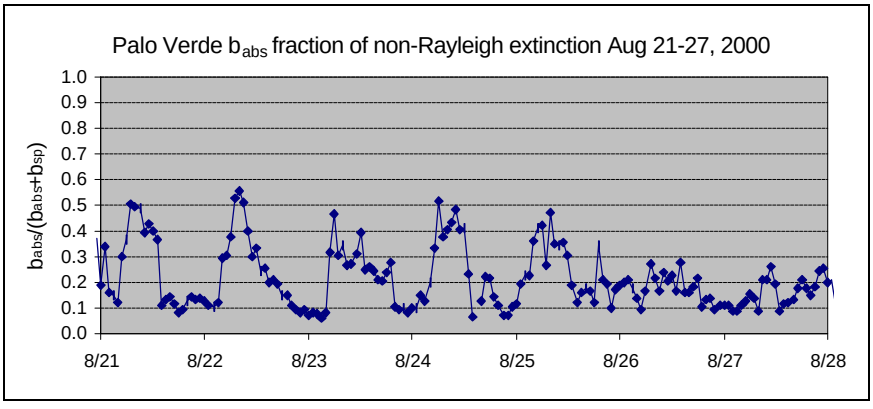


**Figure 5-14.** Hourly averaged fraction of non-Rayleigh light extinction caused by particle light absorption at the Palo Verde site (August 21-27, 2000).

# 6. CHEMICAL COMPOSITION OF HAZE

## 6.1 The Causes of Haze: An Overview of Visibility Science

Haze is caused by scattering and absorption of visible light by particles and gases. Haze is proportional to the light extinction coefficient, which is the sum of scattering and absorption by particles and gases. Symbolically, this can be expressed as:

$$b_{ext}=b_{sg}+b_{sp}+b_{ag}+b_{ap} \quad (6\text{-}1)$$

where $b_{ext}$ is the light extinction coefficient, $b_{sg}$ is the scattering by gases, $b_{sp}$ is the scattering by particles, $b_{ag}$ is absorption by gases, and $b_{ap}$ is absorption by particles. Sometimes $b_{sg}$ and $b_{sp}$ are added and denoted by $b_{scat}$, total light scattering by gases and particles. The scattering, absorption, and extinction coefficients represent the fraction of light energy removed per unit distance: $dE=-b_{ext}Edx$. In this document, we report the coefficients in units of inverse megameters ($Mm^{-1}$), where a megameter is 1 million meters or 1,000 km. For example an extinction coefficient of 100 $Mm^{-1}$ would be 1 per 10 km, and the fraction of light remaining after 10 km would be 1/e or about 37%.

Scattering of light has the effect of blurring views because light from different locations is effectively mixed together. Absorption of light removes light from the atmosphere (converts it into heat), making it hard to distinguish objects.

$B_{sg}$, scattering by gases, is often referred to as Rayleigh scattering and is almost totally from nitrogen and oxygen molecules that comprise 99% of atmospheric gases. Scattering by gases is strongest at the shorter wavelengths of visible light and thus gives the clear sky a blue color. In pristine conditions, $b_{sg}$ is the dominant component of light extinction.

$B_{sp}$, scattering by particles, typically is the largest component of light extinction. All particles (solid or liquid) scatter light. The main components are typically sulfates, nitrates, organic compounds, elemental carbon, and crustal material (soil or dust). Although the scattering is somewhat complicated (theoretically explained by Mie theory), the scattering by a particle is approximately proportional to its cross-sectional area ($\pi r^2$ for a spherical particle). For particles with diameter about the same wavelength of light (0.4-0.7 μm), the scattering is enhanced.

Individual big particles scatter more light than individual small particles, but less per unit mass. This is because scattering is proportional to cross-sectional area: $\pi r^2$, while mass is proportional to volume times density: $\rho\pi r^3$. Thus, scattering efficiency ($m^2/g$) defined as scattering per unit mass is proportional to:

$$\pi r^2/\ \rho\pi r^3=1/\rho r \quad (6\text{-}2)$$

so big particles (large r) are less efficient per unit mass at light scattering than small particles. Dense particles (large ρ) are less efficient than less dense particles.

Under periods of high relative humidity (over about 70% RH), hygroscopic particles (mainly sulfates and nitrate) will go into solution and grow rapidly with increasing relative humidity. Particle water growth is not typically a significant issue in Las Vegas, except for a few days per year. It is very important in much of the eastern U.S. and the west coast.

Light absorption by particles ($b_{ap}$) is dominated by particles containing elemental carbon (black carbon or soot). It is the absorption of light that causes these particles to be very dark. Absorption of light by gases ($b_{ag}$), is nearly all from nitrogen dioxide ($NO_2$). Nitrogen oxide (NO) is formed by high temperature combustion processes such as occurs in vehicles and electric power plants. Further oxidation converts the NO to $NO_2$, which preferentially absorbs light in the shorter wavelengths, leaving a yellow-brown coloring. It is most noticeable in power plant plumes, but also contributes a small amount to haze in urban areas.

## 6.2 Measured and Reconstructed Scattering, Absorption, and Extinction

As described in Sections 2.3 and 2.4, light scattering was measured by nephelometers and light absorption was derived from aethalometer measurements. These instruments give an estimate of all components of light extinction except for absorption by gases ($b_{ag}$). Light extinction can be estimated by adding the nephelometer scattering and aethalometer absorption. There are uncertainties with the measurements. In particular, as discussed in Section 3-5, the nephelometers miss some (perhaps half) of the coarse particle scattering. In addition, absorption due to particles is measured by the aethalometer on a filter tape rather than in the air. The use of aethalometer values could be off by a scaling factor and may systematically bias the results. This will be further discussed later.

In order to estimate the contribution of each major component specie (sulfate, nitrate, organics, elemental carbon, crustal) to haze, we will use literature-derived extinction efficiency factors for each major component. Adding up the scattering over each component gives us "reconstructed" scattering which can be compared to the nephelometer scattering values. If we are using appropriate scattering efficiencies for each component, the reconstructed and measured scattering should compare well. Similarly, we can compare aethalometer-derived absorption with absorption estimated using elemental carbon from the particulate samplers. To properly assign scattering coefficients to a sample, we need to know particle size, shape, and composition. However, good relationships between measured and reconstructed scattering has been achieved using standard scattering coefficients for the major components. Here we will use the scattering efficiencies used for the nationwide IMPROVE program (Malm et. al., 2000).

The following scattering efficiencies in $m^2g^{-1}$ are assumed and are multiplied by the component concentrations in $\mu g/m^3$ to obtain scattering in $Mm^{-1}$.

- $PM_{2.5}$ organic mass = 4, where organic mass = 1.4*organic carbon concentration
- $PM_{2.5}$ sulfate = 3*f(RH), where sulfate is assumed to be mass of ammonium sulfate $(NH_4)_2SO_4 = 1.375*SO_4^=$

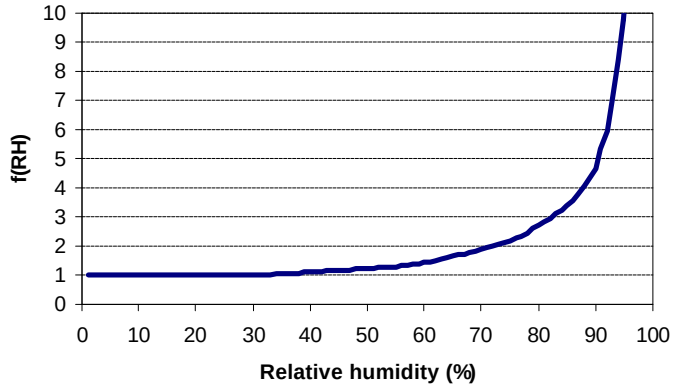


**Figure 6-1.** Relative humidity growth factor f(RH).

- $PM_{2.5}$ nitrate = 3*f(RH), where nitrate is assumed to be mass of ammonium nitrate $NH_4NO_3$ = 1.29*$NO_3^-$

- $PM_{2.5}$ crustal = 1

- Coarse mass ($PM_{10}$ mass-$PM_{2.5}$ mass) = 0.6

The relative humidity growth function f(RH) is shown in Figure 6-1.

We use an absorption efficiency for elemental carbon of 6 $m^2/g$, based upon a comparison of the aethalometer data and the DRI PM sampler elemental carbon concentrations discussed later in this section. This is lower than the 10 $m^2/g$ used for the IMPROVE program and would reduce the effects of elemental carbon upon haze compared to the IMPROVE method.

These calculations are made for all days with chemically speciated fine mass data. For the East Charleston site, the coarse mass was the difference between the DRI $PM_{10}$ and DRI $PM_{2.5}$ measurements. For the Palo Verde and Jean sites, coarse mass was defined as the difference between the Clark County DAQM Beta-attenuation monitor $PM_{10}$ concentration and the DRI $PM_{2.5}$ concentration.

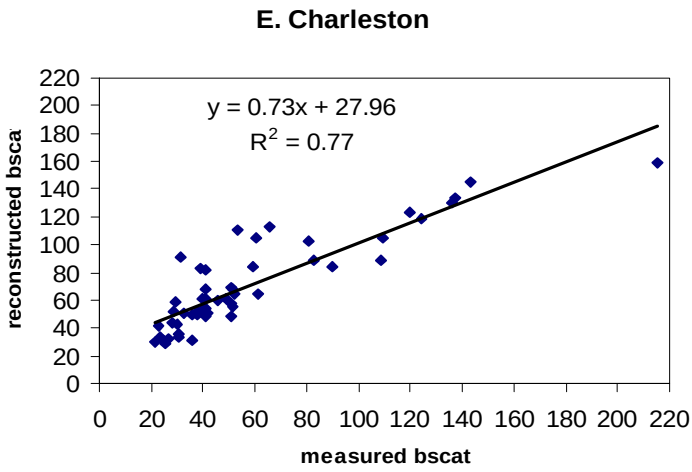


**Figure 6-2.** Measured and reconstructed scattering ($Mm^{-1}$) at East Charleston.

For this study, f(RH) was calculated hourly using data from McCarran airport. It was then averaged over each 24-hour sampling period with speciated chemistry data. For many days, f(RH) was essentially 1. The highest f(RH) for chemistry days was 1.88 on March 2, 2001.

Measured and reconstructed scattering at East Charleston are compared in Figure 6-2. There is a significant intercept, as at low measured $b_{scat}$, reconstructed $b_{scat}$ tends to be higher than measured. $PM_{2.5}$ mass concentration as measured by the Clark County FRM sampler at East Charleston is compared to $b_{scat}$ in Figure 6-3. Even without accounting for species specific concentrations and scattering by coarse particles, an excellent relationship between nephelometer scattering and FRM $PM_{2.5}$ concentration is apparent, with an $r^2$ of 0.95.

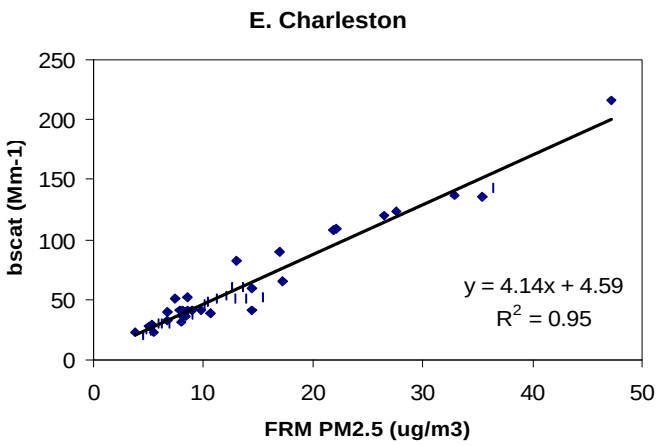


**Figure 6-3.** Measured scattering ($Mm^{-1}$) at East Charleston versus Clark County FRM $PM_{2.5}$ mass concentration ($\mu g/m^3$).

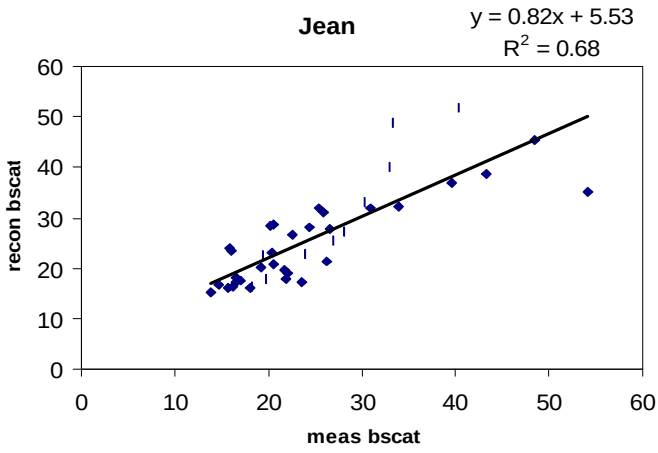


**Figure 6-4.** Measured and reconstructed scattering ($Mm^{-1}$) at Jean.

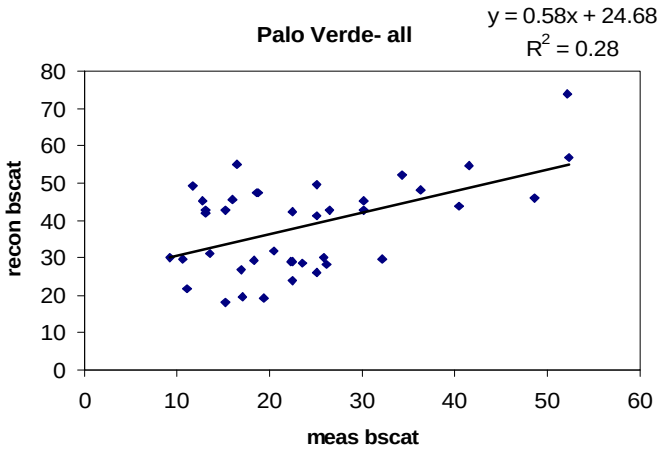


**Figure 6-5.** Measured and reconstructed scattering ($Mm^{-1}$) at Palo Verde.

Figures 6-4 and 6-5 show the measured versus reconstructed scattering at Jean and Palo Verde. These show more scatter than the data at East Charleston, especially at the Palo Verde site. This may be because the coarse mass scattering is a high percentage of total scattering at Palo Verde and is dependent upon differences between the DRI $PM_{2.5}$ SGS filter mass concentration and the Clark County beta attenuation monitor concentration (two very different types of measurements). Also, the coarse mass scattering component is highly dependent upon the particle size distribution which we do not know; thus much uncertainty in inherent in the reconstructed scattering calculation. While on a day-by-day basis there is not good agreement between reconstructed and measured scattering at Palo Verde, we can conclude that coarse particle scattering (due to crustal material) is important there. This will be shown in Section 6.3.

Aethalometer-derived light absorption is compared to elemental carbon concentrations in Figure 6-6. All sites are plotted together. Overall, the squared correlation coefficient ($R^2$) of 0.92 is quite satisfactory. The slope (absorption efficiency) is about 6 $m^2/g$, and the intercept is near zero. The efficiency is at the low end of the literature values, but is not unreasonable. The values for the Jean site appear to be too low for the elemental carbon concentration and would seem to indicate either a low bias for the aethalometer or a high bias for the EC concentration. The slope for the Palo Verde site is a bit higher than for the East Charleston site.

Total reconstructed extinction is compared to the sum of nephelometer scattering and aethalometer absorption for the East Charleston site in Figure 6-7. The $R^2$ for this relationship is 0.89.

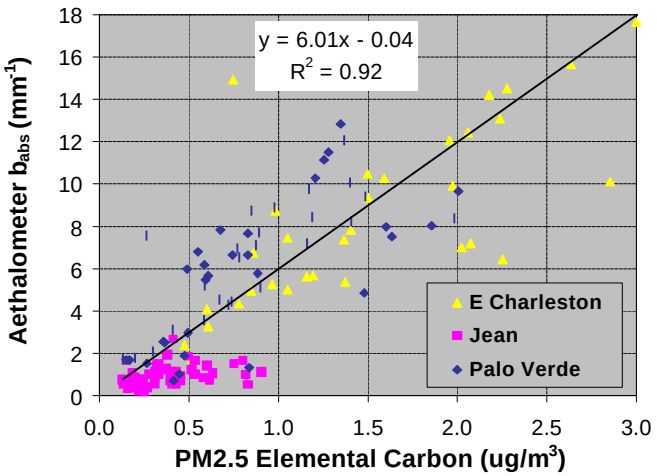


**Figure 6-6.** $PM_{2.5}$ elemental carbon ($\mu g/m^3$) versus aethalometer $b_{abs}$ ($Mm^{-1}$).

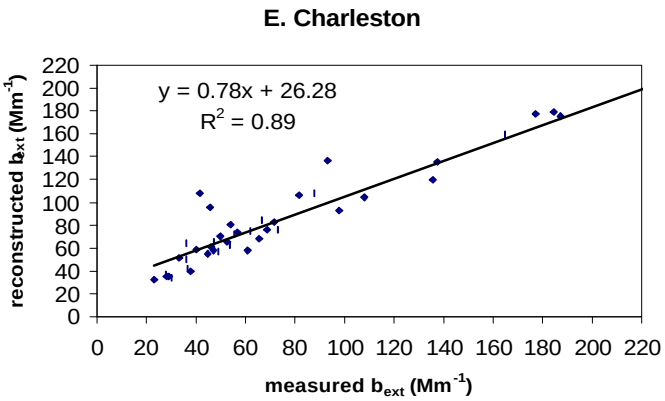


**Figure 6-7.** Measured versus reconstructed extinction for the East Charleston site.

## 6.3 Major Component Contributions to Haze

In this section we address the contributions of each major chemical component to haze at each of the three sites. We rely on reconstructed extinction calculations using the extinction efficiencies given in Section 6.2. Shown first is a summary averaged over the entire study period. Subsequently, the temporal variation of component contributions to extinction is shown.

Figure 6-8 and Table 6-1 show the chemical component contributions to the reconstructed light extinction coefficient in absolute terms ($Mm^{-1}$) at each site. At East Charleston, the values for organic and elemental carbon, in particular are much higher than at the other sites. Fine soil and coarse particle extinction are much higher at the East Charleston and Palo Verde sites than at the Jean site. Sulfate extinction is only a bit higher at East Charleston than at Jean and at Palo Verde it is about the same as at Jean.

Figure 6-9 and Table 6-2 show the percentage contribution of each component to total non-Rayleigh light extinction at each site. The percentage contribution of sulfates is much higher at Jean than the other sites. This is a result of the regional nature of sulfates and the higher concentrations of crustal and carbonaceous compounds at the urban (East Charleston) and suburban (Palo Verde) sites. Fine ($PM_{2.5}$) organic (41%) and elemental carbon (19%) account for fully 60% of the reconstructed extinction at the dirtiest site East Charleston. Fine soil and coarse mass (mostly crustal, some organic) account for 27% of the reconstructed extinction at East Charleston.

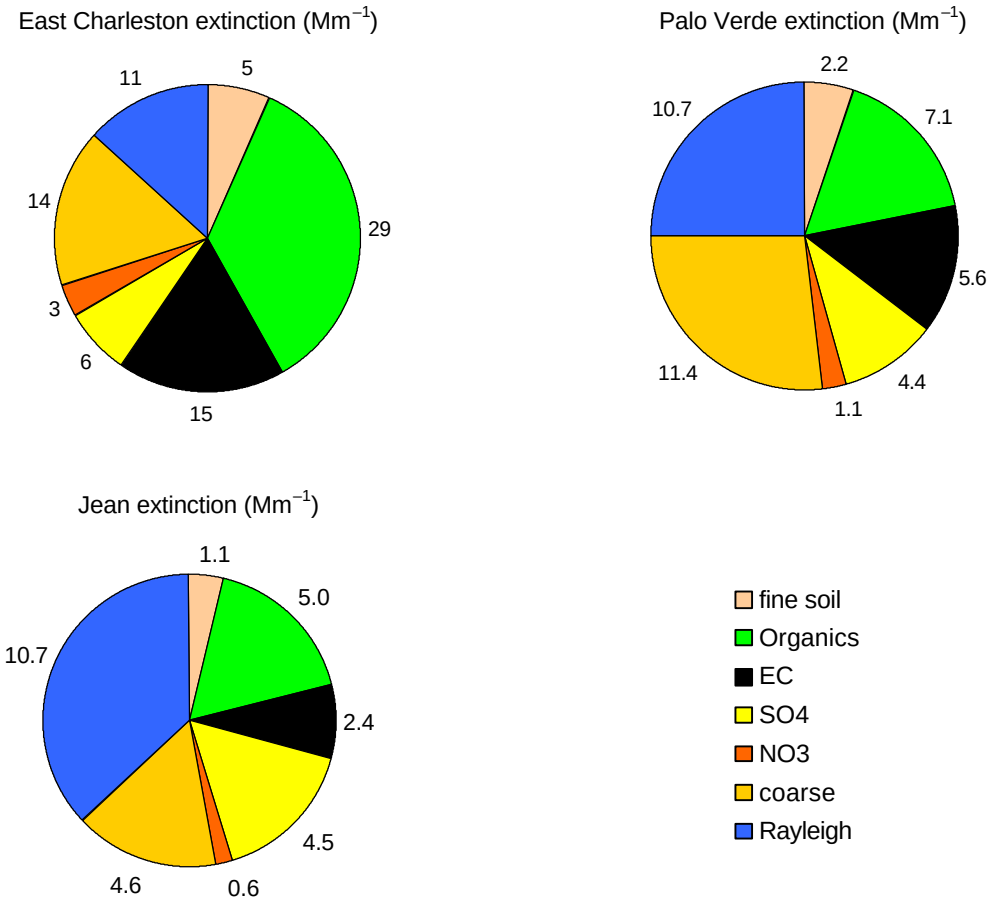


**Figure 6-8.** Contribution to light extinction by component at each site.

**Table 6-1.** Average reconstructed light extinction (Mm$^{-1}$) by component for each site.

| Site | Fine Organic | Elemental carbon | Fine Sulfate | Fine Nitrate | Fine Soil | Coarse Mass | Rayleigh |
|---|---|---|---|---|---|---|---|
| East Charleston | 29.2 | 14.6 | 6.0 | 2.7 | 5.4 | 13.9 | 11.0 |
| Palo Verde | 7.1 | 5.6 | 4.4 | 1.1 | 2.2 | 11.4 | 10.7 |
| Jean | 5.0 | 2.4 | 4.5 | 0.6 | 1.1 | 4.6 | 10.7 |

**Table 6-2.** Average percentage of non-Rayleigh extinction by component for each site.

| | Fine Organic | Elemental Carbon | Fine Sulfate | Fine Nitrate | Fine Soil | Coarse Mass |
|---|---|---|---|---|---|---|
| East Charleston | 41 | 19 | 10 | 3 | 8 | 19 |
| Palo Verde | 21 | 19 | 14 | 4 | 7 | 35 |
| Jean | 23 | 15 | 24 | 4 | 6 | 28 |

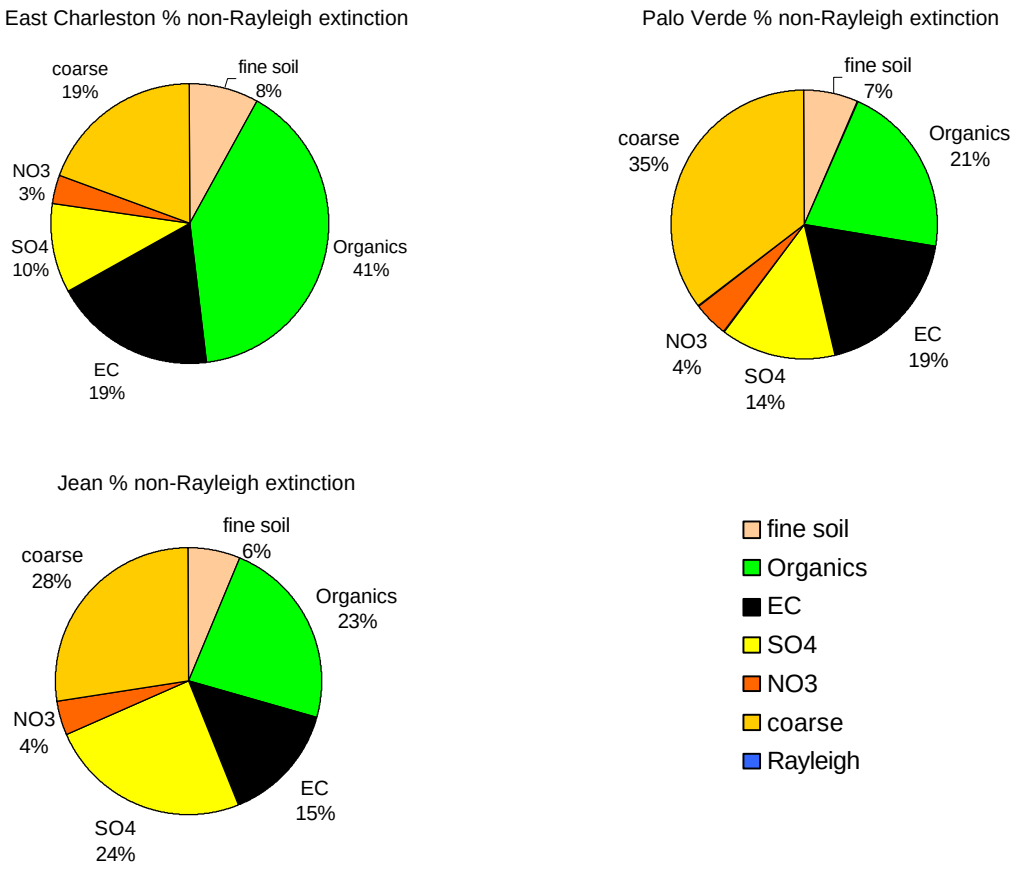


**Figure 6-9.** Percent of non-Rayleigh light extinction for each major component at each site.

At Palo Verde, crustal related compounds and carbonaceous compounds each account for about 40% of the reconstructed extinction. At Jean, the relative contributions of crustal related (34%) and carbonaceous compounds (38%) is also about evenly divided. However, sulfate is about 24% of the reconstructed extinction at Jean, higher than the other sites because the absolute contributions from the other compounds are lower at Jean.

In Figures 6-10 and 6-11, the absolute and relative component contributions to reconstructed extinction are shown for each sample period. These are the equivalent of Figures 6-8 and 6-9 except they show individual sample periods rather than an average over the entire study. Note that on many days in winter, more than half of the light extinction at Jean is attributable to Rayleigh scattering. During these same days at East Charleston, less than 10% of the scattering is attributable to Rayleigh. When haze is greatest at East Charleston, it is the least hazy at Jean. These are winter conditions with light winds, little vertical mixing, and also little transport of pollutants. Thus, at the low-lying urban site of East Charleston, particles build up and it is very hazy. The Jean site does not experience significant transport of pollutant from other areas (such as southern California) and may also be at an elevation that is above any locally generated pollution (e.g., I-15); thus conditions are very clean.

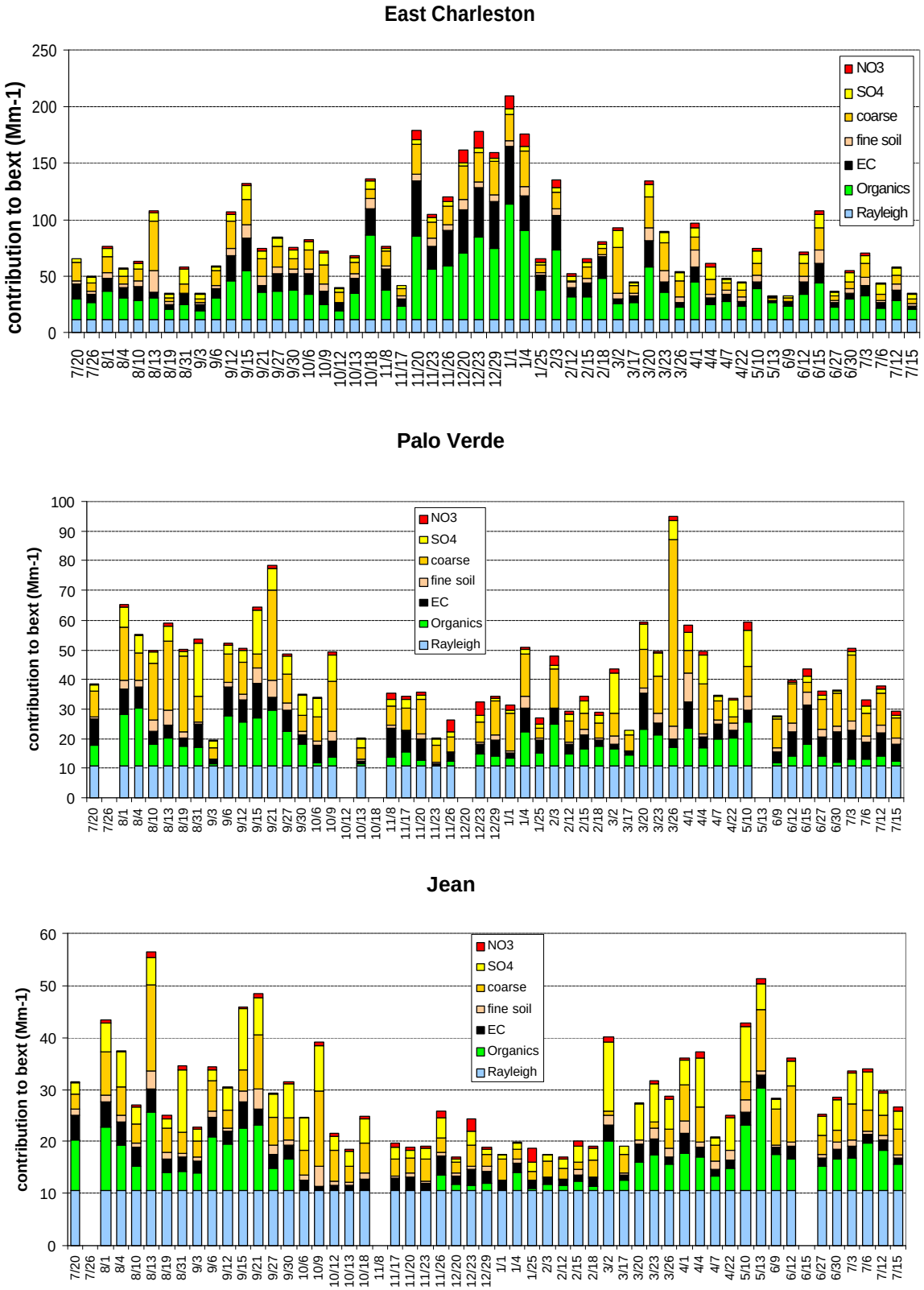


**Figure 6-10.** Daily contributions to $b_{ext}$ ($Mm^{-1}$) by component (07/20/00 to 07/21/01).

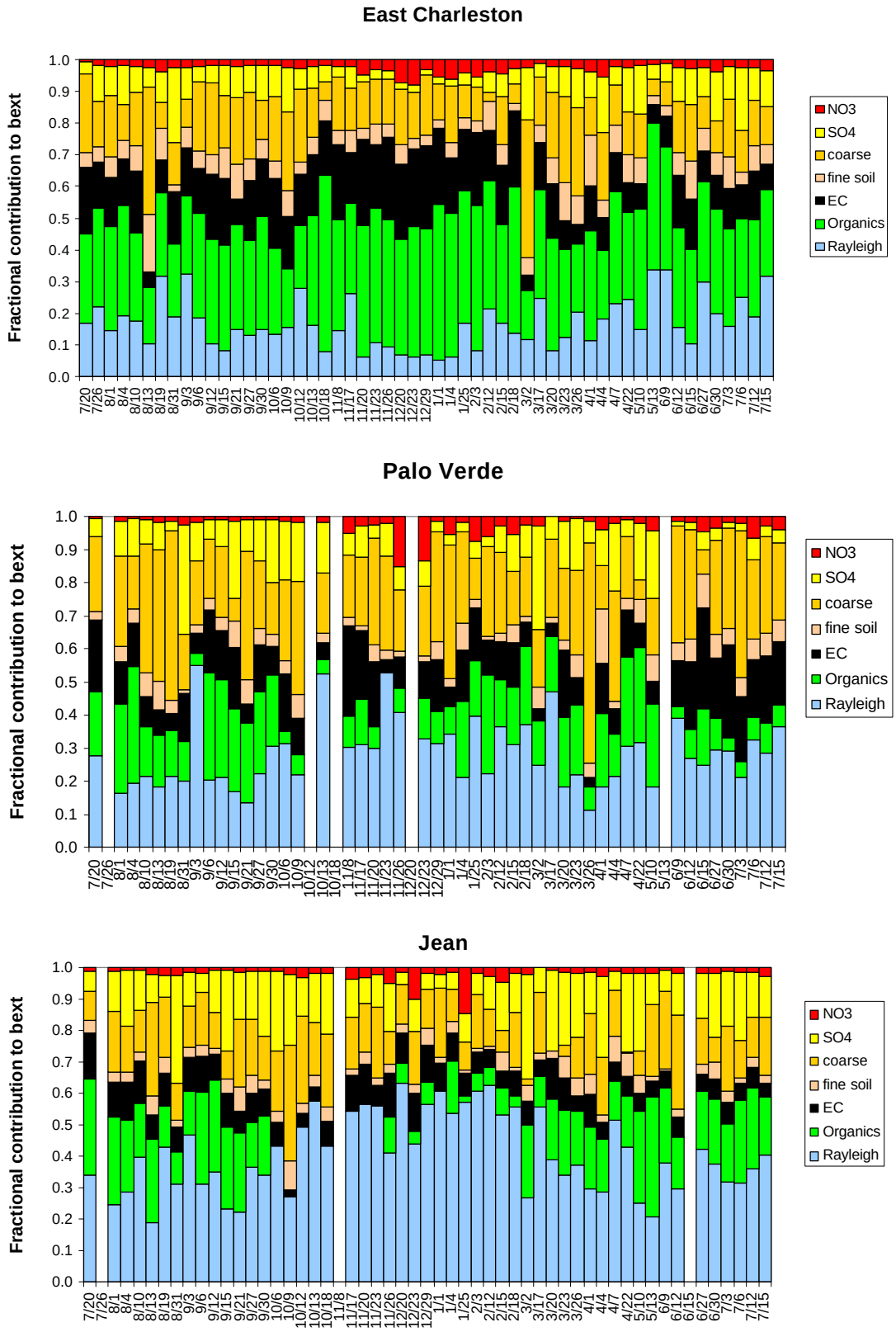


**Figure 6-11.** Daily fractional contributions to reconstructed extinction by component.

## 6.4 Local and Background Contributions to Haze by Chemical Component

When considering the potential benefits of control strategies for locally generated pollutants, it is necessary to know the portion of the problem that is due to local versus regional or background sources. For example, if the background level of haze is high, then controlling local sources would have a rather limited effect. On the other hand, if local sources are responsible for most of the haze, then controlling local sources could lead to substantial improvements in visibility. In this section we give estimates of the local and background contributions to haze in the Las Vegas Valley, specifically at the East Charleston and Palo Verde sites.

Because the prevailing wind flow patterns do not transport emissions from the Las Vegas Valley to the Jean monitoring site, it can be expected on most sampling days to be a background site, representing regional haze levels rather than local influences from the Las Vegas urban area. Winter days when haze is most intense at the East Charleston site are the cleanest days at the Jean site. Summer transport is almost always from the south or southwest, conditions that would transport Las Vegas haze away from the Jean site. Comparisons of the speciated Jean data to remote IMPROVE monitoring sites in the southwest indicate that concentrations of carbon, sulfate, and crustal material may be slightly enhanced at the Jean site (see Malm et al., 2000). The Jean site appears to have some impact from a nearby dirt road and emissions from traffic on I-15. The overall $PM_{2.5}$ annual average concentration at Jean of 3.88 $gm^{-3}$ at Jean is a bit higher than the 3.1 $\mu gm^{-3}$ annual average (1996-1998) at the Grand Canyon and the average $PM_{2.5}$ concentration at Death Valley of 3.5 μgm-3 (1994-1999), (concentrations adjusted to Jean elevation).

With the limitations described above, the $PM_{2.5}$ concentrations at the Jean site can be considered background and the difference between these values and the values at the East Charleston and Palo Verde sites can be attributed to local sources within the Las Vegas Valley (local contributions somewhat underestimated). In order to obtain the effects on haze, the component contributions to extinction can be compared for the local and background sources. Figure 6-12 and Table 6-3 show the amount of non-Rayleigh light extinction at the East Charleston and Palo Verde sites due to local and background sources. Figure 6-13 and Table 6-4 show this information on a percentage basis for each chemical component.

The components with substantial local contributions to haze are fine organics, elemental carbon, and crustal related (fine soil + coarse mass). Overall, about 75% of the non-Rayleigh extinction at East Charleston and 43% of the non-Rayleigh extinction at Palo Verde is from local sources. Only 24% of the sulfate extinction at East Charleston is local, but over 80% of the organic and elemental carbon extinction is from local sources. Nearly 80% of the fine soil and two-thirds of the coarse mass extinction is local at East Charleston. At Palo Verde, all the sulfate extinction is background, but half of the fine soil and 60% of the coarse mass are local. About 30% of the organic extinction and 58% of the elemental carbon extinction is local at Palo Verde. Nitrate extinction ranges from 50% local at Palo Verde to about 80% local at East Charleston, but is low except for a few winter days.

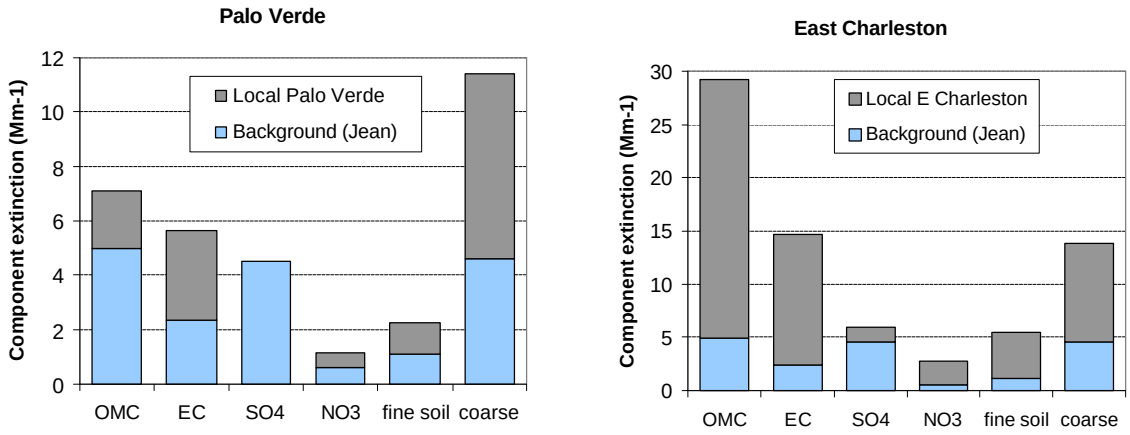


**Figure 6-12.** Local and background contributions to $b_{ext}$ ($Mm^{-1}$) by chemical component at the East Charleston and Palo Verde sites.

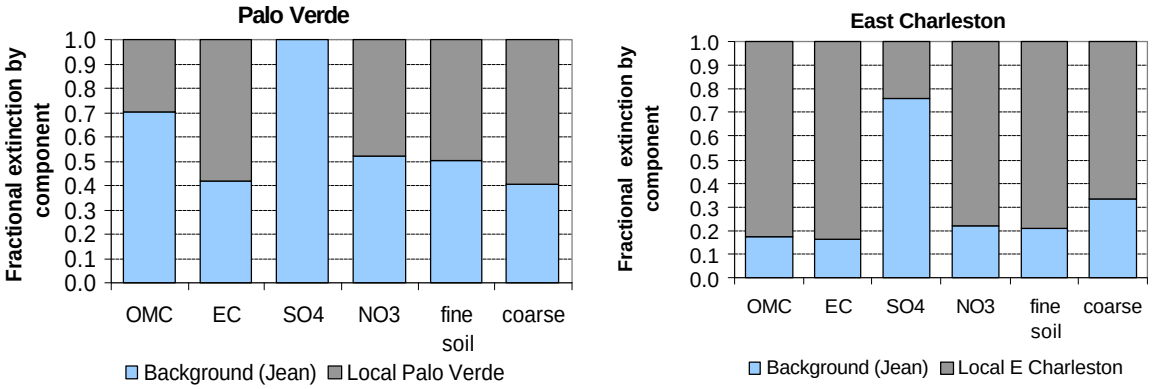


**Figure 6-13.** Fractional local and background contributions to $b_{ext}$ by chemical component at the East Charleston and Palo Verde sites.

**Table 6-3.** Total, local, and background reconstructed $b_{ext}$ by chemical component at the East Charleston and Palo Verde sites.

| | OMC | EC | $SO_4$ | $NO_3$ | Fine Soil | Coarse | Total |
|---|---|---|---|---|---|---|---|
| E Charleston total | 29.2 | 14.6 | 6.0 | 2.7 | 5.4 | 13.9 | 71.9 |
| Local E Charleston | 24.2 | 12.3 | 1.5 | 2.1 | 4.3 | 9.3 | 53.6 |
| Background | 5.0 | 2.4 | 4.5 | 0.6 | 1.1 | 4.6 | 18.2 |
| | | | | | | | |
| Palo Verde total | 7.1 | 5.6 | 4.4 | 1.1 | 2.2 | 11.4 | 32.1 |
| Local Palo Verde | 2.1 | 3.3 | 0.0 | 0.6 | 1.1 | 6.8 | 13.9 |
| Background | 5.0 | 2.4 | 4.5 | 0.6 | 1.1 | 4.6 | 18.2 |

**Table 6-4.** Fractional local and background contributions to $b_{ext}$ by chemical component at the East Charleston and Palo Verde sites.

| | OMC | EC | $SO_4$ | $NO_3$ | Fine Soil | Coarse | Total |
|---|---|---|---|---|---|---|---|
| Local E Charleston | 83.0 | 83.9 | 24.3 | 78.0 | 79.3 | 66.7 | 74.6 |
| Background | 17.0 | 16.1 | 75.7 | 22.0 | 20.7 | 33.3 | 25.4 |
| Local Palo Verde | 30.0 | 58.1 | 0.0 | 48.1 | 49.8 | 59.4 | 43.2 |
| Background | 70.0 | 41.9 | 100.0 | 51.9 | 50.2 | 40.6 | 56.8 |

Figure 6-14 shows the estimated local and background contributions to haze at East Charleston for each day with chemically speciated data. On the haziest days, which occur in winter, the haze is overwhelmingly local. On some summer days and clean winter days, background is equal or greater than local contributions.

These results demonstrate that a majority of the haze in the Las Vegas Valley is from sources within the valley (i.e., is "home-grown"). This affords an opportunity for the community to reduce haze by reducing local emissions. Controlling sources of elemental and organic carbon and crustal material (dust) within the Las Vegas Valley could substantially reduce haze. As discussed below in sections 7 and 8, additional work needs to be done, particularly for sources of elemental and organic carbon, to determine the relative contributions of specific source types to haze and the technical and economic feasibility of reducing emissions from these sources.

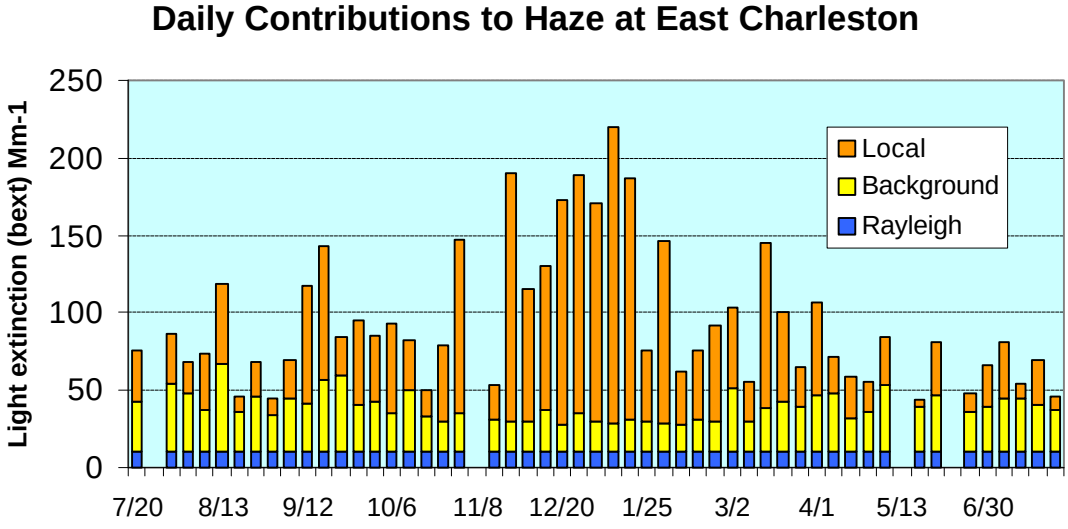


**Figure 6-14.** Local, background, and Rayleigh estimated contributions to haze at East Charleston on days with speciated chemistry data.

# 7. DISCUSSION OF SOURCE TYPE CONTRIBUTIONS TO $PM_{2.5}$ AND HAZE

In Sections 4 and 6, we discussed the contribution of each major chemical component to $PM_{2.5}$ and haze at the urban, suburban, and background/transport sites. $PM_{2.5}$ and haze were far higher at the East Charleston site than at the other locations. For the urban area, the East Charleston and Palo Verde sites are likely representative of the range of conditions from dirty to clean. Typical conditions within the urban area are probably intermediate between these two locations in terms of $PM_{2.5}$ and haze levels. The East Charleston site is in an area with little nearby construction or disturbed vacant land. However, crustal material still constitutes about half of the $PM_{10}$ and an estimated 27% of the haze (non-Rayleigh light extinction). Presumably much of this crustal material is road dust and material transported from upwind areas with disturbed land and construction activity. Areas with extensive disturbed land and construction would be expected to have a higher contribution to haze than the East Charleston site.

At the Palo Verde site, some construction activities were occurring nearby (e.g., the beltway), and crustal components were estimated to contribute 42% of the haze and about 26% of the $PM_{2.5}$, although the SGS sampler may overestimate the $PM_{2.5}$ crustal material due to its use of a cyclone to restrict large particles from entering the sampler. While the percent of haze due to crustal components is larger at Palo Verde than East Charleston, the actual values of the crustal-generated haze at Palo Verde are about two-thirds of those at East Charleston.

Organic and elemental carbon compounds are very significant sources of $PM_{2.5}$ and haze at the East Charleston and Palo Verde sites. Fine carbonaceous compounds account for over half of the $PM_{2.5}$ mass and about 60% of the haze at East Charleston. At Palo Verde, 42% of the $PM_{2.5}$ mass and 40% of the haze are caused by carbonaceous compounds. By comparison with Jean as the background, most (>80%) of the organic mass and elemental carbon at East Charleston is locally (within the Las Vegas Valley) generated (Figure 6-13 and Table 6-4). At Palo Verde, less than half of the organic mass (~30%), but nearly 60% of the elemental carbon are locally produced. At the Palo Verde site for the early part of the study, construction on the beltway west of the school was clearly contributing substantially to both light scattering and absorption due to diesel equipment emissions, which are rich in organic and elemental carbon. However, due to the location of the monitoring site at the entrance/exit of a large parking lot at the high school, it is also likely that impacts from diesel school buses and personal vehicles of the students, faculty, and staff were contributing to carbonaceous and road dust concentrations. Overall, over half of the $PM_{2.5}$ and haze at Palo Verde is estimated to result from sources outside the Las Vegas Valley, using Jean as a background/transport site.

The large contributions of carbonaceous compounds to haze at East Charleston could come from a variety of sources. Previous studies of high CO concentrations in the area suggested that pollutants tend to accumulate in this area from much of the valley, as well as buildup of pollutants from nearby sources (Bowen and Egami, 1994). Diesel and gasoline vehicles would be expected to contribute substantially to the observed concentrations. As the

site is located in a relatively low-income area, there may be a relatively high number of older vehicles with higher emissions. Additional sources could include meat cooking (a restaurant is located adjacent to the site) as well as wood burning during the winter months. Crustal and carbonaceous compounds could also be transported in from sources (e.g., construction activities) in outlying areas.

Fine particulate sulfate is a relatively minor component of $PM_{2.5}$ and haze at East Charleston, a bit more significant at Palo Verde, and fairly significant at Jean. This difference among sites is a result of the regional nature of fine sulfate – fine sulfate is essentially all background at Palo Verde and about 75% background at East Charleston. The sulfur content of gasoline and diesel fuel used in the Las Vegas Valley is low, so substantial concentrations of sulfate from fuel combustion would not be expected, although a small contribution is likely. Some of the excess fine sulfate at East Charleston may in fact be fine $CaSO_4$ (gypsum) rather than from fuel combustion.

Fine particulate nitrate concentrations are generally low at all sites, although they are occasionally elevated at the Palo Verde and East Charleston sites in winter. The ammonium ion data indicates that fine nitrate is in the form of ammonium nitrate, which results from reactions involving ammonia gas and nitrogen oxides. Nitrogen oxide emissions in the valley result from numerous sources including motor vehicles, construction equipment, aircraft, power generation, home heating, etc. Motor vehicles are expected to be the largest source.

Section 8 discusses additional work that would better determine the impact of specific sources types to $PM_{2.5}$ and haze.

# 8. RECOMMENDATIONS FOR ADDITIONAL WORK

Analysis indicates that in the Las Vegas Valley overall, a majority of $PM_{2.5}$ and haze is due to local (within Las Vegas Valley) sources. At the East Charleston site, over 75% of the $PM_{2.5}$ and haze are caused by sources within the Las Vegas Valley. The major local contributors to haze and $PM_{2.5}$ in the valley are sources of crustal (dust) material and organic and elemental carbon. Reducing emissions of these compounds is necessary to improve visibility and reduce $PM_{2.5}$ in the Las Vegas area.

If the measures committed to in the $PM_{10}$ State Implementation Plan submitted to the USEPA are successful, $PM_{10}$ levels will be reduced and the area will be in compliance with the National Ambient Air Quality Standard for $PM_{10}$. While this will have beneficial effects in reducing haze (and $PM_{2.5}$ to a lesser extent), PM levels (both $PM_{10}$ and $PM_{2.5}$) that meet the health-based NAAQS may still result in significant visibility impacts. The major sources of crustal material appear to be well known (construction activities, disturbed vacant land, road dust), but the actual emissions rates and relative importance of these sources are still somewhat uncertain. It is recommended that work on obtaining scientifically sound measures of crustal emissions from the major source types should be continued. For example, paved road dust is considered a major "source", but it is unknown as to the quantities of road dust that are due to atmospheric deposition from sources such as disturbed vacant land and construction activities, or how much is due to sources such as track-out and re-entrainment from unpaved shoulders. Better temporal and spatial measurements of crustal emissions such as the TRAKER method (Etyemezian et al., 2002) are encouraged to better understand the source contributions. Activities to better quantify these uncertainties so that cost-effective control strategies may be developed are strongly encouraged. Continued reductions in crustal emissions are needed for reducing the valley's haze.

Sources of organic and elemental carbon are estimated to contribute more than half of the $PM_{2.5}$ and haze at the East Charleston site, about 40% at Palo Verde, and are expected to be important contributors throughout the valley. Particularly for organic carbon, there are many different carbonaceous source types in urban areas such as gasoline and diesel on-road and off-road vehicles, construction equipment, wood burning, meat cooking, dry cleaning, lawn and garden equipment, vegetation, etc. Due to the sheer numbers, gasoline on-road vehicles are certain to be a large share of these emissions. Due to the large amount of construction activity taking place in the Las Vegas area, emissions from diesel construction equipment need to be better determined. Data from Palo Verde High School indicates that these sources can have very large visibility effects near the sources. As construction sites are widely distributed throughout the valley, especially the edges of the valley, the cumulative impact could be quite significant. In addition, strict standards for on-road diesel are being phased in; without additional controls on off-road diesel, these will take on a greater relative importance in the future.

Better emissions inventories for organic and elemental carbon particulate matter should be developed. This should include improved emissions factors based upon real-world, in-use measurements as well as accurate measures of activity levels.

Speciation of particulate organic carbon may help to apportion the carbon between major source types such as diesel vs. gasoline vehicles, wood smoke, and meat cooking. This involves obtaining a relatively large amount of particulate matter and then performing gas chromatography-mass spectroscopy (GC-MS) on the sample. Certain compounds have been identified as marker species (e.g., Fujita et al., 1998). These were used in Denver to apportion carbon to various sources (Fujita et al., 1998). A limitation in the method is that most of the organic material is composed of compounds that are not identified in the analysis. This leads to inherent uncertainty in the apportionment. Either additional samples could be collected specifically for this purpose, or composites of samples from East Charleston could be used and subjected to the analysis. The East Charleston site has very high levels of carbonaceous materials, and by compositing a month or more of samples, a sufficient mass for the analysis could be obtained. Composites could be made for winter and summer periods, for example. There are both $PM_{10}$ and $PM_{2.5}$ samples at East Charleston that could be used.

As a limitation of the current study is that the $PM_{2.5}$ chemical speciation and light scattering and absorption measurements were made at only two sites in the urban area. These sites probably represented the range of conditions. However, the large differences in $PM_{2.5}$ concentrations and haze levels at the two sites make it problematic to generalize results to the entire valley. It is recommended that chemically speciated $PM_{2.5}$ data be obtained for a few locations in the valley that would represent a better mix of conditions. These could be done for relatively short periods in the winter and summer to get a better idea of the spatial patterns in chemical composition. Aethalometers and nephelometers installed at these sites would also be helpful by providing high-time-resolution light scattering and absorption data.

In the meantime, $PM_{2.5}$ data from the CCDAQM sites should be analyzed for spatial and temporal patterns. It should also be compared to beta-attenuation monitoring $PM_{10}$ at these sites.

# 9. REFERENCES


Bevington, P.R. (1969). *Data Reduction and Error Analysis for the Physical Sciences*. McGraw Hill, New York, NY.

Bowen, J.L.; and Egami, R.T. (1994). Clark County Carbon Monoxide Hotspot Study. Report No. DRI 6460-684-4010.1F1. Prepared for Clark County Health District, Las Vegas, NV, by Desert Research Institute, Reno, NV.

Chow, J.C.; and Watson, J.G. (1989). Summary of particulate data bases for receptor modeling in the United States. In *Transactions, Receptor Models in Air Resources Management*, J.G. Watson, Ed. Air & Waste Management Association, Pittsburgh, PA, pp. 108-133.

Chow, J.C.; Liu, C.S.; Cassmassi, J.C.; Watson, J.G.; Lu, Z.; and Pritchett, L.C. (1992). A neighborhood-scale study of $PM_{10}$ source contributions in Rubidoux, California. *Atmos. Environ.*, **26A**(4):693-706.

Chow, J.C.; Watson, J.G.; Lowenthal, D.H.; Solomon, P.A.; Magliano, K.L.; Ziman, S.D.; and Richards, L.W. (1993a). $PM_{10}$ and $PM_{2.5}$ compositions in California's San Joaquin Valley. *Aerosol Sci. Technol.*, **18**:105-128.

Chow, J.C.; Watson, J.G.; Pritchett, L.C.; Pierson, W.R.; Frazier, C.A.; and Purcell, R.G. (1993b). The DRI Thermal/Optical Reflectance carbon analysis system: Description, evaluation and applications in U.S. air quality studies. *Atmos. Environ.*, **27A**(8):1185-1201.

Chow, J.C.; Fujita, E.M.; Watson, J.G.; Lu, Z.; Lawson, D.R.; and Ashbaugh, L.L. (1994). Evaluation of filter-based aerosol measurements during the 1987 Southern California Air Quality Study. *Environmental Monitoring and Assessment*, **30**:49-80.

Chow, J.C.; and Watson, J.G. (1994). Guidelines for $PM_{10}$ sampling and analysis applicable to receptor modeling. Report No. EPA-452/R-94-009. Prepared for U.S. EPA, Office of Air Quality Planning and Standards, Research Triangle Park, NC, by Desert Research Institute, Reno, NV.

Chow, J.C.; Watson, J.G.; Lu, Z.; Lowenthal, D.H.; Frazier, C.A.; Solomon, P.A.; Thuillier, R.H.; and Magliano, K.L. (1996). Descriptive analysis of $PM_{2.5}$ and $PM_{10}$ at regionally representative locations during SJVAQS/AUSPEX. *Atmos. Environ.*, **30**(12):2079-2112.

Chow, J.C.; and Watson, J.G. (1997). Fugitive dust and other source contributions to $PM_{10}$ in Nevada's Las Vegas Valley. Report No. 4039.1F. Prepared for Clark County Department of Comprehensive Planning, Las Vegas, NV, by Desert Research Institute, Reno, NV.

Chow, J.C.; and Watson, J.G. (1999). Ion chromatography in elemental analysis. In *Elemental Analysis of Airborne Particles, Vol. 1,* S. Landsberger and M. Creatchman, Eds. Gordon and Breach Science, Amsterdam, pp. 97-137.

Chow, J.C.; Watson, J.G.; Crow, D.; Lowenthal, D.H.; and Merrifield, T. (2001). Comparison of IMPROVE and NIOSH carbon measurements. *Aerosol Sci. Technol.,* **34**(1):23-34.

Chow, J.C.; Watson, J.G.; Edgerton, S.A.; and Vega, E. (2002). Chemical composition of $PM_{10}$ and $PM_{2.5}$ in Mexico City during winter 1997. *Sci. Total Environ.,* in press.

Fujita, E.M.; Watson, J.G.; Chow, J.C.; Robinson, N.F.; Richards, L.W.; and Kumar, N. (1998). Northern Front Range Air Quality Study. Volume C: Source apportionment and simulation methods and evaluation. Prepared for Colorado State University, Cooperative Institute for Research in the Atmosphere, Ft. Collins, CO, by Desert Research Institute, Reno, NV. http://charon.cira.colostate.edu/DRIFinal/ZipFiles/.

Green, M.C.; and Chow, J.C. (1997). Program Plan for $PM_{2.5}$ and Urban Haze in the Las Vegas Valley. Prepared for Clark County Department of Comprehensive Planning, Las Vegas, NV, by Desert Research Institute, Reno, NV. December 19, 1997.

Green, M.C.; and Gebhart, K.A. (1997). Clean air corridors: A geographic and meteorologic characterization. *JAWMA,* **47**(3):403-410.

Hansen, A.D.A. (1999). *The Aethalometer*. Magee Scientific Co., Berkeley, CA.

Hering, S.V.; and Cass, G.R. (1999). The magnitude of bias in the measurement of $PM_{2.5}$ arising from volatilization of particulate nitrate from Teflon filters. *JAWMA,* **49**(6):725-733.

Hidy, G.M. (1985). Jekyll Island meeting report: George Hidy reports on the acquisition of reliable atmospheric data. *Environ. Sci. Technol.,* **19**(11):1032-1033.

Lioy, P.J.; Watson, J.G.; and Spengler, J.D. (1980). APCA specialty conference workshop on baseline data for inhalable particulate matter. *JAPCA,* **30**(10):1126-1130.

Lloyd, A.C.; and Cackette, T.A. (2001). 2001 critical review – Diesel engines: Environmental impact and control. *JAWMA,* **51**(6):809-847.

Malm, W.C.; Pitchford, M.L.; Scruggs, M.; Sisler, J.F.; Ames, R.G.; Copeland, S.; Gebhart, K.A.; and Day, D.E. (2000). Spatial and seasonal patterns and temporal variability of haze and its constituents in the United States: Report III. ISSN 0737-5352-47. Prepared by Cooperative Institute for Research in the Atmosphere, Colorado State University, Ft. Collins, CO.

McDonald, J.D.; Zielinska, B.; Fujita, E.M.; Sagebiel, J.C.; Chow, J.C.; and Watson, J.G. (2000). Fine particle and gaseous emission rates from residential wood combustion. *Environ. Sci. Technol.,* **34**(11):2080-2091.

Molenar, J.V. (1997). Analysis of the real world performance of the Optec NGN-2 ambient nephelometer. In *Proceedings, Visual Air Quality: Aerosols and Global Radiation Balance*, I.H. Tombach, L.W. Richards, P.B. Russell, and P. Saxena, Eds. Air and Waste Management Association, Pittsburgh, PA, pp. 243-265.

Optec (1999). Model NGN-2 Open Air Integrating Nephelometer – Technical Manual for Theory of Operation and Operating Procedures. Optec Inc., Lowell, MI.

Pitchford, M.L.; Green, M.C.; Kuhns, H.D.; Malm, W.C.; Scruggs, M.; Farber, R.J.; Mirabella, V.A.; White, W.H.; McDade, C.; Watson, J.G.; Koracin, D.; Hoffer, T.E.; Lowenthal, D.H.; Vimont, J.C.; Gebhart, D.H., et al. (1999). Project MOHAVE Final Report. Prepared by U.S. Environmental Protection Agency, Region IV, San Francisco, CA. http://www.epa.gov/region09/air/mohave/report.html.

USDA (1985). Soil survey of the Las Vegas Valley area, Nevada, part of Clark County. Prepared by U.S. Dept. of Agriculture, National Cooperative Soil Survey, Washington, DC. July 1985.

Vanderpool, R.W.; Peters, T.M.; Natarajan, S.; Gemmill, D.B.; and Weiner, R.W. (2001). Evaluation of the loading characteristics of the EPA WINS $PM_{2.5}$ Separator. *Aerosol Sci. Technol.*, **34**(5):444-456.

Watson, J.G.; Chow, J.C.; Richards, L.W.; Andersen, S.R.; Houck, J.E.; and Dietrich, D.L. (1988). The 1987-88 Metro Denver Brown Cloud Air Pollution Study, Volume II: Measurements. Report No. 8810.1F2. Prepared for 1987-88 Metro Denver Brown Cloud Study, Inc.; Greater Denver Chamber of Commerce, Denver, CO, by Desert Research Institute, Reno, NV.

Watson, J.G.; Lioy, P.J.; and Mueller, P.K. (1989). The measurement process: Precision, accuracy, and validity. In *Air Sampling Instruments for Evaluation of Atmospheric Contaminants*, 7th ed., S.V. Hering, Ed. American Conference of Governmental Industrial Hygienists, Cincinnati, OH, pp. 51-57.

Watson, J.G.; and Chow, J.C. (1992). Data bases for $PM_{10}$ and $PM_{2.5}$ chemical compositions and source profiles. In *$PM_{10}$ Standards and Nontraditional Particulate Source Controls*, J.C. Chow and D.M. Ono, Eds. Air & Waste Management Association, Pittsburgh, PA, pp. 61-91.

Watson, J.G.; Chow, J.C.; Lowenthal, D.H.; Pritchett, L.C.; Frazier, C.A.; Neuroth, G.R.; and Robbins, R. (1994a). Differences in the carbon composition of source profiles for diesel- and gasoline-powered vehicles. *Atmos. Environ.*, **28**(15):2493-2505.

Watson, J.G.; Chow, J.C.; Lu, Z.; Fujita, E.M.; Lowenthal, D.H.; and Lawson, D.R. (1994b). Chemical mass balance source apportionment of $PM_{10}$ during the Southern California Air Quality Study. *Aerosol Sci. Technol.*, **21**:1-36.

Watson, J.G.; Chow, J.C.; Lurmann, F.W.; and Musarra, S. (1994c). Ammonium nitrate, nitric acid, and ammonia equilibrium in wintertime Phoenix, Arizona. *JAWMA,* **44**(4):405-412.

Watson, J.G.; Lioy, P.J.; and Mueller, P.K. (1995). The measurement process: Precision, accuracy, and validity. In *Air Sampling Instruments for Evaluation of Atmospheric Contaminants,* 8th ed., B.S. Cohen and S.V. Hering, Eds. American Conference of Governmental Industrial Hygienists, Cincinnati, OH, pp. 187-194.

Watson, J.G.; Chow, J.C.; and Frazier, C.A. (1999). X-ray fluorescence analysis of ambient air samples. In *Elemental Analysis of Airborne Particles, Vol. 1,* S. Landsberger and M. Creatchman, Eds. Gordon and Breach Science, Amsterdam, pp. 67-96.

Watson, J.G.; and Chow, J.C. (2001a). Source characterization of major emission sources in the Imperial and Mexicali valleys along the U.S./Mexico border. *Sci. Total Environ.*, **276**(1-3):33-47.

Watson, J.G.; and Chow, J.C. (2001b). Estimating middle-, neighborhood-, and urban-scale contributions to elemental carbon in Mexico City with a rapid response aethalometer. *JAWMA,* **51**(11):1522-1528.

Watson, J.G.; Turpin, B.J.; and Chow, J.C. (2001a). The measurement process: Precision, accuracy, and validity. In *Air Sampling Instruments for Evaluation of Atmospheric Contaminants,* 9th ed., B.S. Cohen and C.S.J. McCammon, Eds. American Conference of Governmental Industrial Hygienists, Cincinnati, OH, pp. 201-216.

Watson, J.G.; Chow, J.C.; and Houck, J.E. (2001b). $PM_{2.5}$ chemical source profiles for vehicle exhaust, vegetative burning, geological material, and coal burning in northwestern Colorado during 1995. *Chemosphere,* **43**(8):1141-1151.